# DIFFERENTIAL METASTATIC ADHESION CASCADE OF TUMOR CELLS BEARING SELECTIN-BINDING LIGANDS

A Dissertation

Presented to the Faculty of the Graduate School

of Cornell University

In Partial Fulfillment of the Requirements for the Degree of

Doctor of Philosophy

by

Yue Geng

August 2013

# DIFFERENTIAL METASTATIC ADHESION CASCADE OF TUMOR CELLS BEARING SELECTIN-BINDING LIGANDS

Yue Geng, Ph. D.

Cornell University 2013

A myriad of previous research has suggested that circulating tumor cells (CTCs) can adhere to the blood vessel wall to eventually extravasate and form secondary tumors in a step-wise process similar to the leukocyte adhesion cascade. These steps require the cell, whether CTC or leukocyte, to bear specific surface proteins which can form transient interactions with E- and/or P-selectin expressed on the inflamed endothelium. These interactions facilitate initial cell tethering and rolling which lead to firm cell adhesion and extravasation. However unlike leukocytes, CTCs can originate from various primary sites, e.g. breast, colon, lung, prostate, etc. Moreover, cancer cells from each particular site (and possibly even varying from each person with cancer) can exhibit unique phenotypic expressions of selectin ligands. Briefly from the cell lines studied here, COLO 205 (colon cancer) cells abundantly expressed E-selectin ligands and established stable cell rolling on E-selectin surfaces, however, this cell line proliferates in two separate populations with a differential degree of E-selectin

binding capabilities. The MDA-MB-231 cell line (breast cancer) expressed E-selectin ligands, yet only interacted with E-selectin surfaces with cytokine treatments. The rare childhood eye cancer, retinoblastoma (RB), was found to metastasize without the expression of E-selectin ligands. The mechanism for the RB cell extravasation from the blood stream may proceed via the initial tethering of RB cells to circulating leukocytes where the RB:leukocyte aggregate adheres to the inflamed endothelium. Lastly, the ZR-75-1 cell line (breast cancer) also stably rolled on E-selectin surfaces largely due to the novel E-selectin ligand MUC1. The underglycosylated form of MUC1 was found to facilitate cell tethering when interacting with P-selectin, achieve stable cell rolling when interacting with E-selectin, and even produce firm cell adhesion events when interacting with intercellular adhesion molecule 1 (ICAM-1). Indeed, the challenge of CTC treatment is a major obstacle even when limited to the aspect of selectin ligand expression and cell adhesion to the endothelium. Fortunately, selectin:ligand based devices explored here and by other researchers may offer a viable method to capture CTCs from patient blood for further study and possible personalized treatments.

## BIOGRAPHICAL SKETCH

Yue Geng (耿悦) was born to Xu Geng and Xiaoyin Wang in Shenyang (沈阳), the largest city in northeast China, once the Imperial Palace of the Qing Dynasty. Yue enjoyed traveling even at a young age possibly because her father was a busy journalist who traveled for work almost every week. During her middle and high school years, she spent time in multiple cities in Japan including Kyoto, Tokyo, and Toyama where she became fluent in Japanese. Again influenced by her father, Yue enjoyed social sciences and declared her major in International Studies when she started college at Southern Polytechnic State University in Marietta, Georgia. Yue then developed a strong passion towards science, in part due to the influence of her mother, a physician and editor-in-chief of two medical journals. She then transferred to Georgia Institute of Technology as Chemistry major where she quickly initiated undergraduate research and received multiple awards. However, it wasn't until she met her husband Tait Takatani at Professor David Sherrill's computational chemistry laboratory when she decided to pursue a doctoral degree in science and engineering. During her PhD career at Cornell University under the supervision of Professor Michael King, Yue has made great progress in establishing herself as an independent, creative, and multidisciplinary researcher and looks forward to a career in biotechnology.

To my parents and husband, for their endless love and support.

## ACKNOWLEDGMENTS

It would not have been possible to finish this dissertation without the kind support of people around me, to only some of whom it is possible to give particular mention here.

First and foremost I would like to thank my parents Xu Geng (耿旭) and Xiaoyin Wang (王晓茵) who stood behind every big decision I have made since I was a child as I have changed my mind about what I wanted for my life quite often. People say the hardest part of love is letting go and I can't imagine how difficult it was for my parents when their only daughter made a decision to leave China and see the world on her own. They filled each and every email, weekly skype/google voice calls, and those yearly short visits during school breaks with their love, support, and patience.

My husband Tait Takatani has been the love of my life, best friend, intellectual partner and colleague ever since we met at Georgia Institute of Technology where he completed his PhD in computational chemistry. I often get asked 'How could you stand being with each other for so long everyday?' and the truth is I really don't know how he puts up with me since his existence is nothing but pleasant especially when I get overwhelmed with exams and deadlines.

I feel very privileged to have been mentored by my dissertation advisor Professor Michael King, who has been an amazing and inspiring role model. He patiently provided the vision and encouragement that helped me proceed through the doctoral

program and follow the path to become an independent scientist. Not only did he appreciate my non-engineering background, he also recognized my strength and encouraged me to pursue interdisciplinary collaborations. I enjoyed and will always cherish the conversations I had with both Mike and his wonderful wife Prof. Cynthia Reinhart-King, with whom I had the pleasure traveling to Shanghai, China for a conference. I would also like to acknowledge my committee members Prof. Barbara Baird and Prof. Abe Stroock for their kind support and guidance.

I would also like to acknowledge the King lab (past and present members) especially our lab manager Jeff Mattison and my co-authors including Dr. Tait Takatani, Kimberly Yeh, Siddarth Chandrasekaran, Dr. Jong-Wei Hsu, Mishka Gidwani, Sivaprakash Agastin, Andrew Hughes, Jocelyn Marshall, and Srinivas Narasipura for their productive collaboration, insightful discussion, and friendship. I would like to express my gratitude to Dr. Kuldeep Rana and Carissa Ball for welcoming me to the King lab and providing mentorship as well as friendship. I would also like to thank the awesome BME staff members especially Ms. Belinda Floyd and Ms. Amy Layton who have provided great support during my PhD career.

I have had the privilege to work with wonderful collaborators thanks to the NCI Physical Sciences Oncology Center network. I would like to thank Dr. Gail Seigel from University of Buffalo, Dr. David Nanus and Dr. Gunjan Gakhar from Weill Cornell Medical College, and Srimeenakshi Srinivasan from the Methodist Hospital Research Institute. It was also my great pleasure to have worked with Dr. Mathieu

Provençal and Dr. Pierre Miron from Laboratoire médical FERTILYS (QC, Canada)

I am very grateful for my funding sources throughout my PhD career. I feel honored for being selected as one of the ten Presidential Life Science fellows in 2009 when I entered Cornell University. The Howard Hughes Medical Institute Med-into-Grad fellowship (2010-2011) allowed me to continue the research project that I worked on during the BME summer immersion with Drs. David Nanus and Gunjan Gakhar. Finally, the National Science Foundation Graduate Research Fellowship (2011-2013) supported the rest of my graduate career during which I was provided numerous opportunities to enhance my research and make an impact.

Last but by no means the least, I would like to thank all my friends in Ithaca who have been there for the ups and downs throughout my PhD career. Floor, James, Jochem, Jonathan, Lianyi, Matt, Taylor, and Tina, I enjoyed our countless coffee chats, dinner discussions, game and movie nights very much! Anne, Bailey, Emily, Flor, Mark, Matt, Roanna, and Siddarth, I really appreciate your friendship and support all along and thank you being there for the good, the bad, and the ugly (not too often). To friends outside of Ithaca, Alex, Autumn, Chantelle, Jason, Jay, Jessica, Rodolfo, Tiantian, Wenlong, Xueqiao, and Yue, thank you for keeping in touch with me all these years and encouraging me during this journey!

## TABLE OF CONTENTS

## LIST OF FIGURES

# CHAPTER 1 INTRODUCTION

*This section is adapted from the following publication: Y. Geng, J. R. Marshall, and M. R. King. *Annals of Biomedical Engineering.* 40(4):790-805, 2012

The adhesion and extravasation of circulating tumor cells (CTCs) facilitate the dissemination of tumor cells and eventually secondary tumors. The detection of circulating tumor cells is recognized to hold great potential in cancer prognosis and follow up, yet the basic biophysics of how these cells interact with the endothelium is not fully understood. Formation of metastases by invasive transformed cells accounts for 90% of all deaths in cancer patients.[268] Interactions between CTCs and the endothelial lining of the vasculature are mediated by a variety of cell adhesion molecules that facilitate tethering and arrest of blood borne cancer cells to the blood vessel wall as the initial step in the growth of a metastatic tumor.

The mechanism of leukocyte recruitment from the bloodstream to diseased or inflamed tissue sites can be described as a multistep leukocyte adhesion cascade[239, 177] and has been extensively studied over the past two decades.[34, 244] The cascade begins with capturing events (or tethering) of neutrophils from the bloodstream and subsequent neutrophil rolling along the endothelial layer[34, 244] followed by firm adhesion or arrest and ultimately transendothelial migration into the tissue.[247] Recently, slow rolling, adhesion strengthening, intraluminal crawling, and paracellular and transcellular migration have been included in the cascade as additional steps.[157] Both tethering and rolling are mediated by selectins, a family of adhesion molecules presented by stimulated endothelial cells,[149,150] and represent the first contact between leukocytes and the adhesive ligand (counter-receptor)-bearing endothelial cells.[176, 273, 243]

Hydrodynamic shear force in the bloodstream has been found to control the leukocyte adhesion cascade. When exposed to physiologic shear stress in the

circulation, leukocytes can undergo passive deformation or cell flattening.[63] Cell flattening is the greatest when cells contact the surface and has been correlated with an increase of contact surface area, which also increases the adhesion force of leukocytes to the surface.[118, 124, 46] Moreover, substantial leukocyte microvilli stretching and tethering has been observed by neutrophils perfused over a P-selectin surface.[231] The effect of shear forces on microvilli deformation was hypothesized to play a major role in facilitating cell adhesion dynamics[234] and was supported by computational results.[133] Furthermore, mechanical forces regulate the expression, distribution, and conformation of adhesion molecules present on leukocytes and the endothelial layer[153, 152, 163, 210] as well as the adhesion kinetics with their ligands.[71, 95, 282] Therefore, shear forces are very important to the regulation of leukocyte recruitment.

Similar to leukocyte recruitment, tethering and rolling of CTCs to the blood vessel wall are also mediated by the selectin family.[23, 100] Colon carcinoma cells have been demonstrated to slowly roll over vascular endothelium *in vivo* in a selectin-dependent manner.[126] For leukocytes, firm adhesion to inflamed endothelium is mediated by leukocyte beta-2 integrins (Mac-1, LFA-1) binding to endothelial intercellular adhesion molecule-1 (ICAM-1).[55, 58] Similarly, for epithelial-type CTCs, the mucin MUC1 may play the role of beta-2 integrins, by binding to ICAM-1 to enable firm adhesion and eventually extravasation.[216] Hydrodynamic shear force is also involved in regulating the interactions between cancer cells and the endothelium. Recently, the adhesion dynamics of CTCs under shear flow has been utilized to isolate and target CTCs using selectin-functionalized molecular surfaces.[218] The leukocyte adhesion cascade and CTC tethering, rolling, and firm adhesion on the endothelium

indeed share many paradigms, as summarized in Figure 1.1.

## 1.1 GLYCOPROTEIN GLYCOSYLATION AND CANCER PROGRESSION

Complex carbohydrates, also referred to as *glycans*, are crucial components of the cell membrane and are present in the form of three major groups of glycoconjugates: glycoproteins, comprising a polypeptide covalently bonded to a carbohydrate moiety; glycosaminoglycans, glycans present as free polysaccharides or as part of proteoglycans; and glycosphingolipids, consisting of oligosaccharides glycosidically linked to ceramide, reviewed by Fuster and Esko.[76] Cellular glycans are connected to proteins and lipids via a highly regulated post-translational modification called glycosylation that produces abundant and diverse glycoconjugates.[201, 220] More than a decade ago, Apweiler *et al.* made the prediction that more than half of all eukaryotic protein species are glycoproteins based on the SWISS-PROT protein sequence data bank.[9]

A glycosphingolipid (GSL) is minimally defined as a monosaccharide bound to a ceramide backbone, though the structure of most GSLs is generally more complex. Glycosylation of a GSL begins with the addition of either a glucose or galactose residue to the ceramide creating glucosylceramide and galactosylceramide, respectively. Additional sugar units are then added in a stepwise fashion. Glucosylceramide is commonly combined with a galactose to form lactosylceramide. The addition of sugar units is very ordered and is facilitated by specialized enzyme families (i.e. fucosyltransferases, glucosyltransferase, galactosyltransferase, sialyltransferase).[271]

The role of GSLs in signal transduction has been well studied (reviewed by Hakomori),[94] but more recently, work has been done to distinguish the role in selectin-mediated adhesion of cancer cells to vascular endothelium. GSLs were first shown to adhere to E-selectin through the use of flow chamber dynamic flow assays.[274, 32] In past studies, GSLs are predicted to have a redundant role supporting the adhesion facilitated by glycoprotein selectin ligands.[148,30] For instance, both inhibitors of GSL glycosylation and protease enzymes decreased the adhesion of colon carcinoma cells.[33] However, work done by the Burdick lab has suggested that in head and neck squamous cell carcinoma GSLs, rather than glycoproteins, are the primary E-selectin ligands. (Wood *et al*, unpublished/in review). In addition, GSLs have been shown to play a critical role in the induction of the epithelial to mesenchymal transition (EMT) in mouse mammary cells.[92] Because EMT is hypothesized to be a pivotal step in metastasis (reviewed by Micalizzi *et al*.),[179] understanding the role GSLs play in the CTC adhesion cascade may be critical to understanding the overall metastatic process.

In order to identify and characterize the specific glycoproteins serving as ligands for the selectins, researchers use a variety of scientific approaches. These include, but are not limited to, gel electrophoresis, microarrays, and mass spectrometry. Two-dimensional electrophoresis (2-D electrophoresis) separates protein species based on two characteristics. Proteins are first separated based on isoelectric point (pI) and then on size. The gel can then be stained with silver and analyzed for density of each species. Alternatively, individual protein spots can be excised and extracted from the gel and subjected to further analysis. Mass spectrometry utilizes an electron beam that fractionates the proteins. The result is

charged fragments of proteins. Each fragment is assigned a mass to charge ratio (m/z). The combination of all the m/z values of a protein is the fingerprint. Proteins of interest can be analyzed using mass spectrometry and the resulting fingerprint can be compared to a library of known proteins in order for identification of the protein of interest.[172] In order to study protein-protein interactions, many researchers utilize protein microarrays. Multiple species of proteins are printed onto a glass slide and the slide is then incubated with another protein or antibody and the resulting interactions are observed by colorimetric, fluorescent, or other detection methods. In addition, antibodies can be printed on a glass slide and the slide can then be incubated in a patient's serum. The serum can then be probed for known cancer markers.[245]

Glycosylation occurs via two different pathways: O-glycosylation, where N-acetylgalactosamine is attached to the O-terminus of serine or threonine residues of glycoproteins and N-glycosylation, glycosidic bonds that connect N-acetylglucosamine and the N-terminus of asparagine residues of glycoproteins.[52] It has been shown that glycosylation on the tumor cell surface changes during malignant transformations and that these altered glycans mediate key pathophysiological events during tumor progression.[76, 270] Specifically, glycan alterations include the lack of expression and/or over-expression of certain structures, persistence of incomplete or truncated structures, accumulation of precursors, and the appearance of novel structures.[270] Furthermore, tumor cells are found to express a unique repertoire of glycans. However, correlating the alterations of specific glycans to tumor cell proliferation is difficult in part due to the pleiotropic effects of prevalent N-glycosylated glycoproteins. Examples of glycan families involved in tumor

progression include growth and proliferation, tumor invasion, metastasis, and angiogenesis and have been reviewed in-depth by Fuster and Esko.[76]

The roles of O-linked glycans and mucins in cell differentiation, regulation of cell growth through apoptosis, and proliferation have been extensively studied.[77, 208] O-glycosylation occurs frequently on secreted or membrane-bound mucins that are rich in serine and threonine.[220] Moreover O-glycans, including Lewis antigens, are involved in the adhesion and invasion of cancer cells and are often altered and highly sialylated in cancer cells.[25,182] Therefore, similar to leukocytes, glycosylation is necessary to facilitate cancer cell adhesion and rolling, which are initial steps in metastasis.

## 1.2 METASTATIC CASCADE: ADHESIVE RECRUITMENT OF CANCER CELLS VIA SELECTINS

Selectins are receptors for a variety of O-glycosylated ligands and mediate transient adhesion of cells to the endothelium. These receptor:ligand interactions represent the first contact of cancer cells to the endothelial wall, which facilitates tethering and rolling events.[88, 125, 100, 23, 264] Furthermore, there is a wealth of evidence correlating metastatic potential to selectin mediated events of cancer cells. In particular, highly metastatic cancers, such as colon carcinoma and acute myeloid leukemia, abundantly exhibit E- and P-selectin ligands.[73, 80] E- and P-selectin deficient mice have been shown to form fewer lung metastases from the highly metastatic colon cancer HT29,[11] and E-selectin specifically, has been proven crucial to the metastasis of colon cancer through the vascular wall.[39] These cancer cells have also been shown to slowly roll

over vascular endothelium *in vivo* in a selectin-dependent manner.[84] Therefore, similar to the leukocyte adhesion cascade, also initiated with cell tethering and rolling via selectin mediated interactions, cancer cells displaying selectin ligands are potentially involved in a 'cascade' of events that eventually lead to metastasis, i.e. the metastatic cascade.[23]

It is believed that tumor cells can not only interact with endothelial cells but also form multicellular complexes with platelets and leukocytes, which can then arrest in the microvasculature of distant organs, and eventually extravasate and establish secondary tumor sites.[114, 116, 78] Borsig et al. used P- and L-selectin double deficient mice to demonstrate *in vivo* that the two selectins work synergistically to facilitate cancer metastasis and that L-selectin on leukocytes has a role in facilitating metastasis, following the interactions of platelets with tumor cells mediated by P-selectin.[20] Various types of cancer cells have been found to highly express ICAM-1, a cell surface adhesion protein that can mediate leukocyte firm adhesion through interaction with the CD11/CD18 adhesion complex.[123, 101, 225, 170]

Tumor cells have been reported to undergo extensive interactions with host cells including polymorphonuclear cells (PMNs).[161] Such interactions between cancer cells and PMNs together with the normal interactions between PMNs and endothelial cells have been observed in breast cancer, advanced gastric cancer, colon cancer, and malignant melanoma,[283, 159, 214] and could play important roles in cancer cell transendothelial migration under physiological flow conditions,[160,238] although the mechanism remains unclear. To address this, Liang *et al*. examined the molecular interactions between endothelial cells, PMNs, and melanoma cells under defined

hydrodynamic shear conditions and found that PMN-facilitated melanoma adhesion to endothelial cells is shear dependent.[160] The shear-rate dependency can be explained by the cell aggregation of PMN and melanoma cells through the binding of CD11/CD18 adhesion complex and ICAM-1, which suggests a mechanism for receptor-ligand mediated leukocyte-tumor cell interactions. Recently, our group discovered that ABCG2+ stem-like retinoblastoma cells (RB143 and WERI-Rb27) preferentially express ICAM-1, which can support the heterotypic aggregation of retinoblastoma cells with PMNs in the bloodstream following the same mechanism mentioned above. A step-wise binding mechanism in which the leukocytes and retinoblastoma cells first interact and form small aggregates, roll on the E-selectin surface, and firmly adhere to the endothelial layer has been proposed.[83] Interactions between selectin ligands and fibrin have also been shown to play an important role in cancer cell metastasis. Work done by the Konstantopoulos group has shown that CD44 expressed on colon cancer cells is the main receptor for fibrin, and that the CD44v-fibrin interaction dominates at low shear rates due to the increased interaction time between the two molecules.[7,8,253] In addition, fibrin has also been shown to be a bridging molecule between PMNs and CTCs, allowing for cancer cell-leukocyte aggregation.[290]

A group of important glycosylated ligands consist of oligosaccharides that bear sialic acid, fucose, and sulphate at the tips of O-linked glycans. These ligands are recognized by all three members of the selectin family: E-, P-, and L-selectin (reviewed in Ref 141). Sialic acids are terminal monosaccharides attached to cell surface glycoconjugates and play important roles in many physiological and pathological processes.[89] Lewis type blood group antigens, a class of the ligands

described above, consist of the tetrasaccharide sialyl Lewis x ($sLe^x$; NeuAc α2,3 Gal β1,4 [Fuc α1,3] GlcNAc-R), built on galactose, N-acetylglucosamine and fucose, and its isomer sialyl Lewis a ($sLe^a$; NeuAc α2,3 Gal β1,3 [Fuc α1,4] GlcNAc-R), as illustrated in Figure 1.2.[121, 269, 27] Over a decade ago, researchers found that tumor cells overexpress $sLe^x$ or $sLe^a$ on their surface glycoproteins or glycosphingolipids in lung, colon, gastric, and pancreatic carcinomas.[20, 269, 127] The production and overexpression of $sLe^x$ on tumor cells may be caused, in part, by transcripts of core 2 GlcNAc-T, an O-glycan that harbors $sLe^x$ found to increase in human colon carcinomas.[236]

It is worth noting that the fucose modules of the sialy $Lewis^{x/a}$ motifs are crucial for their functions,[164] requiring fucosylation that is catalyzed by fucosyltransferase enzymes, or FUTs. Each FUT has a distinct function and tissue expression pattern.[49,167] Among the nine already discovered human FUT genes, six FUTs (FUT3-6, FUT7, and FUT9) were found to be involved in the synthesis of sialyl Lewis x ($sLe^x$).[13] Our group demonstrated that colon and prostate cancer cells possess unique FUT s that are distinct from those required by hematopoietic cells and therefore can be targeted therapeutically without compromising immune function.[106] The adhesive interactions between endothelial selectins and their ligands on cancer cells were recreated by perfusing cancer cells through microtubes coated with human recombinant E-selectin. FUT3 siRNA was delivered with a novel flow-based method using P-selectin-conjugated nano-liposomes.[109] At a physiological range of wall shear stress, the number of cancer cells recruited to the microtube surface (rolling/adherent) decreased dramatically after FUT3 knockdown, indicating the essential roles of FUTs in selectin mediated cell adhesion.[106]

To date, a myriad of ligands for the three selectins both on leukocytes and on cancer cells have been discovered. Selectins have been found to interact with $sLe^x$ and related sequences decorating P-selectin glycoprotein ligand 1 (PSGL-1), E-selectin-ligand-1 (ESL-1), CD44, CD34, and mucosal addressin cell adhesion molecule (MadCAM) presented on leukocytes.[121, 57, 213, 17, 250, 248] PSGL-1, first found on the tips of microvilli on leukocyte cell surface, is one of the main physiological ligands for leukocytes and one of the most characterized ligands, which binds to all three selectins with different affinities. PSGL-1 is a sialylated, mucin-like homodimer that displays mostly O-linked glycans. It was found to possess at least one sulfated tyrosine residue at the N- terminus of the molecule.[185, 199, 278, 212] As described above, mucins bearing $sLe^{x/a}$ structures on cancer cells may also function as significant selectin ligands. Interestingly, cancer cells also share multiple well established selectin ligands with leukocytes, including ESL-1 and PSGL-1, first identified on human metastatic prostate cancer cells.[56] Aigner et al. have identified and characterized another mucin like glycoprotein as a ligand for P-selectin. Human CD24 on a breast (KS) and a small cell lung carcinoma (SW-2) cell line, both negative for PSGL-1, were found to bind to P-selectin under static conditions.[3] Using the parallel flow chamber assay, they confirmed the physiological role of CD24 as a ligand for P-selectin on KS cells in the presence of shear stress.[84] Later, Myung et al. reported the role of CD24 on MCF7 breast cancer cells as a ligand for E-selectin under flow[191] by measuring the binding kinetics of CD24 with E-selectin with surface plasmon resonance (SPR). The identification of CD24 as a ligand for both P- and E-selectin may provide better understanding of the adhesion and invasion mechanisms of metastatic breast cancer.

Recently, carcinoembryonic antigen (CEA) and CD44 variant isoforms have been shown to cooperate in mediating colon cancer cell adhesion to L- and E-, but not P-, selectin under physiological flow.[158, 35] Thomas and coworkers also observed sialofucosylated glycoprotein(s) mediated selectin binding in CD44-knockdown cells and identified podocalyxin-like protein (PCLP) as an alternative selectin ligand using immunoaffinity chromatography and tandem mass spectrometry.[271] Shirure *et al*. have also shown that gangliosides, groups of glycosphingolipids on BT-20 and MDA-MB-468 breast cancer cell lines, function as E-selectin ligands that mediate adhesion to activated endothelium.[284] In a 1997 review, Varki stated that selectins could also recognize nonsialylated or nonfucosylated molecules such as heparan sulfate glycosaminoglycans, sulfated glycolipids such as sulfatides, and sulfoglucuronosyl glycosphingolipids.[269] Recently, it was also discovered that E-selectin binding to the breast cancer cell line 4T1 is restricted to $sLe^x$ or closely related structures while P-selectin binding can involve a varied group of compounds, including $Ca^{2+}$ independent but sulfur dependent, heparinase/chondroitinase sensitive binding to non-Lewis structures, implying that P-selectin ligands on the surface of the 4T1 cells are mostly heparin sulfate/chondroitin sulfate proteoglycans.[183] These non-sialylated P-selectin ligands could play a crucial role in tumor cell migration.

## 1.3 EFFECTS OF FLUID MECHANICAL FORCES ON GLYCOPROTEIN MEDIATED CELL ROLLING AND ADHESION

The intravascular environment can dramatically alter tumor cell functionality and viability. In particular, blood circulation creates hydrodynamic shear forces and can

cause cell deformation and activation of signaling cascades. In the case of the colorectal carcinoma cell lines, HT116, shear stress causes an increase in cell proliferation and expression of the transforming growth factor beta 1 and plasminogen activator inhibitor-1 genes.[119] Interestingly, B16 melanoma cell viability significantly decreased when exposed to physiological shear stress over a time frame of minutes to hours.[26] Likely, this type of cell death is caused by mechanical damage to the cell membrane.[5] Under physiologic flow conditions, glycoproteins and glycolipids have been found to mediate adhesion to the vascular wall[33] and, therefore, shear forces help facilitate cancer cell rolling and adhesion in a manner similar to the leukocyte adhesion cascade. The physical interactions of cancer cells with their microenvironment and their modulation by mechanical forces have been shown to play crucial roles in the metastatic process, reviewed by Verdier *et al*. and Wirtz *et al*.[272,279]

Much effort has been made to develop numerical models to describe the important cellular and molecular scale mechanisms of cell rolling. For example, Dong and coworkers described the importance of shear flow and cell deformability in cell rolling mechanics using both an in vitro experimental system and numerical simulation of cell rolling with the finite element method. In their study, the Hookean spring model with a deterministic kinetic equation was used to simulate receptor-ligand interactions under hydrodynamic force. They found that cell deformation/flattening causes fewer disturbances to the flow and therefore reduces the overall shear stress on the cell surface.[61, 62]

Jadhav and coworkers developed a 3-D computational model that simulated

receptor-mediated rolling of a deformable cell on a ligand-coated surface in a linear shear field.[115] In this model, parameters were chosen to describe PSGL-1-mediated leukocyte rolling on a P-selectin- decorated planar surface, where the motion of an elastic capsule near a plane in a linear shear field was simulated. The model successfully predicted the degree of cell deformation at a given shear rate and that the cell-substrate contact area decreases with increasing cell membrane stiffness.

One of the most popular and effective methods to simulate specific adhesive interactions between model cells and surfaces under shear flow is *adhesive dynamics* (AD), developed by Hammer and coworkers.[96] Bond formation and breakage stochastically correspond to the association and dissociation rates, respectively, of the binding receptors and ligands. The basic idea is that adhesion molecules can be modeled as compliant springs, shown in Figure 1.3, and the kinetics of single-bond failure described by the Bell model.[14]

$$k_r = k_r^0 \exp(r_0 F / k_b T)$$

This model has been successful in mapping out a state diagram for an idealized spherical, rigid cell with adhesion molecules randomly distributed about its surface, linking different adhesion dynamics to mechanochemical properties of the adhesion molecules. Furthermore, experimentally measured values of mechanochemical properties of selectins were found to self-consistently fall within the rolling regime of the state diagram.[41] Recently, deformable microvilli parameters were added to this model by Caputo and coworkers.[36] The deformation was predicted to significantly

influence the rolling behavior of leukocytes, an observation also seen in experiments.[206] Using this updated AD model, our group investigated whether force-dependent L-selectin shedding is necessary for L-selectin-mediated neutrophil rolling under flow conditions.[151] It was verified with AD simulations that L-selectin is cleaved from the neutrophil surface during rolling under hydrodynamic shear flow, shown in Figure 1.3, in agreement with previous experimental work.[229] A comparison of an updated state diagram and an adhesive dynamics model without microvilli[41] suggests that deformable microvilli decrease the impact of the reactive compliance on adhesion. Another variant combines Stokesian dynamics,[22] utilizing a Langevin equation for hydrodynamic and thermal forces, and adhesive dynamics.[142]

As the importance of cell-cell collisions and hydrodynamic interactions is being recognized in the adhesive recruitment of cells to surfaces, researchers are now aware of several such mechanisms that contribute to the rate of cell recruitment in concentrated systems that lead to differences between in vitro and in vivo observations.[6, 275] To address this, King and Hammer developed a novel computational approach to simulate cell adhesion to surfaces in a dense multicellular environment, called multiparticle adhesive dynamics (MAD).[132, 131, 135, 130] Fusing a stochastic Monte Carlo simulation of single receptor-ligand bonds and calculations of concentrated suspension flow at low Reynolds number, MAD simulations predict the accelerated recruitment of leukocytes to inflamed endothelium caused by multicellular hydrodynamic interactions and were verified both *in vitro*[132, 131] and *in vivo*.[134, 136] With this success, the MAD program has been expanded to include viscoelastically deformable cells, highly parallel implementations, and intracellular signaling leading

to cell activation.[144] To characterize the dynamics of circulating tumor cells traveling along the endothelium, the interaction constants between tumor cells and the endothelium and their relationships with velocity or loading rates need to be investigated.

Our group has developed a selectin-mediated and flow-based platform technology to capture and enrich cell subpopulations. Mirorenathane (MRE) tubes with an inner diameter of 300 μm were coated with human recombinant endothelial selectin and connected to a pressure driven syringe pump and cell sources. A population of hematopoietic stem and progenitor cells (HSPC) from human bone marrow that express CD34 were isolated when perfused over P-selectin coated microchannels.[281] These P-selectin functionalized microtubes were also used to purify CD45+ mature mononuclear blood cells without alteration of surface phenotypes, which have practical use in the fields of transplantation, regenerative medicine, and gene modification.[195] To date, few methods exist to reduce blood borne metastatic load. The existing methods, although effective, rely on filtration of patient blood through extracorporeal devices, which cause patient discomfort and require very frequent hospital visits.[209, 66, 74, 222, 192] To address this, our group demonstrated a novel biomimetic method to capture CTCs in flow via adhesive interactions with endothelial selectins and induce apoptotic signals with tumor necrosis factor (TNF) related apoptosis-inducing ligands (TRAIL).[59] Compared with cancer cells treated under static conditions, rolling cells on the selectin coated surface under flow conditions showed a much greater apoptotic population.[59] This selectin-based technology has the advantage of capturing viable CTCs that can be further characterized by releasing the bound CTC

in the absence of calcium.[138] Recently, E-selectin-mediated adhesive interactions were utilized inside an E-selectin coated polydimethylsiloxane (PDMS) microbubble system to capture COLO 205 cells under flow conditions.[1] The COLO 205 cells trapped inside the microbubbles were allowed to proliferate and form tumor spheroids for drug toxicity studies.

## 1.4 MUC1 AND CANCER METASTASIS

Another class of glycoproteins is the mucin family of high molecular weight macromolecules. Mucins are normally associated with secreted mucus that provides lubrication between the lumen and cell surfaces and adhere to the epithelial layer for protective purposes.[107, 99] Generally, mucins can be divided into gel-forming, transmembrane, and soluble categories which are summarized in depth elsewhere.[99, 215] Briefly, gel-forming mucins contain cysteine-knot and von Willebrand factor domains, as well as cysteine-rich tandem repeat regions which aid in the formation of oligomers. Transmembrane mucins contain transmembrane domains which connect the mucins to the cell surface. Soluble mucins lack any of the aforementioned domains and are generally smaller than the mucins in the previous categories. All mucins, however, are structurally similar due to their serine, threonine, and proline rich domains. These domains are normally in the variable tandem repeat regions. Therefore, a major hallmark of the mucin family is the ability to be heavily 'sugar-coated' via multiple O-glycosylation sites.[38, 97]

In regards to cancer, transmembrane mucins are by far the most prevalent.[215] Of particular importance is the MUC1 glycoprotein due to its abnormal over-

expression in nearly all types of cancer. MUC1 is normally expressed in mammary (MUC1 was first isolated from human milk[79]), respiratory, female reproductive, gastrointestinal, middle ear, and salivary glandular surfaces[79, 24, 154, 223, 28] and in the pancreas.[171, 258] It has been found to be over-expressed in breast, ovarian, lung, pancreatic, prostate, gastric, and colorectal cancers[221, 31, 86, 4, 292] where the high expression generally correlated with greater mortality rates.[259, 65, 139, 93, 168]

MUC1 is expressed aberrantly on cancer cells in two ways: variant glycoforms and its location on the cell surface. The tandem repeat region of MUC1 consists of 25-150 repeat units of 20 identical amino acid sequences rich in serines and threonines, which have a high propensity for O-glycosylation. With respect to the normal MUC1 glycosylation, MUC1 on cancer cells exhibit fewer glycosylated sites as well as shortened oligosaccharides;[162] both factors lead to the exposure of the core protein, as shown in Figure 1.4.[29,60] Interestingly for pancreatic and colon tumors, glycoforms of MUC1 containing the $sLe^a$ and $sLe^x$ oligosaccharides,[31] and the increased detection of MUC1 carrying $sLe^{x/a}$ have been linked to poor prognosis in patients with lung adenocarcinoma.[113] The second way MUC1 is abnormally expressed is in its uniform distribution across the cancer cell surface.[128, 292] Normally, MUC1 is localized at the apical border of epithelial cells.

There are different hypotheses for the functional role of MUC1 and cancer progression. First, mucins are primarily thought to have lubricating and protective purposes.[292, 128, 257, 285] A study of the MUC1 responses to oxidative stress suggests that MUC1 can protect the cancer cell from cell death via reactive oxygen species.[285] Using atomic force microscopy, another recent study indicated that mucin O-

glycosylation could act as a mechanical barrier, limiting the cytotoxic effects on a multidrug resistant ovarian cell line.[276] Secondly, since MUC1 glycoforms contain several selectin interacting O-glycans (e.g., $sLe^x$ and $sLe^a$), it is reasonable to postulate that MUC1 can facilitate cell adhesion via carbohydrate:selectin interactions. In fact, despite the anti-adhesive role of MUC1 on normal cells, E-selectin:MUC1 interactions have been reported.[289, 288, 69] In particular, the MUC1:E-selectin interaction has been shown to be shear dependent and an order of magnitude more efficient than CD43.[69] Furthermore, for epithelial-type CTCs (e.g., from breast, prostate), MUC1 may play the role of beta-2 integrins, by binding to ICAM-1 to enable firm arrest and transendothelial migration.[216] Recently, kinetic off-rates of monovalent and multivalent interactions between MUC1 epitope and antibody were measured using dynamic force spectroscopy, providing therapeutic opportunities to target the MUC1 core epitope. In conclusion, the mucin family, specifically MUC1, may be important factors in cancer progression either as a protective role and/or as a cell adhesion facilitator, which enhances the cancer cell metastatic cascade.

This thesis will discuss four different types of E-selectin mediated interactions between cancer cells and the endothelial adhesion molecules in the context of metastasis. In Chapter 2, a dynamic COLO 205 population switch presenting unique molecular differences as well as E-selectin functionalized microbubbles as a microfluidic system for 3D tumor spheroid culturing will be discussed. Chapter 3 will cover the effect of human plasma and pro-inflammatory cytokines on increasing the adhesiveness of highly metastatic MDA-MB-231 breast cancer cells. Chapter 4 will describe an alternative metastatic cascade where E-selectin ligand lacking

retinoblastoma cells form aggregates with circulating leukocytes and subsequently establish rolling and adhesion on E-selectin coated surfaces. In Chapter 5, MUC1, a novel ligand for E-selectin and ICAM-1 will be characterized using ZR-75-1 and MCF7 breast cancer cells. The future work section includes plans for animal models to validate the in vitro cell based results as well as the development of non-invasive prenatal diagnostic tools to isolate selectin ligand and EpCAM expressing fetal trophoblasts in circulation.

**Figure 1.1:** Cell adhesion cascade and representative selectin ligands for both leukocyte and cancer cells. The leukocyte adhesion cascade and CTC tethering, rolling, and firm adhesion on the endothelium share many paradigms. Most of the selectin ligands on leukocytes except L-selectin are also present on cancer cells. Recently, novel ligands on cancer cells have been observed to facilitate selectin-mediated rolling on the endothelium.

**Figure 1.1: A schematic of the leukocyte and cancer cell adhesion cascade**

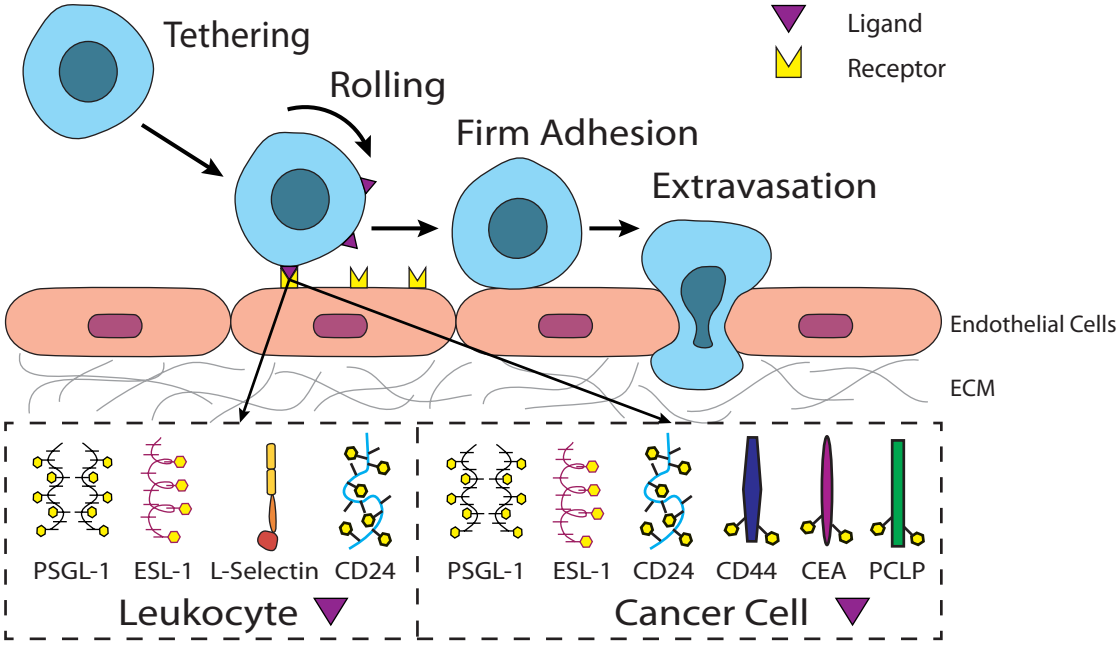

**Figure 1.2:** Selectins only bind to glycosylated ligands. Selectin molecules require glycosylation in order to bind to a receptor. As shown in the above figure, CTCs will not interaction with the vascular endothelium unless their membrane proteins (or lipids) are glycosylated. The insert in the right panel shows the addition of $sLe^x$, a typical glycosylation found on CTCs, to a membrane protein.

**Figure 1.2: A schematic of selectins binding to glycosylated ligands**

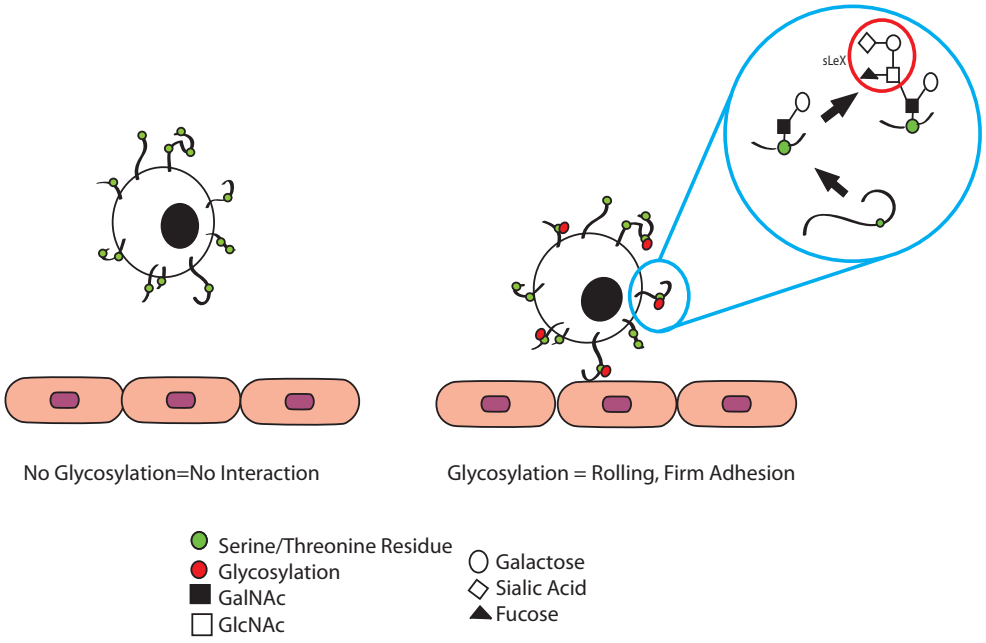

**Figure 1.3:** The adhesive dynamics simulation of cell adhesion under flow. (A) Schematic of the model system: a rigid spherical cell is covered with a random distribution of adhesion molecules, with the appropriate counter-receptor molecules randomly placed on the wall. Individual molecular bonds are modeled as compliant springs. Bonds are randomly formed and broken subject to the appropriate kinetics that depend on the instantaneous force loading determined by the bond endpoints. The cell slowly rolls forward due to the hydrodynamic force and torque exerted by the surrounding fluid flow.[137] (B)-(F) Instantaneous cell rolling velocity in AD simulations and experiments at a shear rate of 400 $s^{-1}$, (B) the average instantaneous velocity of five rolling cells in simulations; (C) a rescaled graph of (B) matching to y-axis with (D)-(F); (D)-(F) the experimental instantaneous rolling velocity of individual neutrophils on a $sLe^x$ coated flow chamber surface.[151]

*Reproduced with permission from Ref. 85 and 95.*

**Figure 1.3: A schematic of the adhesive dynamics simulation of cell adhesion under flow**

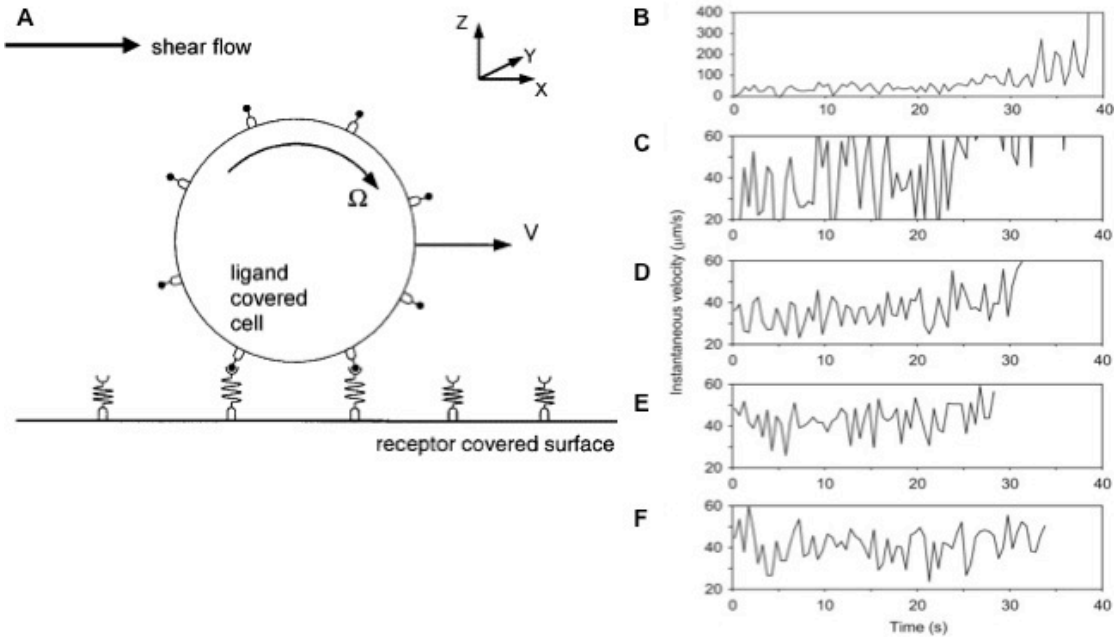

**Figure 1.4:** Involvement of the mucin family in selectin-mediated tumor cell-endothelium interactions. Only the tandem repeat regions are depicted for both MUC1 and MUC4. Compared to the common E-selectin ligands such as PSGL-1 and ESL-1, both mucins are longer (~four times) and display more glycosylated sites, with MUC4 being much longer than MUC1. Carcinoma associated mucins usually involves aberrant localization and underglycosylation (represented by the missing glycans on some of the side branches in this illustration).

**Figure 1.4: Involvement of the mucin family of selectin-mediated tumor cell-endothelium interactions**

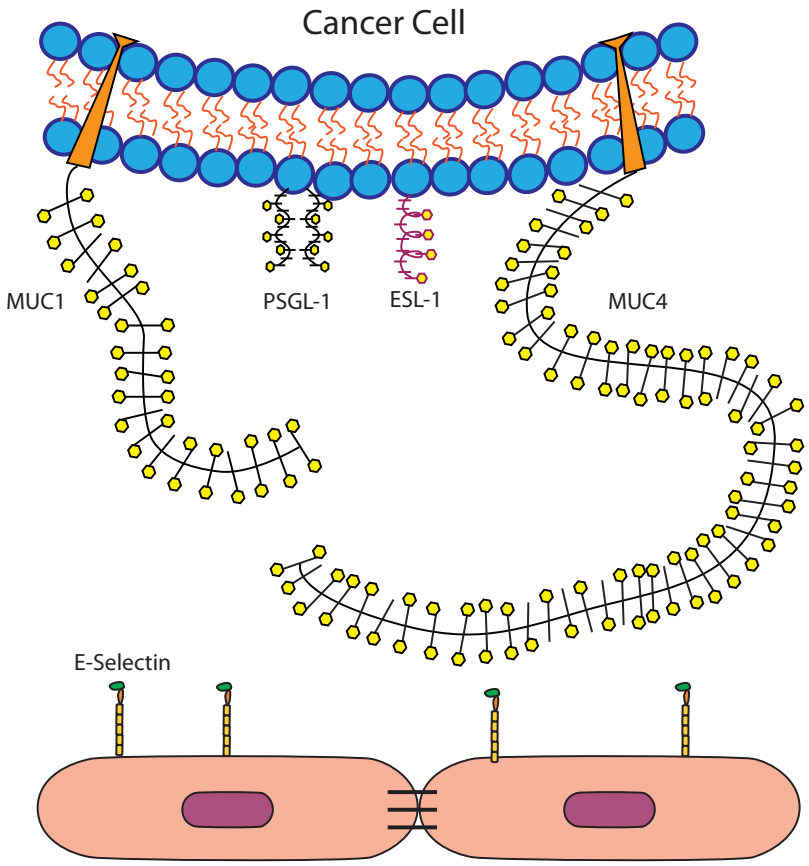

# CHAPTER 2 DIFFERENTIAL ADHESION AND CAPTURE OF COLORECTAL CANCER CELLS MEDIATED BY E-SELECTIN

## 2.1 DYNAMIC SWITCH BETWEEN TWO ADHESION PHENOTYPES IN COLORECTAL CANCER CELLS

### 2.1.1 INTRODUCTION

Colorectal cancer is one of the most frequent human tumors, which can metastasize to liver, lung, and peritoneum. Significant intratumoral genetic heterogeneity has been demonstrated in advanced colorectal carcinoma, indicating the importance to re-evaluate the use of genetic markers for prognosis.[10] Reduction or loss of E-cadherin that mediates homotypic cell-cell adhesion has been shown to promote the progression of several carcinomas including colorectal cancers.[112, 117, 200, 203] This reduced cell-cell adhesiveness permits cells to deviate from normal cell growth patterns, resulting in the destruction of histological structures. As an important member of the cadherin family, the cytoplasmic domain of the $Ca^{2+}$ dependent transmembrane glycoprotein E-cadherin regulates the structural and signaling activities required for adhesion through interactions with β-catenin, α-catenin and plakoglobin (γ-catenin).[255] Wnt signal mediated tyrosine phosphorylation of β-catenin has been established as an important regulatory mechanism behind cytoplasmic protein stabilization as the phosphorylated protein has less affinity to both the APC/GSK-3/Axin complex and E-cadherin.[47]

Metastasis is a complex and highly organized process that involves a series of distinct steps.[198] The formation of metastases by invasive transformed cells accounts for 90% of all deaths in cancer patients.[277] To form secondary tumors, cancer cells must invade the surrounding tissue and enter either the bloodstream or the lymphatic system. Similar to the leukocyte adhesion cascade which is initiated via cell tethering and rolling through selectin mediated interactions, cancer cells displaying

selectin ligands are potentially involved in a series of events that eventually lead to metastasis, i.e. the metastatic cascade.[82, 111, 158, 202]

Following intravasation, selectins can interact with a variety of O-glycosylated ligands and, in turn, mediate the transient adhesion of cells to the endothelium. These receptor-ligand interactions represent the first contact between cancer cells and the endothelial wall, which facilitates tethering and rolling events.[88] Sialic acids are terminal monosaccharides attached to cell surface glycoconjugates and play important roles in many physiological and pathological processes.[89] Over a decade ago, researchers found that tumor cells overexpress sialyl Lewis x ($sLe^x$) or sialyl lewis a ($sLe^a$) on their surface glycoproteins and/or glycosphingolipids in lung, colon, gastric, and pancreatic carcinomas.[20] $sLe^x$-bearing human colon adenocarcinoma cell lines including COLO 205 and LS174T have been shown to undergo extensive adhesive interactions with E- and P-selectin under flow conditions.[1, 98] Recently, we utilized the interaction between E-selectin ligands and human recombinant E-selectin to localize COLO 205 cells into functionalized microbubbles under flow to initiate the growth of tumor spheroids.[1]

The human colon carcinoma cell line COLO 205 was established from the ascetic fluid of a male patient with poorly differentiated colorectal carcinoma by Semple *et al.*[233] Interestingly, this cell line has a unique morphological character in that it grows simultaneously in both adherent and suspended states in culture. We have observed that when separated, both suspended and adherent populations of COLO 205 generate their counterpart populations and re-establish an equilibrium ratio over time. In this study, we examined the kinetics of this phenomenon and investigated the tumor

heterogeneity between the COLO 205 adherent and suspended populations and biochemical factors that modulate this equilibrium ratio.

## 2.1.2 MATERIALS AND METHODS

*Cell Line and Cell Culture*

The COLO 205 cell line was obtained from ATCC (American Type Culture Collection, Manassas, VA). Gibco® RPMI media (Life Technologies, Grand Island, NY), supplemented with 10% Fetal Bovine Serum (Life Technologies), 100 IU/mL penicillin and 10 μg/mL streptomycin (Life Technologies) was used as growth media. Cells were cultured in BD Falcon™ 75 $cm^2$ cell culture flasks at 37ºC in an incubator supplied with 5% $CO_2$. To collect the adherent COLO 205 cells, enzyme free dissociation buffer (Life Technologies) was added after removing the suspended population. 90% cell viability was confirmed with trypan blue dye exclusion using a hemocytometer.

*Cell Population Assay*

Adherent and suspended populations of COLO 205 cells were separated and deposited in 6-well plates. At time points 0, 0.5, 1, 2, 4, 6, and 8 hr, cells were collected and counted as described above. In separate experiments, adherent and suspended COLO 205 cells were separated and labeled with Cell Tracker Green and Orange (Life Technologies, Grand Island, NY), respectively. The adherent green cells were then re-plated at 0.2 million cells per well in a 12-well plate and allowed to reach an equilibrium adherent:suspended ratio for 8 hr. Likewise, the suspended orange cells

were re-plated at the same concentration and equilibrated for 8 hr. The suspended and adherent populations for both the green and orange cultures were separated again. Finally, the orange suspended cells were deposited into the wells containing only the green adherent layer. The numbers of orange and green cells in the suspended and adherent layers were counted from 500 μL cell solutions of each population using a flow cytometer every 2 hr for 10 hr, to assess the rate of phenotype "flip-flop".

*Reverse Transcription*

Total RNA from COLO 205 suspended and adherent cells was prepared and purified separately using RNeasy Plus Mini kit (Qiagen). The 40 μL reverse transcription reaction system includes 10 μg of total RNA, 1 μL of M-MuLV Reverse Transcriptase (New England Biolabs), 0.5 μL of RNase Inhibitor (New England Biolabs), 1 μL of Random Primers (Invitrogen), 2.5 μL of dNTP Mix (New England Biolabs) and 4 μL of MuLV Reverse Transcriptase reaction buffer (New England Biolabs). The reaction mixture was incubated inside the RT-PCR (Bio-Rad) instrument at 42º C for 1 h, followed by an inactivation step at 95º C for 10 minutes.

*Real-Time Quantitative PCR (Qpcr)*

10 ng of cDNA produced by the reverse transcription of total RNA was used in each quantitative PCR reaction. Also included in the 20 μL qPCR reaction system were 10 μL iQ$^{TM}$ SYBR Supermix (Bio-Rad), 1 μL of 2 μM forward primer and 1 μL of 2 μM reverse primer and nuclease free water.

Primer for β-catenin qPCR (product size: 166 bp)

5’-GAAACGGCTTTCAGTTGAGC-3’ (Forward)

5’-CTGGCCATATCCACCAGAGT-3’ (Reverse)

Primer for GAPDH qPCR (product size: 170 bp)

5’-AGAGCACAAGAGGAAGAGAGAGAC-3’ (Forward)

5’-AGCACAGGGTACTTTATTGATGGT-3’ (Reverse)

qPCR reactions were carried out in 96 well real-time PCR plates (Bio-Rad) using a Bio-Rad MyIQ Real-time PCR detection system. The qPCR reaction included 5 min at 95º C to activate the polymerase and 50 PCR cycles (uncoupling step at 95º C for 20 seconds followed by annealing step at 59º C for 20 sec and elongation step at 72º C for 30 seconds), followed by a melting temperature analysis to test for any nonspecific amplification. All the qPCR reactions were performed in triplicate. The expression level of β-catenin gene in each cell population was normalized to the expression level of the standard gene GAPDH.

*siRNA Transfection*

β-catenin siRNA was purchased from Applied Biosystems (Silencer® pre-designed & validated siRNA, ID: s436). Lipofectamine™ RNAiMAX (Invitrogen) reagent was used to transfect the COLO 205 cells with β-catenin siRNA as described by the manufacturer.

*E-Cadherin Coated Bead Incubation*

Protein A coated polystyrene beads (500 µL, 1% w/v, Spherotech, Lake Forest, IL) were first incubated with 2 mL of 50µg/ml mouse anti-human E-cadherin monoclonal

antibodies (Santa Cruz Biotechnology, Santa Cruz, CA) on ice for 45 minutes. Conjugated beads were washed once with 1 mL PBS and then resuspended with 500 µL of fresh media. 250 µL of bead-containing media was added to COLO 205 cells cultured in 6-well plates and incubated for 2 hr at 37ºC before cell counting and mRNA analysis.

*Flow Cytometry*

Adherent and suspended populations of COLO 205 cells were separated, washed with 1X DPBS, and resuspended in 1X DPBS with 1% BSA to a final concentration of 200,000 – 300,000 cells in each sample. Antibodies or appropriate isotype controls were added to cell suspensions and incubated over ice for 45 min. Following the incubations, the cells were washed three times with 1 mL of 1X DPBS to remove any unbound antibody. Flow cytometry samples were analyzed using an Accuri C6 flow cytometer (Accuri Cytometers Inc., Ann Arbor, Michigan, USA) and plots were created using the FCS Express package.

*Proteome Profiler Assay*

Human Phospho-kinase Antibody array kit (R&D systems) was used to analyze the phosphorylation profiles of several key kinases and their protein substrates in both the adherent and suspended COLO 205 cells. Adherent and suspended cells were separated, washed in ice cold PBS buffer, and pelleted before adding the lysis buffer provided with the array kit. Total protein concentrations were determined by Bradford colorimetric assay (Bio-Rad). The nitrocellulose membranes provided with the kit

were processed and developed as per the manufacturer's instructions.

*Immunoblotting*

Whole cell lysate from both subpopulations was freshly made using RIPA lysis and extraction buffer. The lysate protein concentrations were measured using Bradford assay (BioRad). SDS-PAGE was performed using 7.5% polyacrylamide gels and proteins were transferred to a nitrocellulose membrane, incubated with primary antibodies against β-catenin (Biolegend) and β-actin (Santa Cruz Biotechnology) overnight at 4º C. Goat anti-rabbit IgG-HRP (Santa Cruz Biotechnology) and rabbit anti-mouse IgG-HRP (Abcam) were used as secondary antibodies.

*Cell Rolling Assay*

Microrenathane tubing with 640 μm internal diameter (Braintree Scientific) was cut to a length of 50 cm, functionalized with Protein G (10 μg/mL) and Fc chimera E-selectin (20 μg/mL, R&D), and blocked with 5% BSA or milk (Sigma). Functionalized microtubes were then secured to the stage of an Olympus IX81 motorized inverted microscope (Olympus America, Melville, NY). A CCD camera (model no: KP-M1AN, Hitachi, Tokyo, Japan) and DVD recorder (model no: DVD-1000MD, Sony Electronics) were used to record experiments for offline analysis. Adherent and suspended COLO 205 cells were separated and suspended in flow buffer at 1 $x10^6$ cells/mL and perfused through protein coated microtubes using a syringe pump (KDS 230, IITC Life Science, Woodland Hills, CA) at a wall shear stress of 1.0 $dyn/cm^2$.

*qPCR Profiling of EMT-Associated Genes*

RNA was extracted from adherent and suspended cells by TRIZOL method. First strand cDNA was synthesized using the Invitrogen first strand cDNA synthesis kit. Qiagen EMT PCR array including qPCR primers for signature genes during EMT was performed in the Biorad iQ quantitative PCR machine to compare gene expression exhibited by the two populations using the $2^{-\Delta Ct}$ method. Gene expression was normalized to the housekeeping genes GAPDH and β-actin.

*Plasma Isolation and Treatment*

Whole peripheral blood was drawn from informed consenting healthy donors by venipuncture into BD Vacutainer tubes. Collected whole blood was centrifuged for 25 min at 500 rpm. The plasma layer on top was carefully removed without disturbing the interface and passed through a sterile 0.2 μm filter. 50% of the isolated plasma supplemented culture media was used to culture COLO 205 cells at $2 \times 10^5$ cells/well in 6-well plates prior to experiments.

**2.1.3 RESULTS**

*Separation of Adherent and Suspended Subpopulations Resulted in the Re-Establishment of the Equilibrium Ratio*

When cultured in monolayers, COLO 205 cells grow simultaneously in both adherent and suspended states. While the adherent COLO 205 cells grow in small aggregates (2-dimensional islands), the suspended population grows as individual cells. To separate the two populations, suspended cells were collected and plated in a new

culture flask while fresh media was added to the original flask containing the adherent population. Cell counting and viability assay were performed using trypan blue dye and a hemocytometer at various time points including 0, 0.5, 1, 2, 4, 6, and 8 hr. Interestingly, each flask initiated with either all adherent or all suspended cells was observed to re-establish an "equilibrium ratio" of 70% adherent cells to 30% suspended cells within 8 hr, as shown in Figure 2.1. A simple mathematical model was formulated to approximate the kinetics for the adherent (A) and suspended (S) cells to re-establish the equilibrium ratio:

$$\frac{dA}{dt} = -k_1 A + k_2 S \quad (1)$$

$$A + S = N\ (Total\ number\ of\ cells) \quad (2)$$

$$at\ equilibrium, \%\ adherent\ cells = A_{eq}$$

$$\frac{dA}{dt} = 0$$

$$0 = -(k_1 + k_2)A_{eq} + k_2 N \quad (3)$$

*The above differential equation gives the general solution,*

$$A = c_1 e^{-(k_1+k_2)t} + c_2 \quad (4)$$

*with initial conditions*

$$t = 0, A = A_0,$$

*yielding the solution*

$$A = \left(A_0 - A_{eq}\right)e^{-(k_1+k_2)t} + A_{eq} \quad (5)$$

The best-fit solution to this simple model was compared with the experimental data in Figure 2.1, and shows excellent agreement, implying that the phenotypic switch can be approximated with first-order kinetics. These simplified approximations suggest that the changes in gene and protein expressions which cause the dynamic population switches could occur within 30 min.

*Dynamic Switching Between the Suspended and Adherent Cells Occurred Rapidly and Reaches Equilibrium Over Time*

The adherent and suspended cells were separated and labeled with CellTracker green and CellTracker orange dyes, respectively. To determine whether the existence of two subpopulations was maintained by a dynamic switch between the two states, the labeled cells were plated separately at the same seeding density. After they reached the previously observed equilibrium ratio (time to reach equilibrium ratio was determined by previous experiments to be 8 hr), the suspended layer from the originally suspended population (in orange) was added to the adherent layer of the originally adherent type (in green). As shown in Figure 2.2, after 2 hr, a significant number (~30%) of orange suspended cells were identified in the adherent layer (since the percentage of orange cells in the suspended population was 70%) and ~15% of green adherent cells were identified in the suspended layer (since the percentage of green

cells in the adherent population was ~85%), indicating that the cells dynamically switched from one population to the other. At t=4 hr there was an increase in the percentage of orange and green cells in the suspended and adherent populations respectively, indicating that some cells that had switched from one state to the other at t=2 hr switched back again. After t=6 hr both populations stabilized with ~70% of orange cells in the suspended state (30% being in the adherent state) and ~85% of the green cells in the adherent state (~15% in the suspended state). Taken together, our results indicate that there is a dynamic switch between population states to reach an approximate equilibrium ratio of 7:3 (adherent:suspended).

*Phosphorylated Kinases are Upregulated in the Suspended Population*

Relative phosphorylation levels of 12 key kinases and their protein substrates in both adherent and suspended COLO 205 cells were measured. As depicted in Figure 2.3(A), 9 out of 12 key kinases were found to be expressed at relatively elevated levels in the suspended COLO 205 cells compared to their adherent counterparts, among which the phosphorylation of β-catenin showed the greatest increase. The overall increase in the kinase phosphorylation activity in suspended cells can be explained by their significantly higher β-catenin gene expression (Figure 2.3(B)) and excessive Wnt responsive gene activity such as C-myc. The increased phosphorylation of β-catenin protein observed in the suspended cells is also expected to reduce their binding affinity to both E-cadherin and APC, causing the suspended cells to detach and form individual cells in suspension. Increased kinase phosphorylation activity has also been recently reported to inhibit integrin mediated cell-ECM interactions.[242]

*Suspended Cells Show Increased Expression of B-Catenin and Decreased Expression of E-Cadherin*

Immunoblotting results, shown in Figure 2.3(C), indicated that the total (surface + intracellular) β-catenin protein expression was elevated in the suspended COLO 205 cells. Furthermore, flow cytometry results indicated that suspended cells express less E-cadherin and more phosphorylated β-catenin compared to adherent cells (Figure 2.3(D) & (E)).

*Manipulation of B-Catenin and E-Cadherin Expression Result in Increased Number of Adherent Cells*

An average 75% decrease in β-catenin gene expression as measured by qPCR was achieved by treating COLO 205 cells with β-catenin siRNA. As a result of the significant decrease in β-catenin gene expression, the equilibrium ratio between adherent and suspended cells (7:3) shifted towards the adherent state, to a measured ratio of 9:1 (Figure 2.4). This increase in the COLO 205 adherent cell population suggests that β-catenin may play a role in its own gene regulation, in addition to being an important linker protein in E-cadherin mediated cell-cell interactions. It was observed that the β-catenin siRNA was not able to completely abolish β-catenin mRNA expression, leaving enough β-catenin and reduced Wnt signaling to assist the β-catenin:E-cadherin complex mediated homotypic cell aggregation.[102, 197] Likewise, incubating COLO 205 cells with E-cadherin antibody coated microspheres, thereby externally forcing cell-cell adhesion, was also found to induce a significant increase in

the adherent cell fraction, shifting the ratio to 9:1 (Figure 2.4 and inset). Furthermore, β-catenin gene expression decreased by 45% in these artificially clustered cells compared to control.

*Suspended COLO 205 Cells Express More Sialyl Lewis Acids and Show Significantly Stronger Interaction with E-Selectin Coated Surfaces under Physiological Shear Stress*

To further explore the population transition in COLO 205 cells, a flow based adhesion assay was used to investigate the adhesion phenotypes of both adherent and suspended populations. As shown in Figure 2.5(C), suspended COLO 205 cells were found to have a rolling velocity of 1.52 ± 0.05 μm/s under 1 dyne/cm$^2$ shear stress, significantly slower than the adherent cells rolling at 2.10 ± 0.04 μm/s, indicating a more adhesive phenotype on the E-selectin coated surfaces. Compared to adherent cells, suspended cells were found to have elevated $sLe^x$ and $sLe^a$ expression by 60% and 80%, respectively (Figure 2.5(A) and (B)).

*Human Plasma Induces a Pro-Suspension Population Shift and Increased B-Catenin Expression*

To assess whether COLO 205 cells may behave differently once they have entered the bloodstream, human plasma was isolated from healthy donors and added to the culture media. Interestingly, as shown in Figure 2.6(A) and (B), the majority of COLO 205 cells shifted to the suspended state, leaving significantly fewer adherent cells compared to control conditions with area of fluorescence quantified in Figure 2.6(C).

Plasma-treated COLO 205 cells were also found to have greater expression of CD44, an E-selectin ligand, and phosphorylated β-catenin (Figure 2.6 (D) and (E)).

*Suspended Cells Show Increased Expression of Several EMT-Associated Genes*

The adherent-to-suspended transition is reminiscent of the epithelial-to-mesenchymal transition (EMT), which is characterized by a loss of cell adhesion and increased cell invasion in many cancers. Several EMT-associated genes were found to be upregulated in the suspended cells by qPCR. Notably, mRNA of fibroblast growth factor binding protein 1 (FGFBP1), matrix metalloproteinase-2 (MMP-2) and secreted protein that is acidic and rich in cysteine (SPARC) were >3-fold higher in suspended COLO 205 cells, as shown in Figure 2.7.

### 2.1.4 DISCUSSION

Cancer metastasis is a complex process involving a series of steps. The motivation for this study was based on our discovery of distinct adherent and suspended COLO 205 populations that consistently equilibrate to a 7:3 ratio (adherent-to-suspended) over 8 hr. Furthermore, results from Cell Tracker dye labeling revealed that COLO 205 cells dynamically switch from one subpopulation to the other while maintaining the same 7:3 ratio.

The expression levels of phosphorylated kinases show that many kinases and their protein substrates are relatively more active in the suspended cell population compared to the adherent population. This is consistent with previous studies which suggest that the phosphorylation of proteins correlates with the mesenchymal

phenotype of tumor cells.[227, 50] Two of the widely studied markers of epithelial and mesenchymal phenotypes are E-cadherin and β-catenin, respectively.[21] Flow cytometry results reveal that adherent cells express more E-cadherin, while suspended cells express more phosphorylated β-catenin.

Manipulation of the β-catenin gene and surface E-cadherin expression in COLO 205 cells resulted in a shift in the population ratio with an increased number of adherent cells. Transfecting siRNA against β-catenin in COLO 205 cells shifted the adherent:suspended equilibrium ratio from 7:3 to ~9:1. Similarly, by introducing E-cadherin monoclonal antibody coated microbeads to the cell culture, the equilibrium ratio was also altered to ~9:1 and β-catenin gene expression was found to decrease by 50%. Taken together, these results suggest an interesting concurrent 'inside-out' and 'outside-in' regulatory system, where the decrease in β-catenin gene expression within these cells as well as the externally induced elevation of E-cadherin surface expression are both able to drive an increase in the adherent:suspended population ratio.

Interestingly, suspended COLO 205 cells were also found to roll on E-selectin at a significantly slower velocity under physiologically relevant shear stresses when compared to the adherent cell population. This suggests that if given the chance to intravasate into the blood vessel, the suspended cell population may establish stronger interactions with the inflamed endothelium. Recent studies from our group reported that blood plasma triggers an adhesive phenotypic switch of breast cancer cells on E-selectin coated surfaces under flow by upregulating E-selectin ligand and glycan expression.[39, 81] In this study, similarly, plasma treatment was found to elevate CD44 expression for COLO 205 cells, in addition to inducing a preferential shift from the

adherent to the suspended cells, suggesting a more invasive phenotype with stronger interaction with the inflamed endothelium. Furthermore, upregulation of phosphorylated β-catenin expression was also observed. The dynamic population switch observed in this study suggests a potential mechanism which increases the likelihood of extravasation of the circulating tumor cells from the bloodstream to develop secondary tumor sites.

Several EMT-associated genes including FGFBP1, MMP-2 and SPARC are upregulated in suspended COLO 205 cells. FGFBP1 and MMP2 have been previously shown to be upregulated in metastatic colorectal cancers relative to normal colon epithelia.[205, 256] As a mesenchymal cell marker, SPARC expression has been identified during breast cancer EMT which correlates with a basal-like phenotype.[228] In contrast, transforming growth factor beta 1 (TGFB1) was downregulated in the suspended population of COLO 205 cells compared to the adherent population. As TGFB1 is considered to drive EMT through both paracrine and autocrine signaling,[230] its transient upregulation in the adherent COLO 205 population may induce EMT and thus promote the transition to the suspended state. These results strongly suggest that the transition from the adherent to the suspended state creates cells that express both mesenchymal-like phenotype and genotype from a cell line of epithelial origin and may be considered EMT-like.

### 2.1.5 CONCLUSION

The colorectal cancer cell line, COLO 205, uniquely proliferates as adherent and suspended populations where cells can dynamically switch from one population to the

other while maintaining a constant 7:3 (adherent-to-suspended) equilibrium population ratio. The suspended population expressed significantly more phosphorylated β-catenin and less E-cadherin compared to the adherent population. “Inside-out” manipulation, β-catenin siRNA knockdown assays, and “outside-in” manipulation, introduction of E-cadherin coated microspheres, both shifted the equilibrium population ratio to 9:1. Therefore, the expression of β-catenin and E-cadherin regulate the proliferation and switching of COLO 205 cells as two distinct populations.

In the context of metastasis, the suspended COLO 205 population represents a more invasive phenotype. Suspended cells expressed 60% more $sLe^x$ and 80% more $sLe^a$ than adherent cells which resulted in significantly slower rolling velocities on E-selectin coated microtubes. Moreover when cells were cultured in human plasma, the expression of phosphorylated β-catenin increased, shifting the majority of cells into the suspended population where $sLe^x$ and E-selectin ligand CD44 expression both increased as well. Upregulation of the EMT markers FGFBP1, MMP-2 and SPARC within the suspended population suggests mesenchymal-like cells and therefore a much more aggressive population. Future studies could focus on the regulation of phosphorylated β-catenin or E-cadherin to control the aggressiveness of colorectal cancers to help prevent metastases.

**Figure 2.1:** COLO 205 adherent and suspended population reformation and stabilization. Adherent and suspended cells were separated and re-plated in fresh RPMI media (data referred to as 'originally adherent' and 'originally suspended') The originally adherent and suspended culture flasks were monitored over 8 h by performing cell count at 0.5, 1, and 2 h intervals and the fraction of adherent cells in all conditions was plotted against time. A simple ODE model was derived for the adherent fraction as a population balance on adherent and suspended cells. Solutions to the ODE model were plotted for the best-fit model parameters of $k = 0.5\ h^{-1}$ (enough time to allow changes in gene and protein levels) and $A_{eq} = 0.7$.

**Figure 2.1: COLO 205 adherent and suspended population reformation and stabilization**

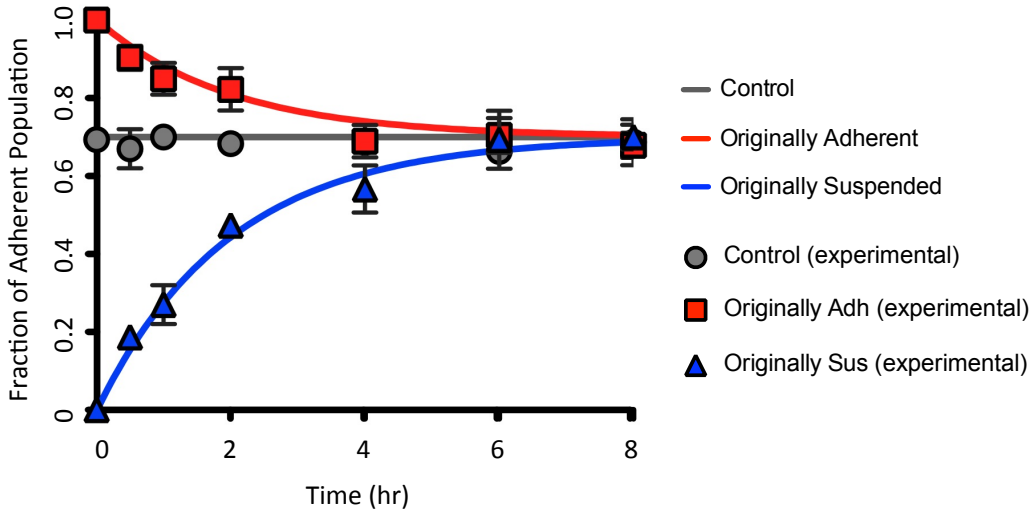

**Figure 2.2:** Dynamic population switch. **(**A)-(C) Dynamic switch between the adherent and suspended COLO 205 population. (D) Percentage of orange cell tracker dye labeled cells in the suspended layer (SUS) and green cell tracker dye labeled cells in the adherent layer (ADH) over 10 hours.

**Figure 2.2: Dynamic population switch of COLO 205 cells**

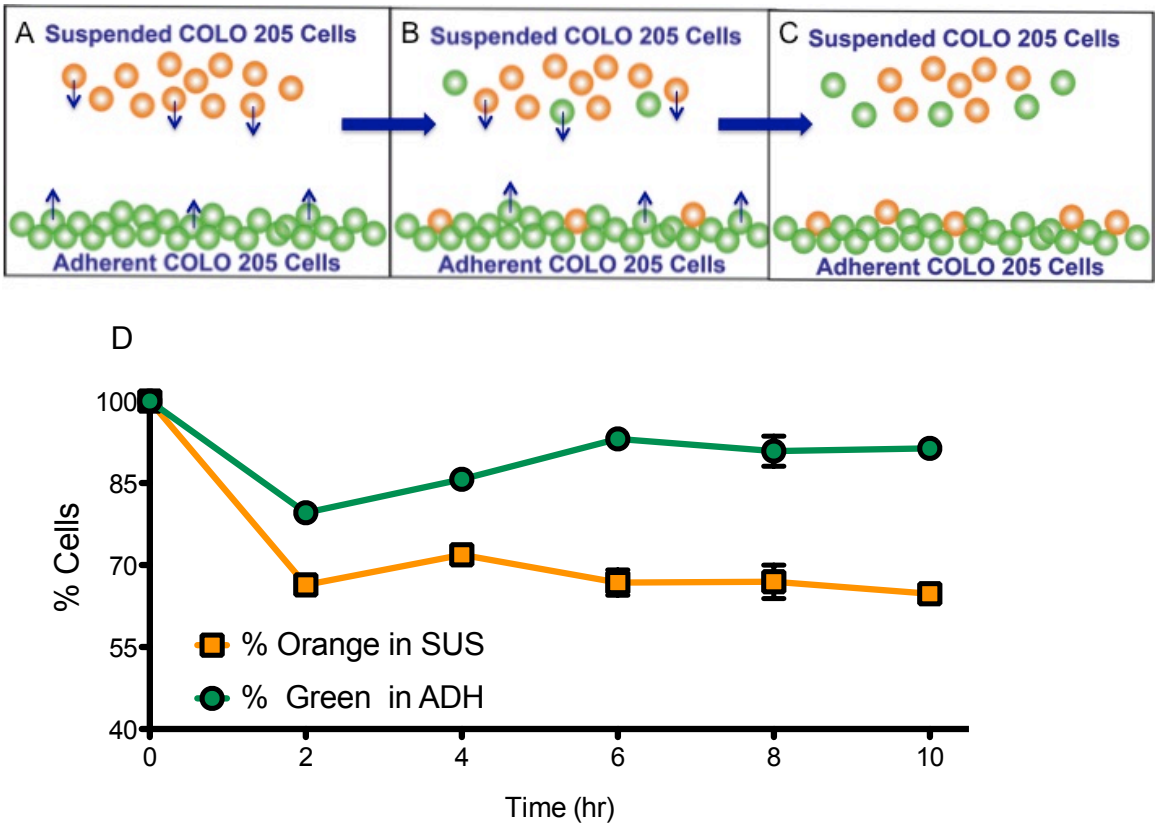

**Figure 2.3**: Differential protein and gene expression between the adherent and suspended COLO 205 cells. (A) Phosphorylation levels of COLO 205 adherent and suspended cells. (B) Relative β-Catenin gene expression comparison between the adherent and suspended population. Suspended cells have an average of 2.5 fold higher β-Catenin expression. (C) Immunoblotting of β-Catenin protein expression in the two populations. (D) and (E) Flow cytometry plots of anti-E-cadherin and anti-phophorylated β-Catenin antibody labeling. Isotypes, suspended population, and adherent population were colored in grey, blue, and red respectively.

**Figure 2.3: Differential gene and protein expression between the adherent and suspended COLO 205 cells**

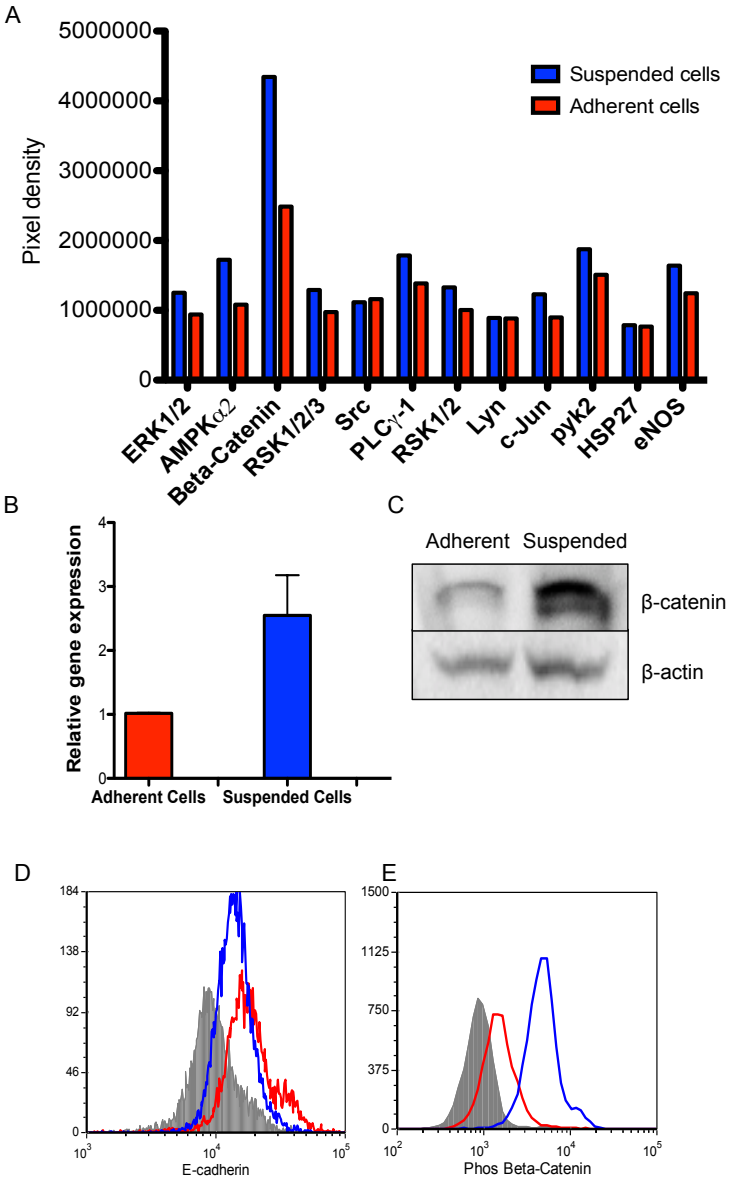

**Figure 2.4**: Gene expression change of β-catenin and population switch after siRNA transfection and microsphere incubation. β-catenin gene expression was reduced after treating the overall COLO 205 population with siRNA. A 20% increase in the adherent cell fraction was observed. In a separate study, the overall COLO 205 cell population was incubated with E-cadherin antibody coated microspheres, which induced an increase in the adherent cell fraction and a 50% decrease in β-Catenin gene expression.

**Figure 2.4: Gene expression change of beta-catenin and population switch after siRNA transfection and microsphere incubation**

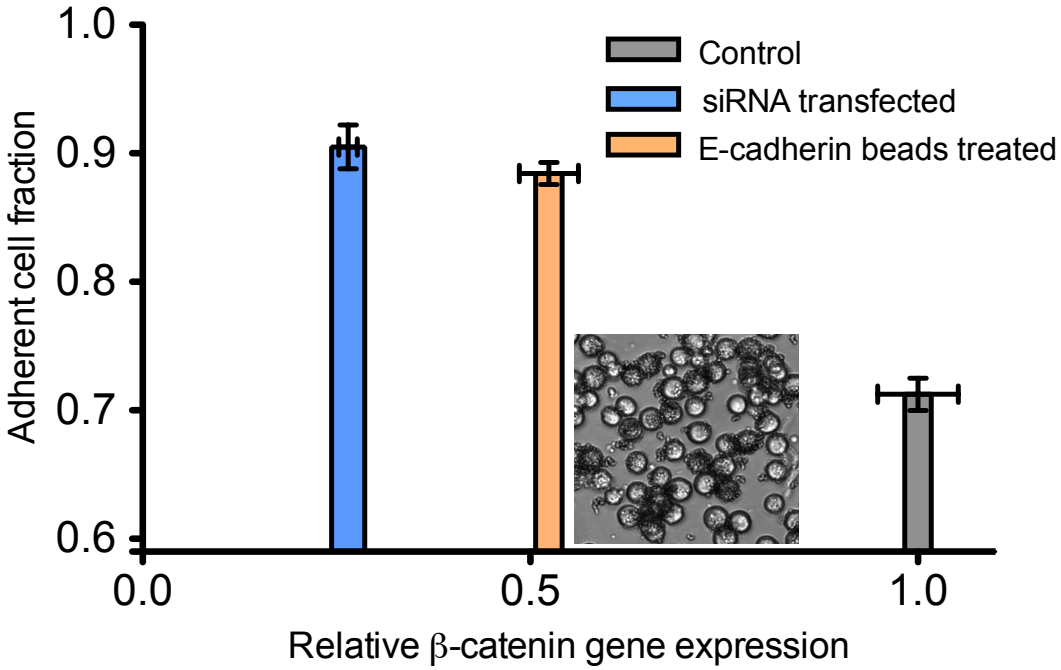

**Figure 2.5**: Differential ligand expression and adhesion profile of adherent and suspended COLO 205 cells. (A) and (B) Flow cytometry histogram plots of COLO 205 adherent (red) and suspended (blue) cells labeled with anti-$sLe^x$ and anti-$sLe^a$ mAbs. Isotype controls are shown in grey. (C) Rolling velocity analysis of adherent (red) and suspended (blue) under 1 dyn/$cm^2$ shear stress. *** $p<0.0001$

**Figure 2.5: Differential ligand expression and adhesion profile of adherent and suspended COLO 205 cells**

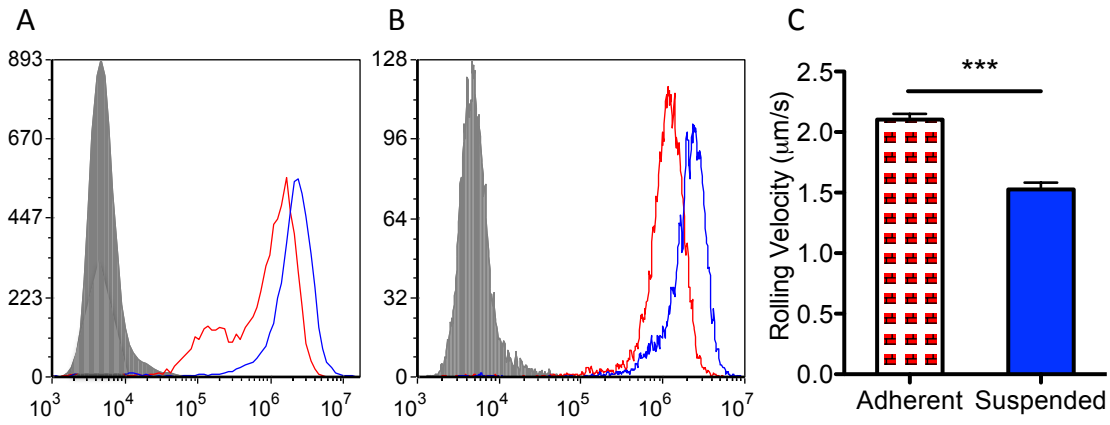

**Figure 2.6:** Phenotypic changes of COLO 205 cells induced by plasma treatment. (A) and (B) Immunofluorescence images of the adherent cells after culturing in control and 50% plasma supplemented media, respectively. Cells were pre-incubated with fluorescently conjugated cell tracker dye prior to plating. (C) Quantification of the relative area of fluorescence with Image J. Two-tailed Student t-test was performed for statistical analysis. $P = 0.008$ (D) and (E) Flow cytometry histogram plots of CD44 expression on cell surfaces and intracellular phosphorylated β-catenin expression on the control (blue) and plasma treated (red), respectively. Isotype control was also performed and shown in grey.

**Figure 2.6: Phenotypic changes of COLO 205 cells induced by plasma treatment**

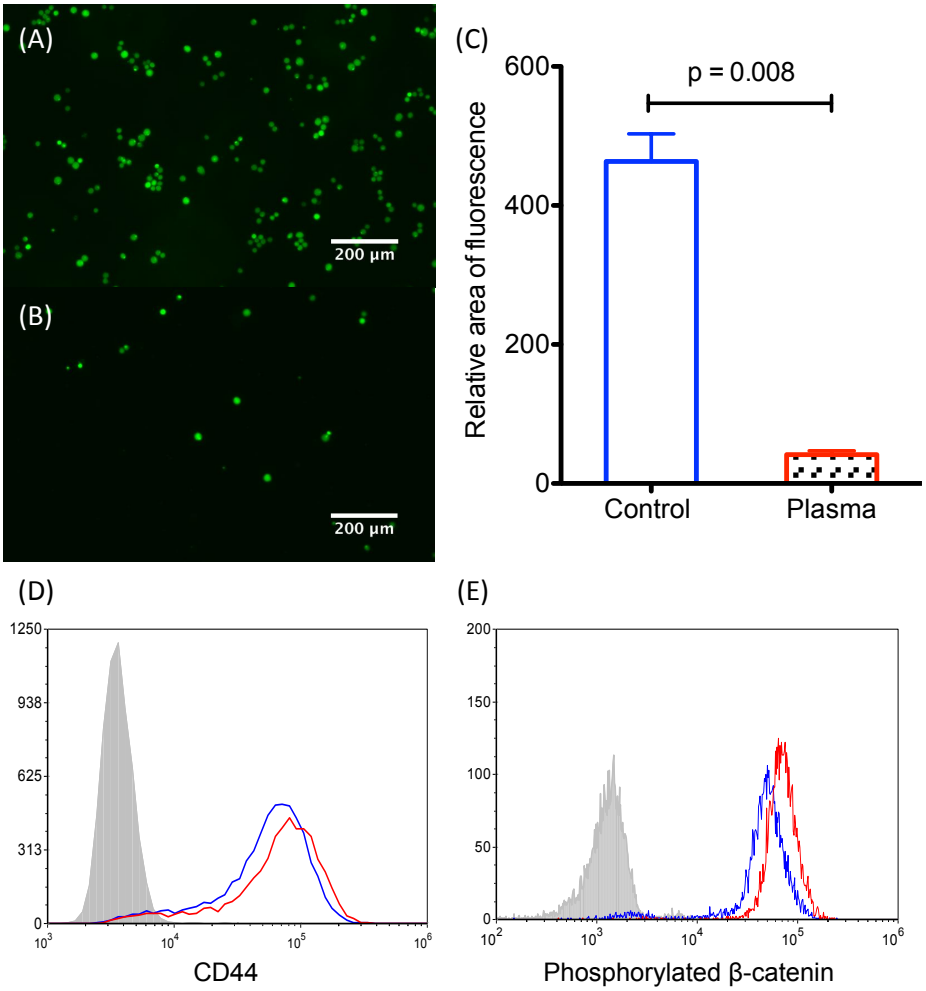

**Figure 2.7:** Real-time PCR of EMT-associated gene expression was performed in both suspended and adherent populations. mRNA expressions with >3-fold change include FGFBP1, MMP2, SPARC and TGFB1. The fold difference is shown in both graph and table below after normalizing to expression level in the adherent cells.

**Figure 2.7: EMT-associated gene expression of the adherent and suspended COLO 205 cells**

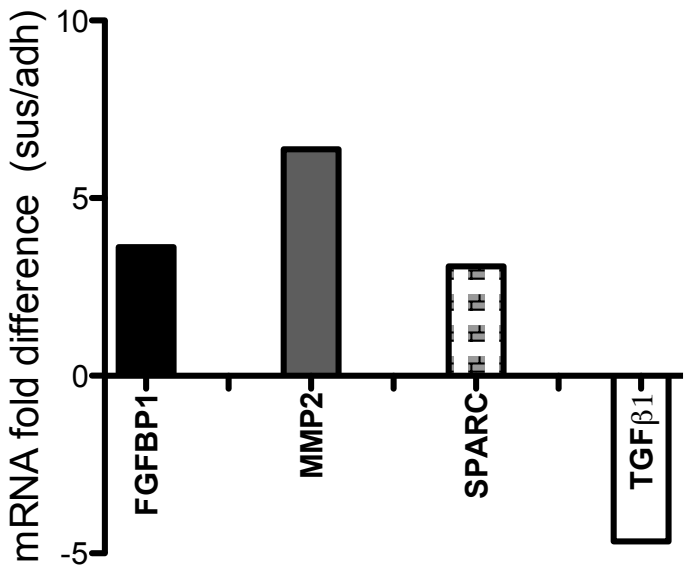


| Genes | FGFBP1 | MMP2 | SPARC | TGFB1 |
|---|---|---|---|---|
| mRNA fold difference (suspended/adherent) | 3.62 | 6.38 | 3.08 | -4.66 |

## 2.2 CONTINUOUSLY PERFUSED MICROBUBBLE ARRAY FOR 3D TUMOR SPHEROID MODEL

* This section is adapted from the following publication: S. Agastin, U. T. Giang, Y. Geng, L. A. DeLouise and M. R. King. *Biomicrofluidics*. 5:024110, 2011

### 2.2.1 INTRODUCTION

Considering the rising costs of developing new anticancer therapies, it is of prime importance to develop efficient, inexpensive, and high throughput anti-cancer therapy testing systems, which more realistically mimic complex *in-vivo* solid tumor pathophysiological conditions. The conventional method to screen therapies and drug targets is to first culture the tumors cells in suspension and/or monolayers. However, recent work has shown that many new therapies and drug targets lose their efficacy when applied in 3D tissue environments, despite their promising results when tested on tumor cells cultured with conventional methods.[11]

Multicellular tumor spheroids (MCTSs) represent a complexity level beyond monolayers of cells in which hypoxic and necrotic cells are surrounded by highly aggressive, metastatic cells. This tumor spheroid structure more closely resembles *in vivo* tumors, which provides insights into the growth of tumors as well as the complexity of the tumor microenvironment. To date, tumor spheroids have been used in cancer research for several decades and have contributed to our current understanding of cancer biology. They have been investigated in the contexts of experimental radiotherapy, photodynamic treatment, hyperthermia, and target specific chemotherapy and immunotherapy.[53, 54, 64, 187, 232] Moreover, recent studies have shown that the gene expression profiles,[19, 224] growth kinetics, and metabolic rates[224] of

MCTSs are similar to clinical conditions and hence, are believed to mimic *in vivo* solid tumors in their response to new drug targets and immunological factors. Therefore, MCTSs could help eliminate less efficient cancer drugs and therapies in earlier stages of testing before they enter expensive animal testing, and promote innovative drug targets that would otherwise fail in the traditional drug screening assays.

Commonly used culture techniques to create tumor spheroids include the hanging drop method,[122, 263] the liquid-overlay technique,[37] and the gyratory rotation technique.[254] In the hanging drop method, spheroids are grown in hanging drops placed on an inverted microplate. In the liquid-overlay technique, cells are grown on culture plates covered with a thin film of agar, preventing cells from attaching to the surface so that individual cells can grow into aggregates or spheroids. In the gyratory rotation technique, trypsinized cells are cultured in a stirred flask, thus preventing them from adhering to the substrate and favoring cell-cell interactions. All these techniques have disadvantages such as the formation of unequal sized spheroids, long cultivation time, inaccessibility for testing in the growth platform, and difficulty to adapt to high throughput screening platforms. Current efforts to develop new systems are underway using modern microfabrication techniques to generate uniformly sized spheroids over shorter time frames.[75, 193, 226] Our group recently reported the growth of homogenously sized 3D melanoma aggregates in microbubble compartment arrays[266] that were fabricated using polydimethylsiloxane (PDMS) gas expansion molding.[85]

MCTSs are a frequently used *in vitro* model of avascular tumor growth and the physiological tumor microenvironment. Avascular tumors occur at early stages of

tumor growth in which nutrients from the blood are obtained by the tumor mass only through its outer surface as blood vessels are not yet formed within. Similar conditions occur again when the tumor progresses into a metastatic state and cells escape and migrate to a new location. The continuous perfusion culture enables one to recapitulate the tumor microenvironment with realistic concentration gradients and establish physiologically relevant drug profiles in the exposed spheroids.

In this study, we exploit the microbubble technology and develop a simple microfluidic device to maintain uniformly sized tumor spheroids in an array format. Tumor spheroids are created and allowed to proliferate under flow condition in this device, mimicking *in vivo* avascular tumor conditions and are accessible for imaging and analysis.

### 2.2.2 MATERIALS AND METHODS

*Cell Culture*

Colon cancer COLO 205 cell line (ATCC number CCL-222) and breast cancer cell line MDA-MB-231 (ATCC number HTB-26) were obtained from ATCC (Manassas, VA). COLO 205 and MDA-MB-231 cell lines were maintained in RPMI 1640 (Sigma) and DMEM media respectively with 10% (v/v) fetal bovine serum and 100 U/mL Penicillin-streptomycin at 37°C in a 5% $CO_2$ incubator.

*COLO 205 Spheroids*

COLO 205 MCTS formation was initiated using a modified hanging drop method. COLO 205 cells cultured in culture flasks were trypsinized for 5 min and then

resuspended in fresh RPMI 1640 media at a concentration of $1.5\times10^6$ cells/ml. An array of 5 µl droplets of cell suspension was then placed on the lid of the 60 mm Petri dish. The lid with droplets was then inverted over the Petri dish containing 5 ml of RPMI medium. Aggregate formation was examined using bright field microscopy after incubating for 12 h. The formed spheroids were transferred by pipette and gently resuspended in 1X DPBS with $Mg^{2+}$ and $Ca^{2+}$ (Invitrogen) at a concentration of $2\times10^5$ cells/ml and used in cell capture experiments. Spheroid aggregates larger than 100 µm in diameter were subjected to gentle pipetting to generate smaller aggregates.

*COMSOL Simulation*

Before culturing cells inside the microfluidic system, a COMSOL simulation model was developed to understand the flow characteristics within the microbubbles under physiological shear flow. The Navier-Stokes equation with no slip boundary conditions was used to solve the model. A Newtonian fluid with density 1 x $10^3$ kg/ $m^3$ and viscosity 0.01 Pa.s was used to represent the flow buffer. Shear stresses in the range of 2 - 10 dyn/$cm^2$ were used for the COMSOL simulations and spheroid seeding into the microbubbles. Fluid was perfused through the microbubbles containing tumor spheroids at 0.6 dyn/$cm^2$ to mimic the fluid mechanical environment of the microcirculation and postcapillary venules.[174]

*COLO 205 Cell Preparation For Cell Capture Experiments*

COLO 205 cells were trypsinized from the tissue culture flask using Accutase™ (Sigma) and then incubated in fresh media at 37°C in a shaker for up to 3 h for surface

receptor recovery. The cells were then resuspended in 1X DPBS containing $Mg^{2+}$ and $Ca^{2+}$ to a concentration of $2\times10^5$ cells/ml. Cell viability of > 95% was confirmed by the trypan blue exclusion test prior to each cell capture experiment.

*PDMS Microbubble*

Microbubbles in the size range of 200-500 μm in diameter with 50-200 μm top openings (in square, circular and triangular shapes) were fabricated in PDMS using the gas expansion molding (GEM) technique described in detail elsewhere85. A vacuum-assisted coating (VAC) technique[85] was used to completely fill up the microbubble with liquid and remove any trapped air bubbles. 1X DPBS was pipetted on top of the microbubbles to completely cover the top openings before placing the microbubbles inside a vacuum chamber. Negative pressure was applied for 30 minutes to draw out the air trapped inside the microbubbles and cause the injection of PBS buffer into the microbubble cavities. The primed PDMS microbubbles were then used in the perfusion chamber assembly. The average size of the microbubbles used in this spheroid capturing experiment was 207 ± 9.7 μm in diameter with 99 ± 1.8 μm circular top openings. For each experiment, a microbubble array consisting of 25-30 microbubbles was used.

*Perfusion Chamber*

The perfusion chamber was assembled by mounting a rectangular parallel plate flow chamber (Glycotech, Rockville, MD) on top of the PDMS microbubble array. A 125 μm thick rubber gasket was used to seal the device with the PDMS surface and create

a rectangular path for the perfusion flow. To create a tight sealing and prevent any airbubbles from entering, the top plate with the gasket was connected to the vacuum pump by a Tygon tubing. The top of the parallel plate chamber is made of transparent polycarbonate that allows for easy imaging. Medical grade Tygon tubing was used to connect the chamber inlet to the cell suspension and the outlet to the syringe. Ethanol (70% v/v) was perfused through the chamber for 15 s to sterilize the tubing and flow chamber. Sterile 1X DPBS buffer was perfused to remove any residual ethanol prior to cell capture experiments.

*PDMS Surface Preparation*

The PDMS surface was incubated with 0.5 μg/mL of recombinant E-selectin/Fc Chimera (R&D systems) in PBS for 45 min. To prevent nonspecific binding of cells, the surface was then incubated with 3% filter sterilized bovine serum albumin (BSA) for 90 min.

*Cell Capture Inside PDMS Microbubbles*

PDMS surfaces were prepared as described above for both spheroid and single cell capture inside the microbubbles, mimicking the postcapillary venules where activated endothelial cells express selectins on their luminal surface. COLO 205 cells were suspended in PBS and perfused through the parallel flow chamber at 2 dyn/cm$^2$ shear stress. Interactions between the E-selectin counter ligands expressed on the cell membrane surface and immobilized E-selectin facilitate tethering and rolling of the cells on the functionalized PDMS surface. The rolling cells were trapped in the

microbubble cavity as they approached the microbubble openings under flow conditions. The microfluidic system with cells trapped inside was then maintained at 37°C in a 5% $CO_2$ incubator with perfusion of fresh RPMI media at 0.6 dyn/ $cm^2$ shear stress.

Before the cell capture experiments, the assembled apparatus was secured to the stage of an Olympus IX81 motorized inverted epifluorescence microscope (Olympus Americam Melville, NY). A CCD camera (Hitachi, Tokyo, Japan) and DVD recorder (Sony Electronics) were used to perform image capture for offline data analysis.

*Cell Staining and Doxorubicin Toxicity Assay*

Viable COLO 205 and MDA-MB-231 cells were stained by incubation with 10 μM CellTracker Green and CellTracker Blue (invitrogen) for 45 min at 37°C. Cells were washed twice with PBS buffer to remove excess dye. The CellTracker probes stay within living cells through several generations and are inherited by daughter cells after cell fusion. Dead cell staining was performed using propidium iodide (PI) which intercalates into free double stranded nucleic acids in unhealthy cells. Doxorubicin was added to the RPMI culture medium at a concentration of 10 μM to test its toxicity on both monolayer and spheroid cultures.

*Imaging and Data Analysis*

Tumor cells and spheroids cultured inside the microbubbles were imaged using a Zeiss 710 laser scanning confocal microscope. A 25× lens was used to acquire confocal z-

stacks of depth of 50-200 μm with a z-stack interval of approximately 2 μm. Images were uploaded to the Zen 2009 software (Carl Zeiss MicroImaging GmbH) for analysis. The number of cells within a spheroid mass was estimated from the volume of the 3D spheroid image reconstructed from z-stacks divided by the average volume of a tumor cell (1200 $\mu m^3$).

### 2.2.3 RESULTS AND DISCUSSION

It is well understood that the tumor microenvironment plays a critical role in the tumor growth, progression, metastasis and drug resistance. Recent studies show that the mechanical microenvironment plays a major role in modulating tumor cell responses, tissue development and maintenance.[42, 235] It is shown that flow induced shear stress in tumor cells up-regulate some key genes (cyclin B1 and $p21^{CIP1}$) and down-regulate several other genes (such as cyclins A, D1, cyclin dependent protein kinases). In addition to creating physiological shear stress inside the microbubbles, perfusion flow also establishes a physiologically relevant drug concentration profile to the exposed spheroids.

Figure 2.8 shows the streamline directions, shear stress profile, velocity profile, and complex flow paths created inside the microbubble by the perfusion flow. The fluid velocity decreases sharply in magnitude with distance from the bubble top opening. To characterize the streamlines inside the microbubble and to determine the flow rate range at which the cells can be kept inside the bubble, 5.27 μm diameter polymer beads (Bangs Labs) were introduced into the microbubbles under perfusion

flow. Here the consistent sizes of the beads made the characterization process simple and efficient. The beads were observed to travel slowly at the lower end of the circular motion and then gain momentum as they approach the bubble top opening, as shown in Figure 2.9a and 2.9b. Cells and microbeads trapped inside the microbubble cavity were found to travel in circular trajectories and rarely escape from the bubble when the fluid velocity was less then 2.21 cm/s (10 dyn/cm$^2$ shear stress) at the bubble opening. The experimental system used for spheroid capture inside the microbubble cavity and perfusion culture is illustrated in Figure 2.9c and 2.9d.

COLO 205 cells were captured inside the microbubble by rolling on the E-selectin functionalized planar PDMS surface of the microbubble chip via ligand:receptor interactions and fall into the microbubbles, as shown in Figure 2.10a and 2.10b. Captured COLO 205 cells were cultured inside the microbubbles for 2 days to form loose aggregates (Figure 2.10). This technique was also used to capture spheroids initiated by the falling drop method inside the microbubbles followed by culture for up to 5 days with fresh RPMI media in perfusion. The sizes of the spheroids captured inside each bubble were controlled by the duration of the perfusion. This technique was also effective in controlling the spheroid size variability between microbubbles. In an experiment with 20 microbubbles, the average number of cells captured in each bubble was 95.8 ± 5.6 SD. The spheroids then formed inside each microbubble and proliferated. The fluid flow inside the bubble pushes the spheroids to the bottom and sides of the spheres resembling hemisphere-shaped spheroid clusters with raised edges.

Confocal images of the cultured spheroids were taken and pseudo-colored to

indicate distance from cells to the microbubble bottom surface, as shown in Figure 2.11a(1) and 2.11a(2). Figure 2.11b shows the viability of cell spheroids cultured inside the microbubble system. Dead cells inside the spheroids were counted using PI staining and 3D confocal imaging. A greater number of dead cells were detected at the bottom of the spheroids near the microbubble spheroid junction. Results from the toxicity assay of a common chemotherapy drug, doxorubicin (10μM), on COLO 205 cells cultured in a monolayer (Figure 2.12a), COLO 205 spheroids in static culture (Figure 2.12b), and COLO 205 spheroids cultured inside the microbubble perfusion culture (Figure 2.12c) are demonstrated in Figure 2.12. COLO 205 spheroids showed greater resistance to doxorubicin compared to the monolayer COLO 205 cells, consistent with previous research on drug resistance of colon and breast spheroid cultures.[178, 188] This increased doxorubicin resistance in the spheroid cells may be due to cell-cell contact responses, internal protective mechanisms, and/or mass transfer limitations. Higher drug resistance in spheroids cultured inside the microbubble in perfusion flow compared to spheroids cultured in static suspension culture was also observed. The difference in the drug toxicity is likely due to limited exposure of cells to doxorubicin within the microbubbles, which may resemble the conditions prevailing in avascular tumor growth *in vivo*. The increased resistance demonstrated by spheroids in perfusion culture is similar to standard MCTS models studied by others.[59, 105, 253]

Cells located at the top of the spheroids exposed to the media reflect the situation of actively growing tumor cells adjacent to capillaries *in vivo*. The cells at the microbubble bottom, on the other hand, become quiescent and undergo necrosis or apoptosis to form a secondary necrotic core. This arrangement of heterogeneous cell

populations and the creation of pathophysiological gradients within the spheroids in microbubbles are similar to the micrometastases and avascular tumor microregions.

The advantages of the microbubble array technique include the ability to maintain the size uniformity of the spheroids and easy non-invasive testing during their growth. Attempts were also made to improve specific cell capturing efficiency of the microfluidic system. For instance, COLO 205 cells were mixed with MDA-MB-231 cells that do not roll on the E-selectin coated PDMS surface in different ratios. The different adhesion phenotypes were used to sort the cells in the capture experiment (Figure 2.13). Good enrichment of COLO 205 cells was observed over the range of concentrations studied. The specific cell capture capability and easy control over the size uniformity of the spheroids make this model well suited for the development of co-culture spheroids. This separation process could be further improved through the optimization of the microbubble arrangements and opening shapes. Later in Chapter III, the MDA-MB-231 cell line, a highly metastatic breast cancer cell line that lacks E-selectin interactions, was used as a model to study the adhesive phenotype changes when exposed to cytokines and other factors.

### 2.2.4 CONCLUSION

A cost-effective 3D spheroid culture system which reflects the *in vivo* behavior of the cells in tumor tissues holds great potential for future drug development. We developed a simple microfluidic approach to culture tumor spheroids in perfusion culture that creates a 3D microenvironment, which resembles disease conditions. COLO 205 spheroids created using the hanging drop method were captured and kept viable inside

the microbubbles for 5 days with a continuous perfusion of fresh culture. Doxorubicin toxicity was compared between COLO 205 monolayer cells, spheroids cultured in suspension culture under static conditions, and spheroids cultured in the microbubbles by perfusion culture. Greater resistance was observed in spheroids cultured in the bubbles, likely due to a combination of cell-cell contact responses, mass transfer limitations, and limited exposure of the cells to the drug. The microenvironment inside the microbubbles and flow conditions produced by the microfluidic system may resemble conditions prevailing in avascular tumor growth. The described technique is advantageous due to its low cost, ability to be automated and its usefulness for high throughput drug screening. Moreover, this model could be used to study therapeutic problems related to metabolic and proliferative gradients and 3D cell-cell and cell-matrix interactions. Further investigations on the enrichment of specific cell types and the capture of primary tumor cells within microbubbles to create spheroid co-cultures are currently under way.

**Figure 2.8:** A COMSOL model was used to demonstrate the flow characteristics inside the PDMS microbubbles that were assembled within a Glyotech parallel plate flow chamber. Streamline side view (a) and top view (b) show the three-dimensional circular flow paths produced inside one microbubble. The COMSOL model slice plot (c) shows the flow velocity magnitude inside one microbubble. The velocity decreases sharply with distance from the bubble top opening. The shear stress plot (d) shows the shear stress magnitude exerted by the perfusion flow at the inner surface of the microbubble. COMSOL simulation conditions: Perfusion flow rate: 0.403 ml/min; fluid velocity: 2.12 cm/sec; shear stress at the PDMS surface: 10 dyn/cm$^2$; 600 μm diameter microbubble with circular 100 μm top opening.

**Figure 2.8: COMSOL model demonstrating the flow characteristics inside the PDMS microbubbles**

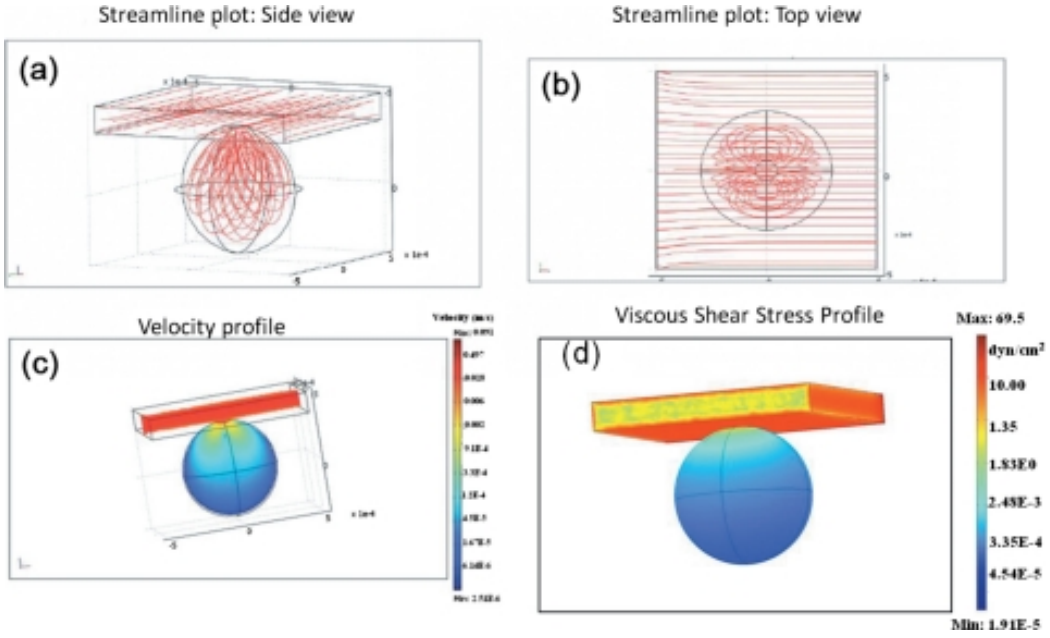

**Figure 2.9:** Micrographs of microbead trapping, parallel flow chamber setup, and hanging drop assay. (a) Sequential images of the microbeads trapped and circling inside the microbubble. Black arrows indicate the direction of the perfusion flow. Red and green arrows follow two different beads in their circular trajectories. These values are in agreement with the COMSOL simulation results (Figure 2.2.1c). (b) The circular paths taken by the two beads were highlighted using ImageJ software, (c) Schematic of the parallel plate flow chamber set up. (d) Micrograph of the experimental set up used for the spheroid perfusion culture including syringe pump, parallel flow chamber, and cell solution, (d3) Microdroplets placed on the petri dish lid for COLO 205 spheroid formation.

**Figure 2.9: Micrographs of microbeed trapping, parallel flow chamber setup, and hanging drop assay**

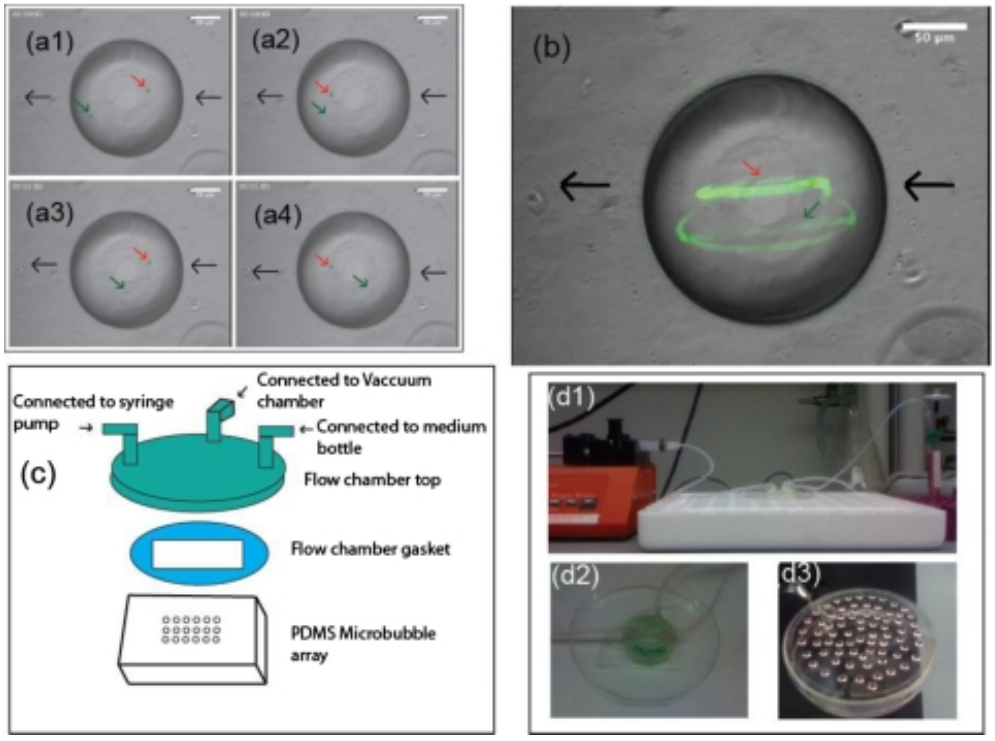

**Figure 2.10:** Micrographs of E-selectin functionalized microbubbles. (a) Micrograph showing COLO 205 cells rolling on the PDMS surface functionalized with E-selectin recombinant protein at a shear stress of 2 dyne/cm$^2$. The edges of the microbubble and its triangular top opening are outlined in green. (b) Higher magnification micrograph showing rolling cells entering the microbubble openings. (cl, c2, and c3) Micrographs showing COLO 205 cells captured inside the microbubbles and cultured for two days under flow condition at 37 °C and 5% $CO_2$ at humidified conditions. (dl, d2, and d3) Micrographs showing COLO 205 tumor spheroids cultured inside the microbubbles in 4X, 10X, and 20X, respectively.

**Figure 2.10: Micrographs of cells cultured in E-selectin functionalized microbubbles**

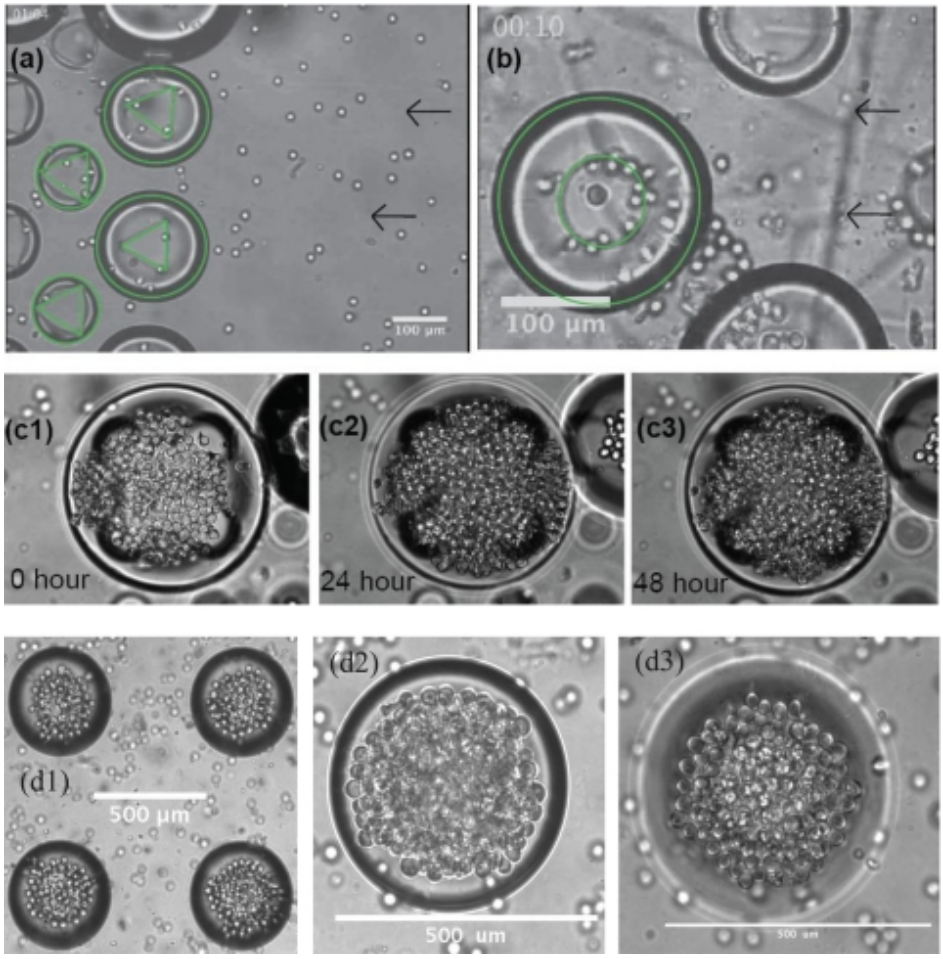

**Figure 2.11:** Top view (al) and side view (a2) of a spheroid cultured inside a microbubble. The spheroids are pseudo-colored to indicate the distance from the microbubble bottom surface, (b) 3D image of the COLO 205 spheroid cultured inside a microbubble by perfusion, stained with Propidium Iodide (PI) and imaged with confocal microscopy for the cell viability assay. Live cells were stained using Invitrogen Celltracker probe. (c) Viability of COLO 205 spheroids cultured inside the microbubbles by perfusion culture as a function of seeding duration.

**Figure 2.11: Top and side view of a spheroid cultured inside the microbubble**

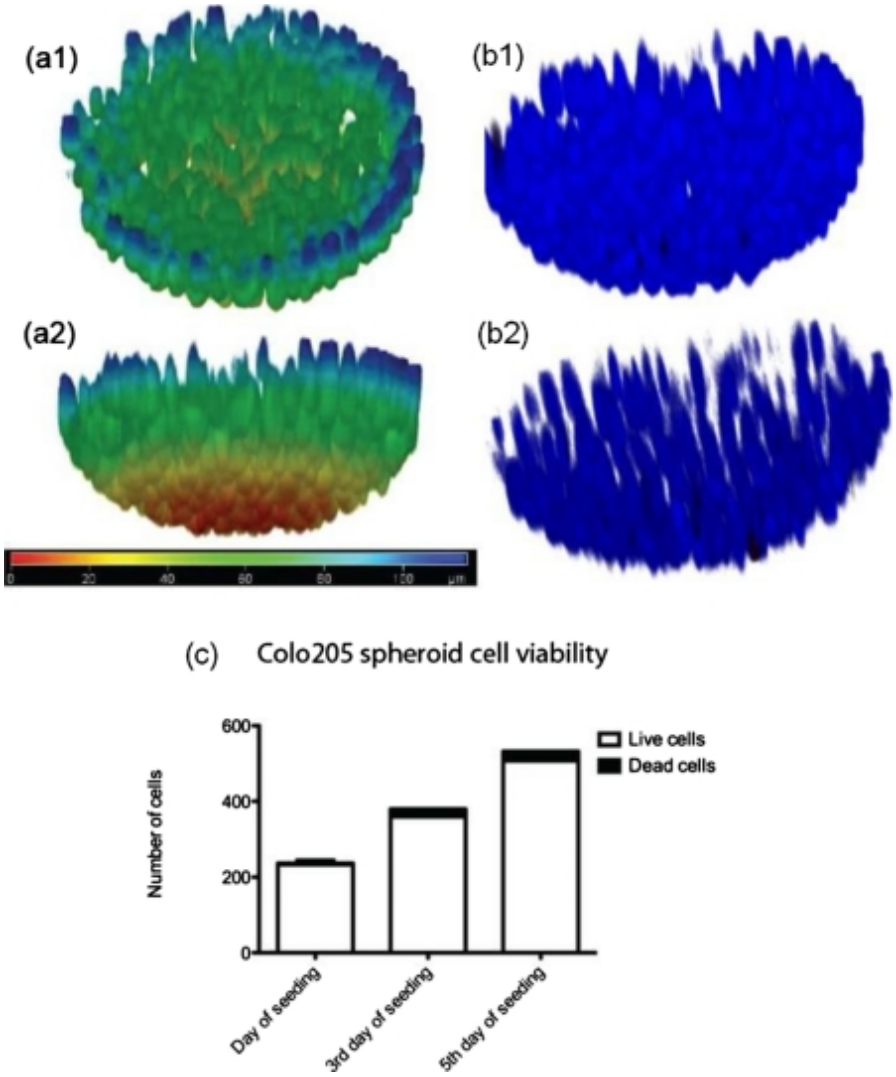

**Figure 2.12:** Toxicity assay of COLO 205 cells cultured in monolayer and spheroids. (a) Toxicity of doxorubicin drug on COLO 205 cells cultured in monolayers. The percentage of cells viable after 48 h was 16.67%±1.49 SD. (b) Doxorubicin toxicity on COLO 205 spheroids cultured in agar-coated plates under static conditions. The percentage of cells viable after 48 h of treatment was 42.85%±3.97 SD. (c) Doxorubicin toxicity on COLO 205 spheroids captured and cultured inside microbubbles by perfusion flow. The plotted values are the average number of viable cells in each microbubble. Three microbubbles were used for the perfusion experiments and two microbubbles for the untreated group. The percentage of cells viable after 48 h of perfusion culture was 51.36%±1.93 SD. Doxorubicin at 10 μM concentration was used in all three conditions.

**Figure 2.12: Toxicity assay of COLO 205 cells cultured in monolayer and spheroids**

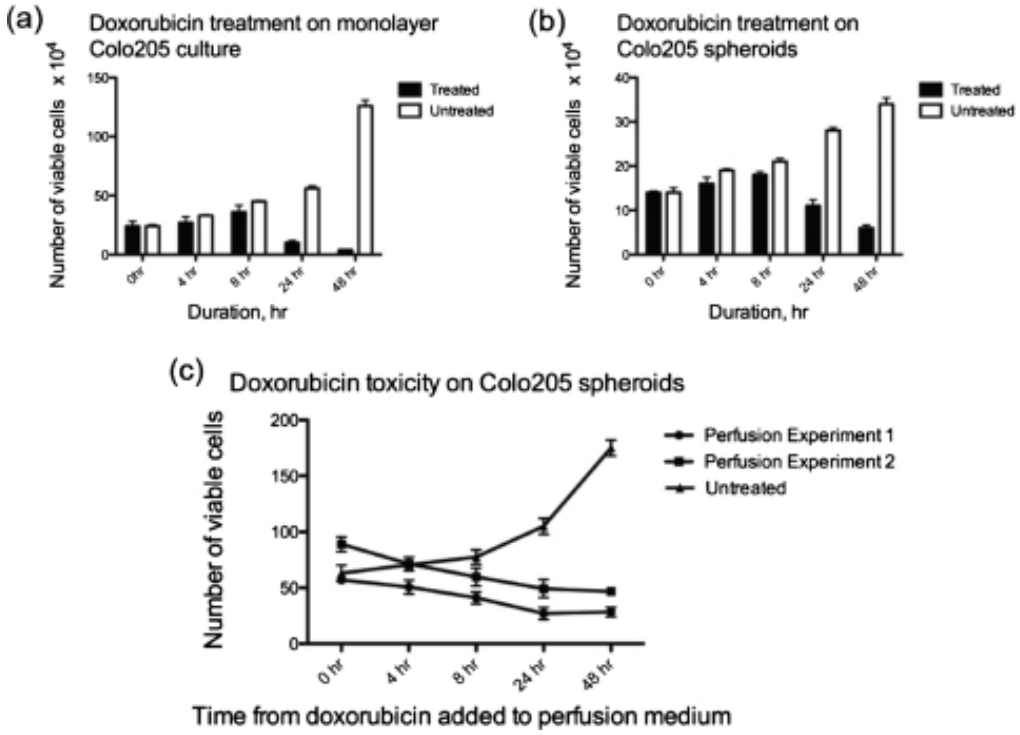

**Figure 2.13:** Results of specific cell capture and enrichment study. COLO 205 tumor cells stained with Invitrogen CellTracker Green were mixed with MDA-MB-231 tumor cells stained with Invitrogen CellTracker Blue at different ratios and used for cell rolling and capture inside the bubbles. MDA-MB-231 cells did not roll on E-selectin coated PDMS. The principal mechanism behind the enrichment is that the perfused cells rolling on the PDMS surface have an elevated probability of entering the bubbles compared to non-rolling cells.

**Figure 2.13: Specific cell capture and enrichment using E-selectin coated microbubbles**

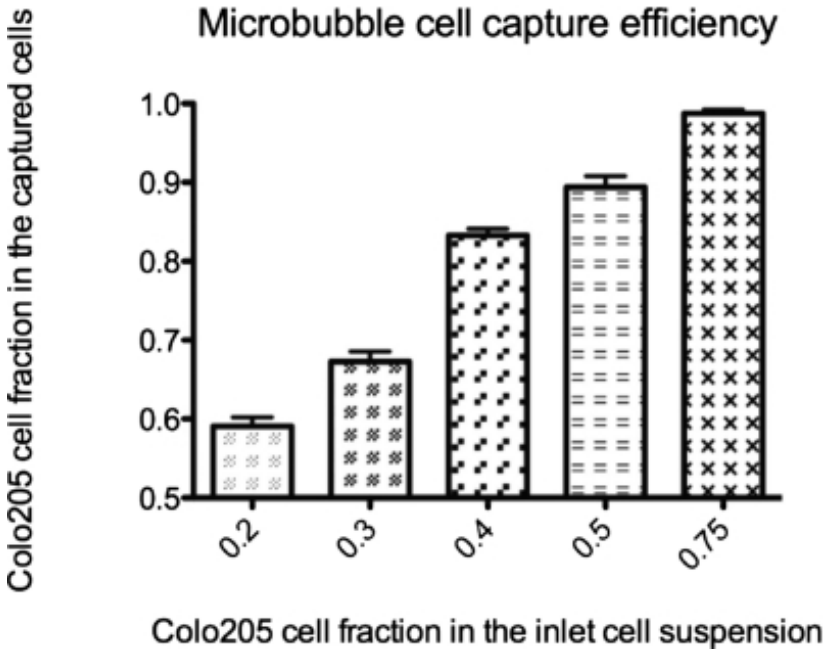

# CHAPTER 3 PHENOTYPIC SWITCH IN BLOOD: EFFECTS OF PRO-INFLAMMATORY CYTOKINES ON BREAST CANCER CELL AGGREGATION AND ADHESION

* This section is adapted from the following publication: Y. Geng, S. Chandrasekaran, J. W. Hsu, M. Gidwani, A. Hughes, and M. R. King. *PLOS ONE*. 8(1): e54959, 2013

## 3.1 INTRODUCTION

Cancer mortality is predominantly caused by the dissemination of cancer cells from the primary tumor to distant organs where secondary sites are formed via a metastatic progression. Breast cancer, one of the most diagnosed forms of cancer, still causes high mortality rates due to the emergence of invasive, therapy-resistant cancer cells.[251] There are conflicting ideas on the nature of these invasive cells, from their population size within the primary tumor[211, 217] to their methods of dissemination (lymphatic[204] or hematogeous[82]) and the process of metastasis within blood vessels.[262, 83, 286]

One mode of cancer metastasis is through the bloodstream, which involves the escape of cancer cells from the primary tumor site into the circulatory system via intravasation. Circulating tumor cells (CTCs) can then interact and adhere to the endothelial lining of the vasculature through a series of receptor-mediated events, commonly referred to as the metastatic adhesion cascade. This cascade mimics the leukocyte adhesion cascade (reviewed in 82) where the initial contact between cancer cells and the endothelium is facilitated by a family of endothelial adhesion molecules called selectins.[88, 125] Firm adhesion of CTCs on the endothelium then allow extravasation and subsequent secondary tumor site formation.

There are several factors in the blood that are secreted by lymphocytes and macrophages known to facilitate the metastatic progression and potentially interact with CTCs within the bloodstream. In particular, interleukin-6 (IL-6) and tumor necrosis factor-alpha (TNF-α) have been reported to be elevated in the blood serum of patients diagnosed with advanced stage breast tumor and correlate with an increased

number and size of metastatic sites.16, 143 IL-6 and TNF-α have been shown to promote the growth and invasiveness of colon and prostate cancer epithelial cells *in vitro* and *in vivo*.[12, 155] Studies have also shown that cancer cell chemokine receptors also play a role in determining the destination of metastases.[189]

MDA-MB-231 is a well characterized metastatic breast cancer cell line isolated from pleural effusion of a patient with adenocarcinoma suffering from widespread metastasis, and is known as a 'basal' or 'triple-negative' cell line with stem cell-like or post-Epithelial-Mesenchymal Transition (EMT) features and fails to express estrogen receptors, progesterone receptors or human epidermal growth factor receptor 2 (HER2). MDA-MB-231 cells have been previously reported to express E-selectin ligands such as CD44V4 as well as selectin-binding moieties such as sialyl lewis x ($sLe^x$).[196, 287] Despite their expression of functional E-selectin ligands, it was observed that MDA-MB-231 cells do not adhesively interact with E-selectin coated microtube surfaces under flow, as reported here. In the present study, the effect of plasma, cytokine treatments, and 3-D spheroid culture conditions on altering the adhesion phenotype of MDA-MB-231 cells on E-selectin functionalized microtubes was investigated. It was hypothesized that human plasma, tumor spheroid culture, and exposure to pro-inflammatory cytokines such as IL-6 and TNF-α could induce robust interactions between metastatic breast cancer cells in circulation and the inflamed endothelium. The findings of this study suggest new therapeutic approaches targeting specific cytokine(s) and their receptor(s) to help prevent the metastatic progression of breast cancer cells in transit.

## 3.2 MATERIALS AND METHODS

*Reagent*

Recombinant E-selectin-$IgG_1$ chimera was purchased from R&D systems (Minneapolis, MN). Blotting grade blocker non-fat dry milk was obtained from Bio-Rad Laboratories (Hercules, CA) and Protein-G was purchased from EMD Biosciences (San Diego, CA). FITC Mouse IgG1 k isotype control, purified mouse anti-human CD15s (clone CSLEX), and APC rat anti-mouse IgM were all purchased from BD Biosciences (San Jose, CA). FITC mouse anti-human CD44V4 was obtained from AbD Serote (Germany). $Ca^{2+}$ and $Mg^{2+}$ free DPBS (Invitrogen, Camarillo, CA, USA), calcium carbonate (Sigma Chemical Co., St. Louis, MO, USA), low endotoxin (1 ng/mg), and essentially globulin-free Bovine Serum Albumin (Sigma Chemical Co., St. Louis, MO, USA) were used to prepare flow buffer for cell adhesion assays. Nuclear ID™ cell viability reagent was obtained from Enzo Life Sciences (Farmingdale, NY).

*Breast Cancer Cell Culture*

Breast cancer cell line MDA-MB-231 was purchased from ATCC and maintained in 10% Fetal Bovine Serum (FBS; Cellgro), 1% penicillin-streptomycin (Invitrogen), and high glucose Dulbecco's Modified Eagle Medium at 37°C with 5% $CO_2$ in a humidified incubator.

*Plasma Isolation and Treatment*

Whole peripheral blood was collected from informed consenting healthy female donors using sodium–heparin tubes with a venoject vacuum system. Collected whole blood was centrifuged for 25 min at 500 rpm. The plasma layer on top was carefully removed without disturbing the interface and passed through a sterile 0.2 μm filter. 50% of the isolated plasma was used for cell culture while the rest was stored in -80°C for other assays. MDA-MB-231 cells were plated at 2 x $10^5$ cells/well in 6-well plates. Isolated plasma and culture medium at a 1:1 ratio were used to treat cells for 48 h.

*Tumor Spheroid Generation Using PDMS Coated Plate*

*Dow Corning*'s Sylgard® 184 silicone elastomer kit in a 10:1 base to curing agent ratio (w/w) was used to cure PDMS 40. The pre-polymer components were manually mixed with a pipette tip in a 50 mL tube for 60 s. 300 μL of PDMS pre-polymer was pipetted into each well of a 24-well plate and allowed to settle at room temperature (RT) for 30 min. The plates were then cured at 60 °C for 4 h. MDA-MB-231 cells were plated at 5 x $10^4$ cells/well and cultured for 48 h.

*Pro-Inflammatory Cytokine and Metformin Treatment*

Human recombinant IL-6 (R&D) and TNF-α (R&D) were added to the culture media at a range of concentrations from 1-25 ng/mL. Cell rolling assay and flow cytometry were performed after 48 hr treatments (single cytokine or combined). For blocking/neutralization experiments, 0.1 mM Metformin (1,1-dimethylbiguanide hydrochloride) or 1 μg/mL of mouse anti-human IL-6R monoclonal antibody was added with the IL-6 treatment.

*Neuraminidase Treatment*

After IL-6 treatment and prior to rolling experiments, MDA-MB-231 cells were treated with 0.1 U/ml Vibrio Cholerae neuraminidase (Roche Biochemicals, Indianapolis, IN) for 45 min at 37°C to cleave terminal sialic acid residues. After enzyme treatment cells were washed and incubated with 0.1% BSA to block nonspecific interactions.

*MTT Assay*

MDA cells were seeded into each well of a 24-well culture plate. After 12 hr in culture, the medium was withdrawn and replaced with 0.5 mL fresh DMEM culture medium or cytokine spiked medium. After 2 days in culture, all media was withdrawn and replaced with 0.5 mL fresh DMEM medium. Next, 50 µl MTT stock solution (5 mg MTT powder/1 ml PBS) was added into each well and incubated at 37°C for 1 hr. Media was then removed and replaced with 0.5 mL DMSO for 5 min incubation at RT. Absorbance was measured at a wavelength of 570 nm with background subtraction at 660 nm.

*Cell Viability Assay*

The Nuclear-ID™ Blue/Red cell viability reagent (GFP-Certified™), a mixture of a blue fluorescent cell-permeable nucleic acid dye and a red fluorescent cell-impermeable nucleic acid dye that is suited for staining dead nuclei was used to determine cell viability. MDA-MB-231 cells with various treatments including

control, plasma, IL-6, IL-6 + Metformin, and TNF-α were grown in imaging ready glass coverslip mounted 24-well plates at 5 x $10^4$ cells/well. Cells were incubated with the Nuclear-ID reagent at 1:1000 dilution for 30 min at 37°C and imaged with a Zeiss 710 confocal microscope (10X objective) with a dual filter set for DAPI (Ex/Em: 350/470nm) and Texas Red (Ex/Em: 540/605 nm).

*Flow Cytometry*

After 48 h in culture, untreated and treated (plasma, tumor spheroid, IL-6, and TNF-α) MDA-MB-231 cells were removed from culture plates using an enzyme-free cell dissociation buffer solution to preserve membrane proteins and prevent clumping. After washing with PBS, the cells were resuspended in 1% BSA in DPBS to a final concentration of 250,000 cells per sample. Antibodies against CD44V4 and $sLe^x$ or appropriate isotype controls were added to the cell suspensions and incubated over ice for 45 min. Following incubation, cells were washed twice with 500 µL of 1% BSA to remove any unbound antibody. Flow cytometry samples were analyzed using an Accuri C6 flow cytometer (BD Bioscience, San Jose, CA).

*Cell Rolling Assay*

Micro-renathane tubing with 640 µm internal diameter (Braintree Scientific) was cut to a length of 50 cm, functionalized with Protein G (10 µg/mL) and Fc chimera E-selectin (20 µg/mL, R&D), and blocked with 5% BSA or milk (Sigma). Functionalized microtubes were then secured to the stage of an Olympus IX81 motorized inverted microscope (Olympus America, Melville, NY). A CCD camera

(model no: KP-M1AN, Hitachi, Tokyo, Japan) and DVD recorder (model no: DVD-1000MD, Sony Electronics) were used to record experiments for offline analysis. MDA-MB-231 cells were suspended in flow buffer at 1 x$10^6$ cells/mL and perfused through protein coated microtubes using a syringe pump (KDS 230, IITC Life Science, Woodland Hills, CA) at a wall shear stress of 1.0 dyn/$cm^2$. "Rolling" cells were defined as those observed to translate in the direction of flow with an average velocity less than 50% of the calculated hydrodynamic free-stream velocity 153.

*Quantification of cytokine concentration using enzyme-linked immunosorbent assay (ELISA)*

Healthy donor plasma was isolated as described above. Conditioned media was harvested from both 2-D culture and 3-D tumor spheroid culture. Anti-human IL-6 and TNF-α ELISA kits from eBioscience (San Diego, CA) were used to quantify the cytokine concentration. Standard curves were performed per instruction and the concentration of cytokines in each sample was calculated accordingly.

*Real-time quantitative PCR (qPCR)*

10 ng of cDNA produced by the reverse transcription of total RNA was used in each quantitative PCR reaction. Also included in the 20 μL qPCR reaction system were 10 μL iQ™ SYBR Supermix (Bio-Rad), 1 μL of 2 μM forward primer and 1 μL of 2 μM reverse primer and nuclease free water.

Primer for CD44 qPCR

5'-TATAAGCTTTTCGCTCCGGACACCAT-3' (Forward)

5’-ATAAGATCTTTCTGGAATTTGGGGTG-3’ (Reverse)

Primer for GAPDH qPCR

5’-AGAGCACAAGAGGAAGAGAGAGAC-3’ (Forward)

5’-AGCACAGGGTACTTTATTGATGGT-3’ (Reverse)

qPCR reactions were carried out in 96 well real-time PCR plates (Bio-Rad) using a Bio-Rad MyIQ Real-time PCR detection system. The qPCR reaction consisted of 5 min at 95º C to activate the polymerase and 50 PCR cycles (uncoupling step at 95º C for 20 sec followed by annealing step at 59º C for 20 sec and elongation step at 72º C for 30 sec), followed by a melting temperature analysis to test for any nonspecific amplification. The expression level of CD44 gene in MDA-MB-231 cells with different treatment was normalized to the expression level of the standard gene GAPDH.

## 3.3 RESULTS

*Blood Plasma Triggers an Adhesive Phenotypic Switch of Breast Cancer (Bca) Cells on E-Selectin Coated Surfaces under Flow*

When grown in 2-D monolayers with culture media, highly metastatic MDA-MB-231 breast cancer cells showed no adhesive interactions with E-selectin coated surfaces under flow conditions (Figure 3.1a) despite the expression of the E-selectin ligand CD44V4 and the binding moiety $sLe^x$ (Figure 3.1b). This is contradictory to its reported high metastatic potential from *in vivo* studies where MDA-MB-231 cells were found to efficiently metastasize to distant organs through the bloodstream,180 where selectin-mediated tethering and rolling events have been shown to play

important roles, as reviewed in.[146, 280]

A more physiological method of culturing cancer cells is presented where human blood plasma is used in combination with culture media. The plasma treatment was found to switch the MDA-MB-231 cells from non-interacting to adhesive (Figure 3.1a) where conventionally cultured MDA-MB-231 cells (control) exhibited no rolling cells on an E-selectin coated surface and plasma cultured cells exhibited strong rolling behavior with rolling velocities of 5.72 ± 0.32 μm and a 10-fold increase of cell flux compared to control cells (Figure 3.1c). It was found that $sLe^x$ expression was upregulated on cells cultured in plasma compared to control cells (Figure 3.1b), which may contribute to the resulting adhesive phenotype.

*Pro-Inflammatory Cytokines IL-6 and TNF-A Induce Adhesive Recruitment of Bca Cells and is Blocked by the Anti-Inflammatory Drug Metformin*

Pro-inflammatory cytokines have been linked to poor prognosis in metastatic breast cancer patients with elevated IL-6 and TNF-α cytokine in their blood plasma.[16, 143] Similar to culture in plasma, MDA-MB-231 cells cultured in IL-6 and TNF-α supplemented media also induced the adhesive phenotypic switch resulting in cell rolling velocities of 11.90 ± 0.28 μm/s and 14.22 ± 0.85 μm/s for IL-6 and TNF-α conditions, respectively, twice that of plasma and the combination of IL-6 and TNF-α treated cell rolling velocities (Figure 3.2a). Treatment with IL-6 and TNF-α at physiologically relevant concentrations such as 25 pg/mL also induced rolling on E-selectin coated microtubes at rolling velocities of 15.43 ± 1.31 μm/s and 17.03 ± 2.21 μm/s, respectively. Furthermore, whereas TNF-α upregulated both CD44V4 and $sLe^x$

expression compared to control cells, IL-6 only upregulated $sLe^x$ (Figure 3.2b) suggesting the importance of increased $sLe^x$ moieties. Blocking the IL-6 receptor with anti-IL-6R monoclonal antibody effectively hindered the adhesive phenotype resulting in nearly abolished cell flux on the E-selectin surfaces (Figure 3.2a). Treating cells with an isotype control for the monoclonal antibody did not affect the IL-6 induced MDA-MB-231 cell rolling on E-selectin coated microtubes (data not shown). In some experiments, IL-6 treated MDA-MB-231 cells were incubated with neuraminidase for 1 hr to cleave $sLe^x$ from the cell surface. Interactions between MDA-MB-231 cells and the E-selectin coated surfaces were abolished after neuraminidase treatment, indicating that the rolling behavior of MDA-MB-231 cells is E-selectin:$sLe^x$ dependent (Figure 3.2a). Interestingly, the anti-inflammatory drug Metformin (1,1-dimethylbiguanide hydrochloride), a frequently used drug to treat type 2 diabetes, showed similar effects to the IL-6R antibody. Metformin has been shown to target Stat3 and induce apoptosis in triple-negative breast cancers as well as significantly decrease serum IL-6 level in breast cancer patients.[51, 165]

*Plasma, IL-6, and TNF-A Promote Breast Cancer Cell Growth as Aggregates*

When plated in a 24 well plate with imaging ready glass coverslip built-in wells, control cells were found to grow as monolayers with very little occurrence of aggregation (Figure 3.3a). Monitoring the cell proliferation and viability under various cytokine treated culture media conditions demonstrated that not only do MDA-MB-231 cells proliferate at an increased rate in the presence of IL-6 and TNF-α (Figure 3.3g), an increased number of aggregates (Figures 3.3b, d, and e) was observed. A

similar and enhanced effect was observed in human plasma (Figure 3.3f) where the large degree of aggregation is reminiscent of tumor spheroids. Therefore, the cell growth and formation as aggregates may cause the adhesive phenotypic switch, especially considering that MDA-MB-231 cells grown in IL-6 and Metformin formed a negligible number of aggregates (similar to control cells, Figure 3.3c). MTT assay also indicated increased cell proliferation when MDA-MB-231 cells were treated with high concentrations of IL-6 and TNF-α (Figure 3.3g).

*3-D Tumor Spheroid Culture Increases the Interactions between BCa cells and E-selectin Coated Surfaces by Upregulating CD44V4 and sLe$^x$ Expression*

Similar to elevated cytokine concentrations, the increased occurrence of tumor spheroids and circulating tumor microemboli has been linked to poor prognosis and increased metastatic potential.[70, 87] Culturing MDA-MB-231 cells as 3-D tumor spheroids in conventional culture media (Figure 3.4a) had an even greater effect on cell adhesiveness to an E-selectin coated surface. Comparable to plasma and cytokine treated conditions, cells grown as spheroids also showed significantly increased CD44V4 and sLe$^x$ expression (Figure 3.4b) while inducing more stable rolling on E-selectin coated surfaces under flow. Moreover, as shown in Figure 3.4c, MDA-MB-231 cells grown in tumor spheroid conditioned media also demonstrated the adhesive phenotypic switch with an average rolling velocity of 7.72 ± 0.32 μm/s, although significantly faster than MDA-MB-231 cells grown in 3-D spheroids (4.02 ± 0.17 μm/s). mRNA expression of CD44 was also measured for all conditions (IL-6, TNF-α, tumor spheroid, and plasma) via real time quantitative PCR (qPCR). As shown in

Figure 3.4d, all conditions resulted in upregulation of CD44 mRNA expression compared to control.

*IL-6 and TNF-α Concentrations in Blood May Regulate the Recruitment of BCa Cells to the Inflamed Endothelium*

Interestingly, the tumor spheroid (3-D) conditioned media contained significantly higher concentrations of both IL-6 and TNF-alpha (Figure 3.5a) than that of healthy donor plasma. Conditioned media from 2-D culture was also assayed and the concentrations of both IL-6 and TNF-alpha were significantly lower than physiological cytokine concentrations sufficient to have an effect on the phenotype of MDA-MB-231 cells. To explore the effects of cytokine concentration on the adhesive behavior of MDA-MB-231 cells, human recombinant IL-6 was added to cell culture medium at a range of concentrations consisting of 1, 5, 10, and 25 ng/mL. MDA-MB-231 cells treated with 25 ng/mL of IL-6 demonstrated the strongest interactions with the E-selectin coated surface with a rolling velocity of $5.46 \pm 0.31$ μm, comparable to the rolling velocity of plasma cultured cells (Figure 3.5b). Overall, MDA-MB-231 cells showed more robust interactions with E-selectin coated surfaces as the concentration of IL-6 was increased, resulting in greater numbers of cells recruited via the adhesion cascade.

## 3.4 DISCUSSION

There is compelling evidence supporting the strong interplay between various types of inflammation and cancer progression suggested by numerous clinical and

epidemiological studies.[45, 90] The recruitment of tumor-associated immune cells during the inflammation that accompanies tumor progression, has been shown to promote tumor growth and contribute to angiogenesis, invasion, and metastasis.[44] Infiltration of these tumor-promoting immune cells as well as various inflammatory cytokines, particularly TNF-α and IL-6, has been found in the breast tumor microenvironment.[15]

A clinical study reported elevated levels of pro-inflammatory cytokines in the serum of breast cancer patients when compared to healthy individuals.[166] As one of the well characterized 'triple-negative' breast cancer cell lines, MDA-MB-231 has been reported to also be mesenchymal stem cell-like.[156] Furthermore, 'triple-negative' breast cancers have been found to correlate with inflammatory states such as obesity and diabetes where pro-inflammatory cytokines, including IL-6, are highly expressed.

The lack of interaction between culture medium grown MDA-MB-231 cells with E-selectin coated surfaces, as observed in this study, was rather unexpected considering their reported high metastatic potential from both *in vitro* and *in vivo* studies. Human plasma, IL-6, and TNF-α supplemented culture conditions have been shown to induce an adhesive phenotypic switch, allowing MDA-MB-231 cells to establish stable rolling on E-selectin coated surfaces under physiological flow. Plasma factors such as fibrinogen as well as other cytokines such as IL-1β and IFN-γ have also been shown to promote cell adhesion.[147, 169, 290] In this study, cytokines such as IL-6 and TNF-α were studied in particular due to their association with poor prognosis for breast cancer patients. The concentration of cytokines used for the *in vitro* experiments was based on similar studies that have investigated the effect of these cytokines on invasiveness of breast cancer cell lines.[252] CD44V4, a major E-selectin

ligand for breast cancer cells, was found to be upregulated on MDA–MB-231 cells treated with TNF-α. TNF-α has been reported to increase CD44 expression on ovarian cancer cells upon the activation of the c-Jun $NH_2$-terminal kinase[190] and, although not in the context of cancer, affects the glycosylation and sulfation of various glycoproteins.[48] On the other hand, IL-6 has been shown to induce a significant increase in the expression of α1,3/4-fucosyltransferases (FUT11 (fucosyltransferase 11 gene) and FUT3) as well as the amounts of $sLe^x$ and 6-sulfo-$sLe^x$ epitopes in human bronchial mucosa.[91] Although CD44V4 is a major E-selectin ligand for breast cancer cells, there are other ligands such as MUC1 which play an active role in rolling and firm adhesion of breast cancer cells on inflamed endothelium, as reported in our recent study.[84] The flow cytometry results of the present study comparing control and IL-6 treated MDA-MB-231 cells suggest that IL-6 also promotes the synthesis of $sLe^x$ on breast cancer cells, potentially providing more opportunity for $sLe^x$: E-selectin mediated heterotypic interaction between cancer cells and the activated endothelium.

Selectin-based technology has been used to capture viable circulating tumor cells (CTCs) that can be further characterized by releasing the bound CTCs in the absence of calcium.[110, 111] Recently, E-selectin-mediated adhesive interactions were utilized inside an E-selectin coated polydimethylsiloxane (PDMS) microbubble system to capture colon CTCs under flow conditions.1 Presently, most CTC studies have focused on the survival and metastasis of individual tumor cells in the circulation. However, emerging evidence supports the importance of circulating tumor microemboli (CTM) during cancer progression.[108] CTM represent a “collective migration” of tumor cells and have been found to exhibit higher metastatic potential

than that of individual CTCs.[207] It has been proposed that these multicellular clumps of tumor cells can metastasize by becoming mechanically trapped in the smallest capillaries due to their large size.[70] Tumor spheroid/aggregate grown MDA-MB-231 breast cancer cells were found to upregulate their number of E-selectin ligands and binding moieties and demonstrated the most robust rolling behavior on E-selectin coated surfaces, compared to MDA-MB-231 cells from plasma and cytokine treatments, suggesting that CTMs may efficiently escape the bloodstream via a metastatic adhesion cascade.

Highly metastatic tumor cells have been reported to exhibit increased homotypic aggregation, gaining resistance to apoptosis.[87] There is also evidence to suggest that breast cancer cells cultured as 3-D spheroids express a higher level of IL-6 mRNA.104 A recent study by our group reported that homotypic and heterotypic interactions in breast cancer cells cultured as 3-D spheroids alter their adhesion phenotype. These interactions were shown to increase the interaction of breast cancer cells with human recombinant E-selectin.[39] Furthermore, when MDA-MB-231 cells were cultured as 3-D spheroids in media, high concentrations of IL-6 and TNF-α were found in the spent media and cell adhesion to E-selectin surfaces were found to be dependent on IL-6 concentration.

A novel mechanism (Figure 3.6) was proposed that may explain the aggressiveness of 'triple-negative' breast carcinoma. First, the pro-inflammatory cytokines act on single cells to induce an aggregated morphology and an increased proliferation rate. Cell aggregation then upregulates the secretion rate of IL-6 and TNF-α thereby increasing cytokine concentrations. This may cause a positive

feedback mechanism where the increased cytokine concentrations cause more aggregation and proliferation that further stimulate cytokine secretion. The ultimate effect of aggregation is the increased expression of E-selectin ligands and binding moieties that facilitate stable rolling on the inflamed endothelium to enable subsequent extravasation.

In summary, results from this study indicate that plasma and cytokines can promote homotypic aggregation and that cell proliferation as tumor spheroids can change the adhesion phenotype of cancer cells to immobilized E-selectin under physiological flow, which may contribute to the higher metastatic potential of CTM. Taken together, these results suggest that therapeutic approaches targeting cytokine receptors and adhesion molecules on cancer cells may help reduce the likelihood of metastasis and deserve further attention.

**Figure 3.1:** Plasma triggers an adhesive phenotypic switch of breast cancer (BCa) cells on E-selectin coated surface under flow**.** (a) Left: Untreated MDA-MB-231 cells (2-D culture with regular medium) show no interactions with the E-selectin coated surfaces under flow. Right: Cells establish stable rolling on E-selectin coated surface after 48 h plasma treatment. (b) Flow cytometry results of CD44V4 (left) and $sLe^x$ (right) expression on untreated and plasma treated MDA-MB-231 cell surfaces. Mean fluorescence intensity ratio of sample over isotype has been included. (c) Left: Average rolling velocity of untreated (control) and plasma treated MDA-MB-231 cells (n =35 cells). Shear stress of 1 $dyn/cm^2$ was used. Right: Average numbers of cells interacting with the E-selectin coated surface per 5 x $10^5$ $\mu m^2$ of untreated (n = 30 frames) and plasma treated (n = 36 frames) MDA-MB-231 cells. Bars represent mean ± SEM. $P < 0.0001$, two-tailed unpaired student t-test.

**Figure 3.1: Plasma triggers an adhesive phenotypic switch of breast cancer cells on E-selectin coated surface under flow**

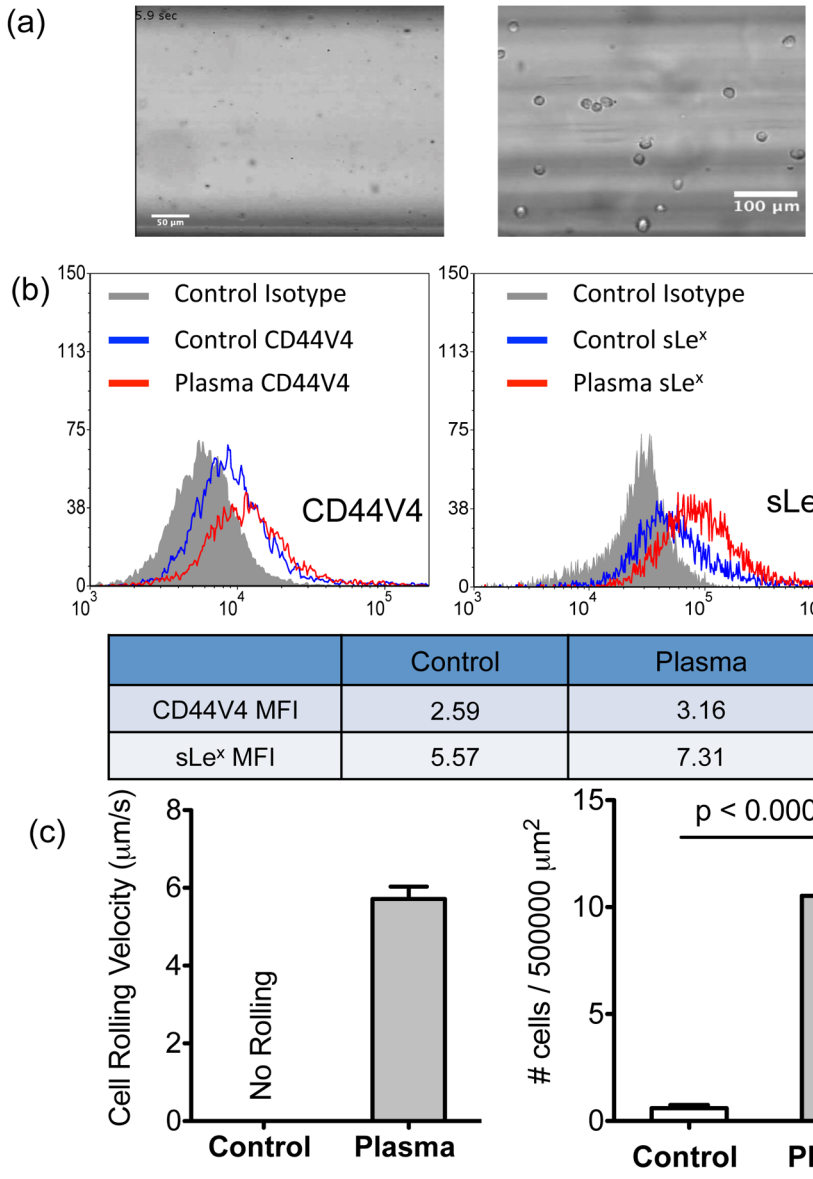


| | Control | Plasma |
|---|---|---|
| CD44V4 MFI | 2.59 | 3.16 |
| sLe$^x$ MFI | 5.57 | 7.31 |

**Figure 3.2:** Pro-inflammatory cytokines IL-6 and TNF-α also induce adhesive recruitment of BCa cells and is blocked by the anti-inflammatory drug Metformin. (a) Average rolling velocity (left) and average number of MDA-MB-231 cells interacting with E-selectin coated surfaces (right) after treatments including 5 ng/mL of IL-6 (n=71), 5 ng/mL TNF-α (n = 48), IL-6 + TNF-α (5 ng/mL each), 5 ng/mL of IL-6 with 0.1 mmol Metformin, 5 ng/mL of IL-6 with 1 μg/mL anti-IL-6R MAb, 5ng/mL of IL-6 with neuraminidase treatment prior to rolling experiment. For conditions where MDA-MB-231 cells were treated with IL-6 with MAb, Metformin, or neuraminidase (after IL-6 treatment), there were insufficient numbers of cells found on the E-selectin coated surface for velocity analysis. Bars represent mean ± SEM. $P < 0.0001$, two-tailed unpaired student t-test. Average number of MDA-MB-231 cells from control experiment was found to be significantly less than all other conditions ($P<0.0001$). (b) Flow cytometry measurements of CD44V4 (left) and $sLe^x$ (right) expression on untreated, IL-6 (5 ng/mL), and TNF-α (5 ng/mL) treated MDA-MB-231 cell surfaces. Mean fluorescence intensity ratio of sample over isotype has been included.

**Figure 3.2: Pro-inflammatory cytokines also induce adhesive recruitment of breast cancer cells and is blocked by Metformin**

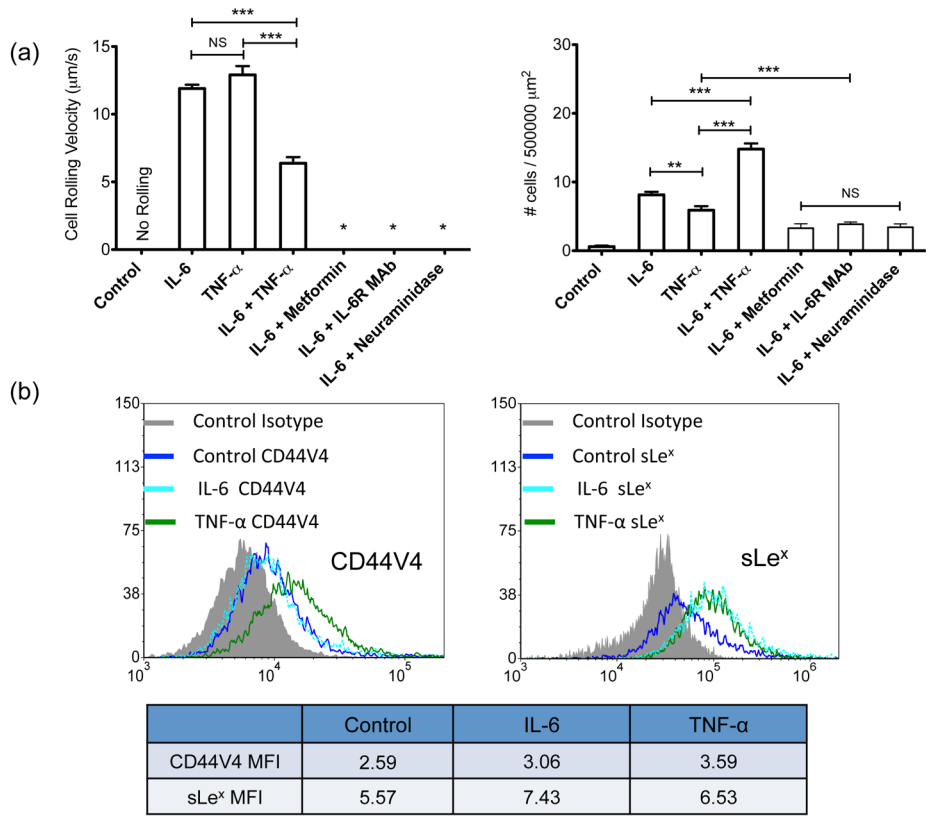


| | Control | IL-6 | TNF-α |
|---|---|---|---|
| CD44V4 MFI | 2.59 | 3.06 | 3.59 |
| sLeˣ MFI | 5.57 | 7.43 | 6.53 |

**Figure 3.3:** Plasma, IL-6, and TNF-α promote breast cancer cell growth as aggregates. Morphology and viability of MDA-MB-231 cells cultured in (a) regular medium, (b) IL-6 (5 ng/mL) spiked medium, (c) IL-6 (5 ng/mL) and 0.1 mmol Metformin added medium, (d) TNF-α (5 ng/mL) spiked medium, (e) IL-6 and TNF-α (5 ng/mL each) spiked medium, and (f) healthy donor plasma. A blue fluorescent cell-permeable nucleic acid dye (for live cell staining) and a red fluorescent cell-impermeable nucleic dye (for dead cell staining) were used to visualize the live and dead populations. (g) Cell proliferation results via MTT assay of control media, IL-6, TNF-α, and Metformin treated MDA-MB-231 cells.

**Figure 3.3: Plasma, IL-6, and TNF-alpha promote breast cancer cell growth as aggregates**

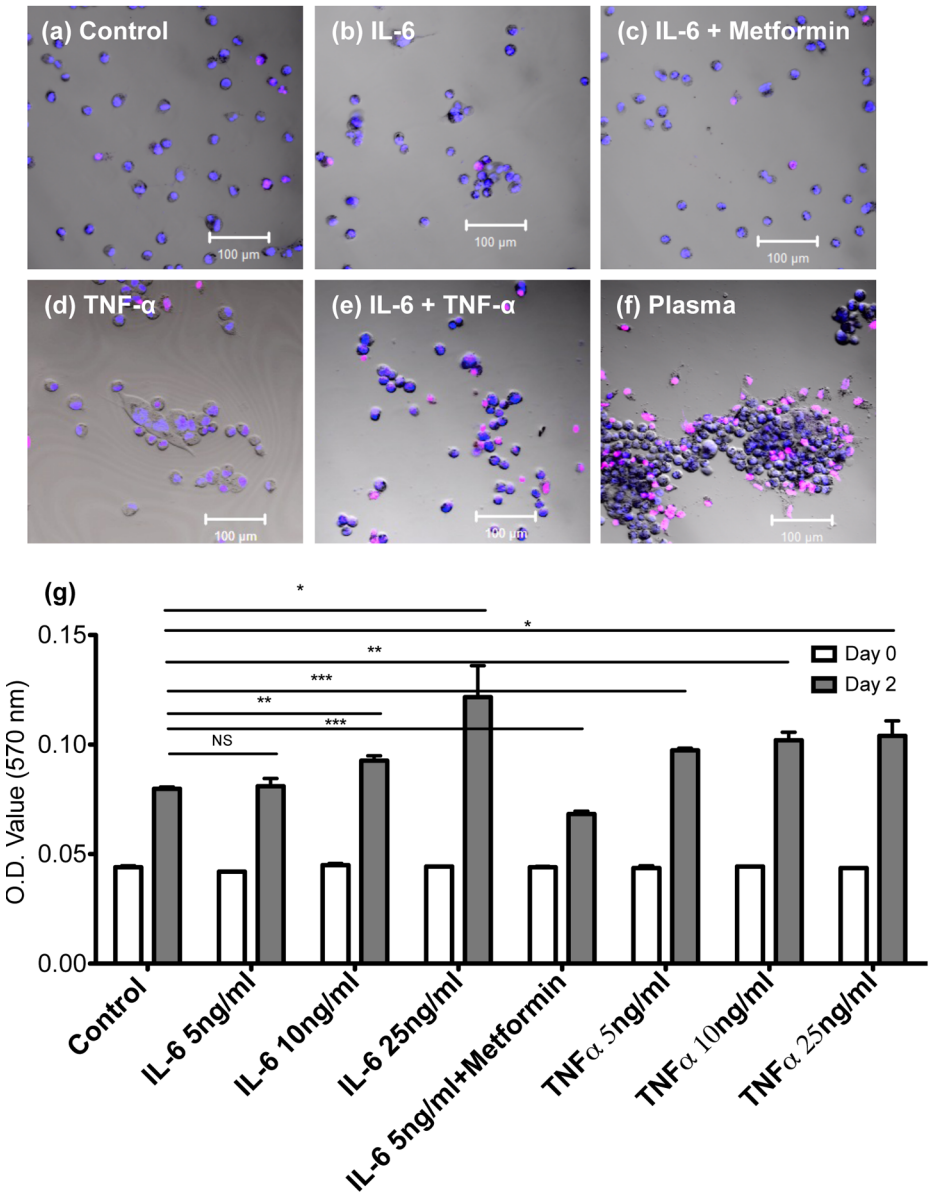

**Figure 3.4:** 3-D tumor spheroid culture further increases the interactions between BCa cells and E-selectin coated surfaces by upregulating CD44V4 and $sLe^x$ expression. (a) Micrographs of MDA-MB-231 cells cultured in 2-D monolayer (left) and 3-D spheroid on PDMS (right). (b) Flow cytometry results of CD44V4 (left) and $sLe^x$ (right) expression on untreated (2-D monolayer grown) and tumor spheroid cultured MDA-MB-231 cells. Tumor spheroid cultured cells were treated with enzyme free dissociation buffer prior to experiments to obtain mostly single cell populations. Mean fluorescence intensity ratio of sample over isotype has been included. (c) Average rolling velocity (left) and average number of MDA-MB-231 cells found interacting with E-selectin coated surfaces (right) cultured in medium (untreated), 3-D spheroid, and spheroid conditioned medium. Bars represent mean ± SEM. Two-tailed unpaired student t-test was used. (d) CD44 mRNA expression of MDA-MB-231 cells that are cultured in control, IL-6, TNF-α, tumor spheroid, and plasma conditions, respectively, measured via qPCR.

**Figure 3.4: 3-D tumor spheroid culture further increases the adhesive interactions by upregulating CD44V4 and glycan expression**

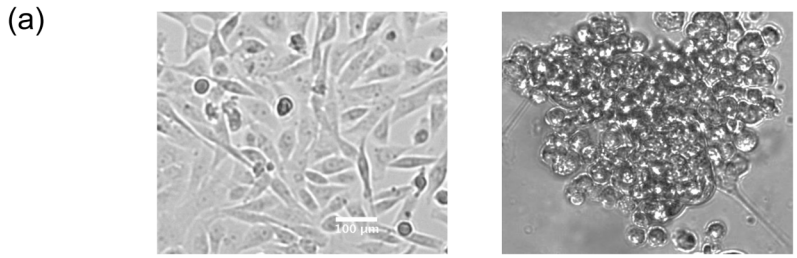


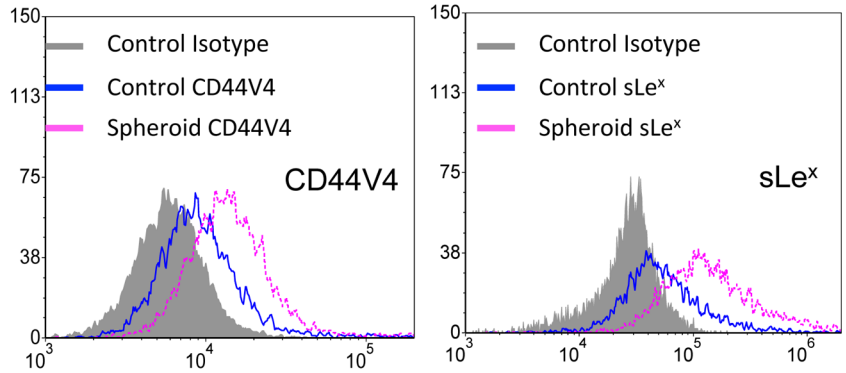


| | Control | Tumor Spheroid |
|---|---|---|
| CD44V4 MFI | 2.59 | 6.35 |
| sLe$^x$ MFI | 5.57 | 11.8 |

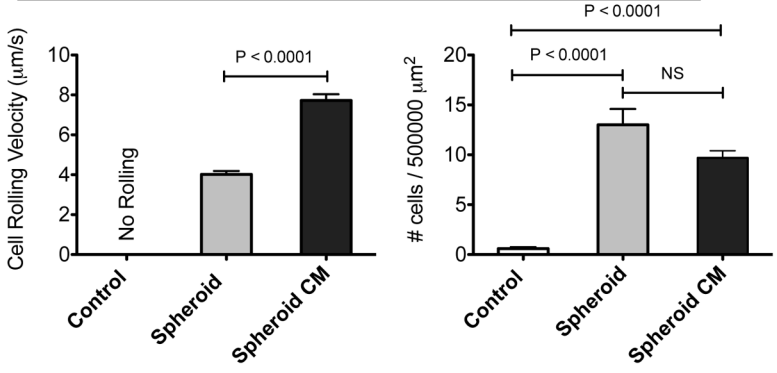

**Figure 3.5:** IL-6 and TNF-α concentrations in blood can regulate the recruitment of BCa cells to the inflamed endothelium. (a) Calculated concentrations of IL-6 (left) and TNF-α (right) of healthy female donor plasma and tumor spheroid conditioned media on ELISA standard curves. IL-6 concentration in the tumor spheroid conditioned media was diluted with equal volume of culture media to remain in the detectable range (0-200 pg/mL) of the ELISA kit. (b) Average rolling velocities (left) and average numbers of MDA cells found interacting with E-selectin coated surfaces (right) from untreated conditions and culture media spiked with a range of IL-6 concentration including 1, 5, 10, and 25 ng/mL. For the cell number analysis, all conditions are significantly different ($p < 0.0001$) except for the 5 and 10 ng/mL treatments. Bars represent mean ± SEM. Two-tailed unpaired student t-test was used.

**Figure 3.5: IL-6 and TNF-alpha can regulate the recruitment of breast cancer cells to the endothelium**

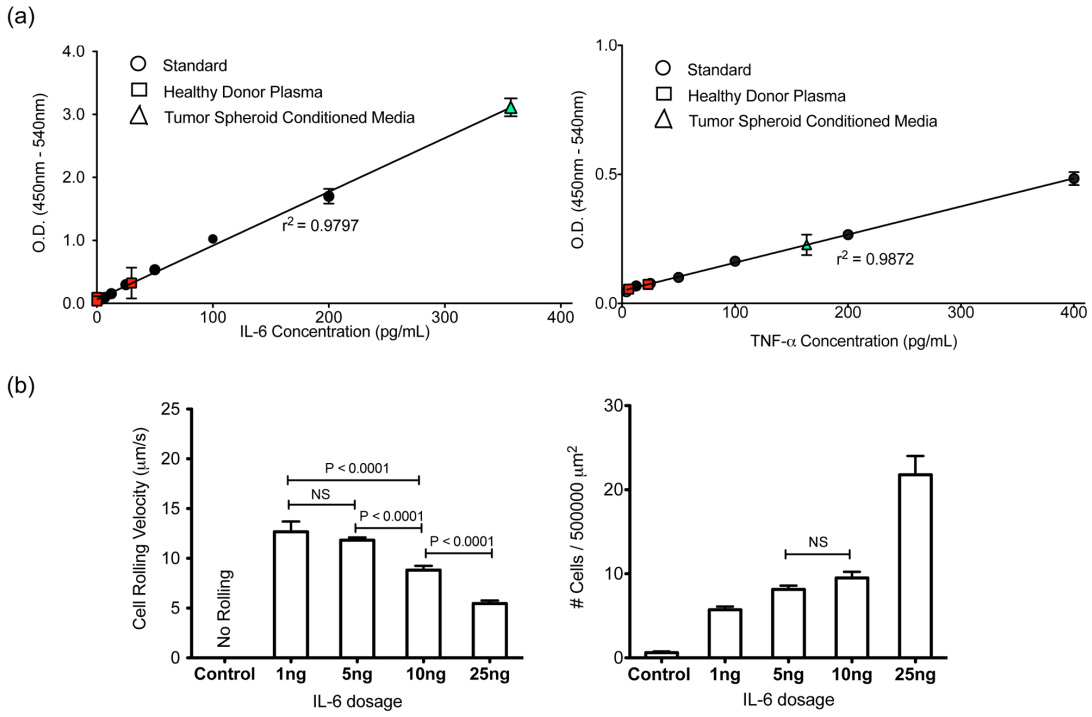

**Figure 3.6:** A positive feedback loop: activation and maintenance of the adhesive phenotypic switch**.** Step A: Tumor cells encounter proinflammatory cytokines such as IL-6 and TNF-α secreted by tumor promoting immune cells in the microenvironment. Step B: Cytokine conditioned tumor cells form aggregates. Step C: Aggregates/spheroids of tumor cells release more IL-6 and TNF-α, turning on a phenotypic switch for more tumor cells nearby by upregulating E-selectin ligand and binding moiety expressions, and promote heterotypic interactions between tumor cells and the inflamed endothelium. Step D: Tumor cells ready to invade the endothelium.

**Figure 3.6: A schematic of the positive feedback loop: activation and maintenance of the adhesive phenotypic switch**

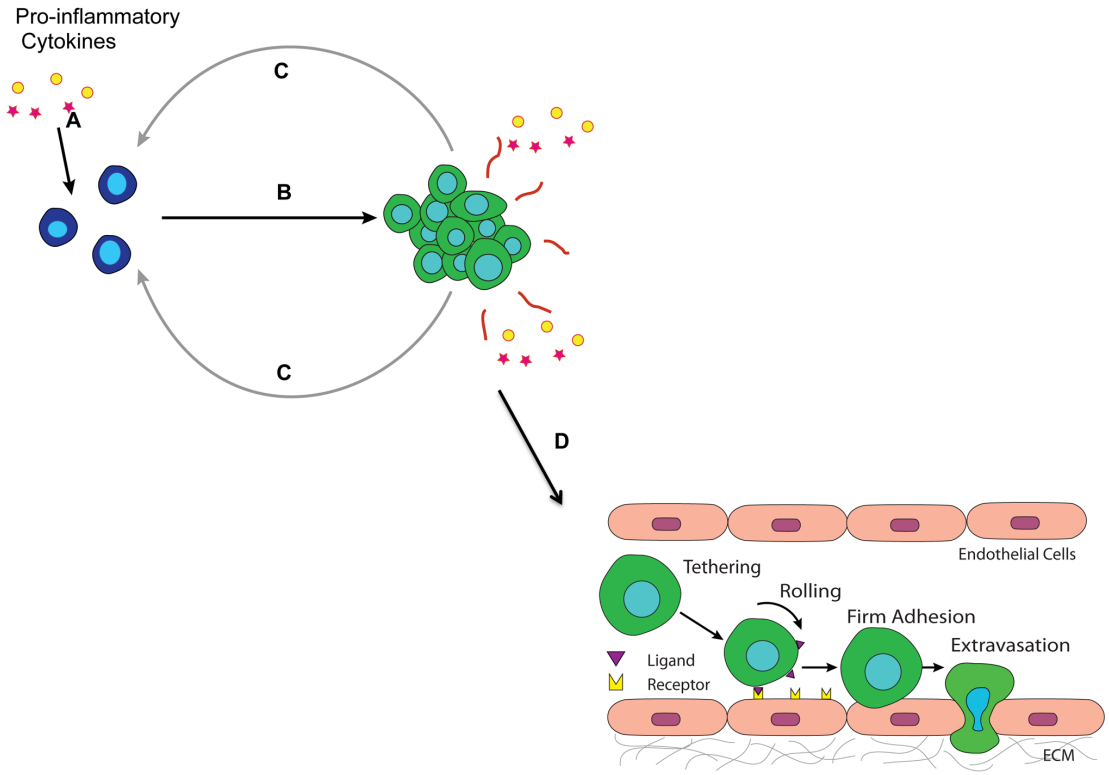

# CHAPTER 4 VASCULAR RECRUITMENT OF HUMAN RETINOBLASTOMA CELLS BY MULTI-CELLULAR ADHESIVE INTERACTIONS WITH CIRCULATING LEUKOCYTES

* This section is adapted from the following publication: Y. Geng, G. M. Seigel, S. Narasipura, and M. R. King. *Cellular and Molecular Bioengineering*. 3:361-8, 2010

## 4.1 INTRODUCTION

Retinoblastoma (RB) is a malignant tumor of the neural retina that affects approximately 250-350 children under the age of six every year in the United States.[18] In some Central and South America countries, retinoblastoma is one of the most common solid tumor malignancies in children.[26] Retinoblastoma usually manifests before the age of three and the tumors can grow locally within the eye as well as extend outside the globe by migrating down the optic nerve into the central nervous system and the cerebrospinal fluid. In addition, the tumors can spread through the vasculature to form metastases in distant organs. Patients with hereditary RB have a much higher risk for developing secondary malignancies later in life, mainly soft tissue sarcoma, osteosarcoma, and melanoma.[4,10] Reports have indicated that the rate of secondary tumor formation in these patients is increased by radiation treatment and possibly in combination with chemotherapy.[3] Chemoresistant, radiation-resistant stem-like cells exist in many forms of cancer[20,22] and may relate to these secondary malignancies. One hallmark of many stem-like cell populations is the presence of ABCG2 (BCRP), a stem cell marker[32] and a cell surface transmembrane pump that can confer resistance to a wide variety of chemotherapy agents, including anthracyclines, mitoxantrone, and camptothecins.[17] The calcium-dependent transporter activity of ABCG2 has been used to identify and isolate stem-like cells from a variety of normal and malignant tissues based on the ability of ABCG2 positive cells to exclude Hoechst dye 3334.[1,7,27] Seigel and colleagues have identified subpopulations of cancer stem-like cells in retinoblastoma that express stem cell markers such as ABCG2, as well as human embryonic stem cell markers, such as Nanog and

Oct3/4[24,25] that provide an intriguing model for the study of tumor cell adhesion and metastasis.

The basic mechanisms of how neutrophils adhere to the vascular endothelium and migrate to inflammatory sites have been studied extensively over the past two decades. To start the neutrophil recruitment cascade, the initial capture of neutrophils from the bloodstream and rolling along the vessel wall is mediated by P-selectin and E-selectin presented by stimulated endothelial cells.[11,12] Activated beta-2 integrins (CD11a/CD18 or LFA-1, and CD11b/CD18 or Mac-1) on neutrophils then facilitate the firm arrest of neutrophils by binding to ICAM-1 on endothelial cells.[6] Circulating tumor cells such as colon carcinoma[3] and acute myeloid leukemia[19] express selectin ligands and integrins, which allow them to interact directly with the endothelium and metastasize through the blood stream. Other circulating metastatic cancer cells, however, have been found to adhesively associate with neutrophils in the circulation, to escape the circulation and engraft in the extravascular space.[14,16] The similar properties shared between metastatic cancer cells and leukocytes such as the ability to interact with endothelium and cause basement membrane degradation suggests that leukocytes may play a role in promoting tumor growth and survival, as well as transendothelial migration.[23,30] The interaction between cancer cells and leukocytes has been found in breast cancer, advanced gastric cancer, colon cancer, and malignant melanoma.[15,21,31]

It has been established that the accumulation of neutrophils at inflammatory sites is a collective phenomenon.[8] Homotypic interactions between neutrophils were found to be responsible for enhancing the accumulation of neutrophils rolling on P-

selectin surfaces *in vitro*.[29] Walcheck *et al*. showed that transient tether formation between a rolling neutrophil and a cell suspended freely in the fluid can cause the rolling and capture of free-flowing cells near the surface.

It is not clear how retinoblastoma cells may adhere to the endothelium and subsequently extravasate through it under flow conditions in the microcirculation. In this study, it was shown that retinoblastoma cancer stem cells can interact with a model endothelial surface via secondary recruitment by activated leukocytes, as a potential mechanism for metastatic spread.

## 4.2 MATERIALS AND METHODS

*Reagents*

FITC-conjugated mAb for anti-human CD 338 (ABCG2) clone 5D3, PE-conjugaged mAb for anti-human CD 54 (ICAM-1) clone HCD54 and FITC-conjugated Mouse IgG2b, κ isotype control were purchased from BioLegend, (Sandiago, CA). PE-conjugaged Mouse IgG1, κ isotype control was purchased from eBioscience (San Diego, CA). Recombinant E-selectin-IgG chimera was obtained from R&D Systems (Minneapolis, MN). Trypan blue stain (0.4%) was obtained from Lonza (Wilkersville, MD). Blotting grade blocker non-fat dry milk was obtained from Bio-Rad Laboratories (Hercules, CA). Protein-G was purchased from EMD Biosciences (San Diego, CA). $Ca^{2+}$ and $Mg^{2+}$ free HBSS (Invitrogen, Camarillo, CA, USA), $Ca^{2+}$ and Mg2+ free DPBS (Invitrogen, Camarillo, CA, USA), calcium carbonate (Sigma Chemical Co., St. Louis, MO, USA), endotoxin free water (MO BIO Laboratories, Carlsbad, CA, USA), endotoxin free human serum albumin (Sigma Chemical Co., St.

Louis, MO, USA), and low endotoxin (1 ng/mg), essentially globulin-free BSA (Sigma Chemical Co., St. Louis, MO, USA) were used to make buffer solutions for neutrophil isolation and flow experiments.

*Retinoblastoma Cell Cultures*

Retinoblastoma cell lines RB143 (a gift from Dr. Bruce Ksander) and WERI-Rb27 (a gift from Dr. John Ludlow) were maintained in Dulbecco's Modified Eagle's Medium (Sigma), with 20% calf serum for RB143 cells and 10% calf serum for WERI-Rb27 cells (Hyclone, Logan UT) at 37ºC in a 5% $CO_2$ incubator.

*Immunocytochemistry*

The following primary antibodies were used for immunocytochemistry:
10 μg/ml rabbit anti-Nestin (Sigma), 4.16 μg/ml rabbit anti-ICAM-1 (Cell Signaling Technologies, Danvers, MA), 1 μg/ml goat anti-doublecortin (Santa Cruz Biotechnology, Santa Cruz, CA), 5 μg/ml mouse anti-CD147 (Neurothelin, EMMPRIN, Basigin; BD Pharmingen, Franklin Lakes, NJ), and 1:200 dilution of mouse anti-ABCG2 (Abcam, Cambridge, MA).

For diaminobenzidine (DAB) staining, RB143 cells were prepared as cytospins by centrifugation and resuspension in cytospin fixative (72% isopropyl alcohol, 19% acetone, 7.6% glycerol). After at least 10 min of fixation, the cell suspensions were spun onto slides at 1000g for 5 min in a Shandon Cytospin 2. Cytospins underwent immunocytochemistry using the following protocol: Cytospin slides were incubated for 5 min with PBS, 5 min with 3% $H_2O_2$ and rinsed twice with PBS. Cells were

blocked for 15 min with 2% bovine serum albumin, followed by a PBS wash. Cells were incubated in primary antibody or isotype control antibody for 1 h, washed twice with PBS, and incubated with 1 μg/ml of appropriate biotinylated secondary antibody (anti-mouse, rabbit or goat from Vector Laboratories, Burlingame, CA) for 45 min. After two PBS washes, the cells were incubated for 20 min with horseradish peroxidase-labelled avidin (ABC Elite kit, Vector Laboratories, Burlingame, CA). The cells were washed twice with PBS and then treated with DAB (Zymed Laboratories, Carlsbad, CA) for 5 min to develop the brown reaction product. Cells were then viewed by brightfield microscopy with Nomarski optics (Nikon Eclipse, ES600).

For double immunofluorescent staining, cells were fixed and maintained in suspension. After PBS wash, cells were incubated at 4ºC with primary antibodies (mouse anti-ABCG2 and rabbit anti-ICAM-1 or isotype control antibody) for 1 h, rinsed twice, then incubated for 1 h with a mixture of fluorescent secondary antibodies (2.5 μg/ml each of FITC anti-rabbit Ig and TRITC anti-mouse Ig, Sigma). Cells were rinsed, placed on a slide and coverslipped for viewing with fluorescence microscopy (Nikon Eclipse, ES600).

*Flow Cytometry*

Both RB143 and WERI-Rb27 cells were de-clumped prior to antibody incubation using an enzyme-free cell dissociation media that preserves the cell surface receptors rather than cleave them. After two washes with 1X DPBS, the cells were resuspended in 1X DPBS to a final concentration of 200,000-300,000 cells in each sample.

Antibodies or appropriate isotype controls were added to cell suspensions and incubated over ice for 45 min. Following the incubations, the cells were washed three times with 1mL of 1X DPBS to remove any unbound antibody. Flow cytometry samples were analyzed using an Accuri C6 flow cytometer (Accuri Cytometers Inc., Ann Arbor, Michigan, USA) and plots were created using the FlowJo v. 7.6.3 (Tree Star Inc., Ashland, Oregon) software package.

*Preparation of Immobilized Protein Surfaces*

Polyurethane microtubes with an inner diameter of 300 μm (Braintree Scientific Inc., Braintree, MA, USA) were cut to a length of 50 cm. Recombinant human E-selectin-IgG chimeric protein was dissolved in 1X PBS to a final concentration of 5 μg/mL. The microtube surface was first rinsed with 75% ethanol and then 1X PBS. The surface was subsequently incubated with 10 μg/mL of protein-G solution for 1.5 h, followed by a 2 h incubation with selectin chimera then blocked with 5% milk protein in PBS for 1 h. Control tubes were blocked with 5% milk protein in PBS for 1 h.

*Neutrophil Isolation and Activation*

Human peripheral blood was collected from consenting healthy adult donors (as per IRB-approved protocol). Neutrophils were isolated by centrifugation at 500g for 50 min at 23°C using 1-Step Polymorphs (Accurate Chemical and Scientific Corporation, Westbury, NY, USA.), creating separate visible layers of plasma, mononuclear cells, neutrophils, and erythrocytes and platelets. The neutrophil layer was extracted and washed twice in $Ca^{2+}$ and $Mg^{2+}$ free HBSS to remove the polymorph residue, and any

remaining red blood cells were lysed hypotonically with 1:6 and 10X PBS. Neutrophils were then resuspended at various concentrations of HBSS containing 0.5% HSA, 2mM $Ca^{2+}$, and 10 mM HEPES, buffered to 7.4. Prior to flow experiments, neutrophils were stimulated with 1nM IL-8 (R&D Systems Inc., Minneapolis, MN, USA) for 10 min at RT on a rocker (Rocker II Model 260350, Boekel Scientific).

*Recruitment of Retinoblastoma Cells by Association with Neutrophils under Flow*

Microtubes with functionalized E-selectin surfaces were secured on the stage of an Olympus IX81 inverted microscope (Olympus America Inc., Melville, NY, USA). After mixing IL-8 stimulated neutrophils and CTG-labeled RB cells for 5 min on a rocker, the cell solution was introduced into the microtube using a syringe pump (KDS 230, IITC Life Science, Woodland Hills, CA) at a wall shear stress of 1.0 dyne/$cm^2$. The dynamic adhesion between RB cells and human peripheral leukocytes was characterized over a physiological range of wall shear stress values (0.2-5 dyn/$cm^2$).

*Data Acquisition*

Videos of flowing and adhering RB-neutrophil aggregates were recorded using a microscope-linked Hitachi CCD camera KP-M1AN (Hitachi, Japan) and a Sony DVD Recorder DVO-1000MD (Sony Electronics Inc., San Diego, California, USA). For each flow experiment, a 12 cm functionalized E-selectin surface was scanned and the aggregates were quantified and normalized. The average ratio of leukocytes to cancer cells per aggregate was measured as a function of shear stress, receptor density, and

cell concentration.

*Statistical Analysis*

Adhesive interactions of RB143 and WERI-Rb27 cells with neutrophils at various ratios were quantified and plotted using Prism 5.0b for Microsoft (GraphPad Software, San Diego, CA, www.graphpad.com). Rolling cells were defined as those translating in the direction of flow with an average velocity less than 50% of the calculated hydrodynamic free stream velocity. Two-tailed unpaired t-test and ANOVA were employed with a significance level of $\alpha$=0.05 where applicable.

## 4.3 RESULTS

When RB143 and WERI-Rb27 cells were perfused through E-selectin coated microtube surfaces without neutrophils, neither demonstrated rolling adhesion as defined above. No expression of E-selectin ligands was found via flow cytometry in either the RB143 or WERI-Rb27 cell line (data not shown). There was, however, an ABCG2+ stem-like cell subpopulation within both cell lines that co-expressed high levels of ICAM-1 (Figure 4.1). ICAM-1 is a beta-2 integrin ligand and a surface marker that correlates with tumor metastatic potential.[28] As shown in Figure 4.1, ~90% of ABCG2+ RB143 cells expressed ICAM-1, compared with less than 20% expression of ICAM-1 in ABCG2- cells. This co-staining for ABCG2 and ICAM-1 is also demonstrated in the micrograph of Figure 4.1B.

Results from the aggregation assay indicate that RB-leukocyte aggregate formation is ICAM-1 dependent (Figure 4.2). In these experiments, RB143 and WERI-

Rb27 cell concentrations were held constant at 1 million/mL while varying neutrophil concentrations from 2 million/mL to 5 million/mL. The total number of aggregates observed (including adhering and rolling/flowing) from all four different conditions (RB143 1:2, RB143 1:5, WERI 1:2, WERI 1:5) were not significantly different ($p = 0.0814$). Approximately 80% of the captured events in all four conditions were RB cells rolling or flowing with their anchoring neutrophils on the microtube surface. Significantly fewer events were observed in blocking and control experiments, as seen in in Figure 4.2. Overall, RB-neutrophil aggregate formation showed no correlation with initial cell ratios or cell lines ($p = 0.814$, ANOVA). It was also observed that some flowing neutrophils are captured by a retinoblastoma:neutrophil aggregate attached to the surface; such cells were recorded as "tethered" neutrophils since they were available for future collisions with flowing retinoblastoma cells.

To further characterize the size of aggregates formed, the number of neutrophils that bound to RB cells in each aggregate (both adhering and rolling/flowing) was quantified for two experiments with RB143 cells, for two different initial RB143:neutrophil cell ratios of 1:2 and 1:5. The normalized results showed no significant difference in the number of aggregates captured. In the experiment in which the RB143:neutrophil initial ratio was 1:2, the aggregation profile exhibits an approximately binomial distribution. Overall, the majority of aggregates captured were one-to-one (i.e., one RB with one neutrophil) binding events, shown in Figure 4.3. Over 40 adhering one-to-one binding events were analyzed in which both RB and neutrophil were attached to the E-selectin surface (shown in Figure 4.4). The orientation angle and center-to-center distance of the captured RB cell, relative to the anchoring neutrophil,

was quantified for each observed heterotypic adhesion event. It was found that 90% of these one-to-one aggregates, RB cells and neutrophils formed angles between 0° and 180°, i.e., downstream to their anchoring neutrophils.

## 4.4 DISCUSSION

The goal of this study was to address the mechanism by which RB cells adhere to the endothelium that could allow subsequent extravasation and metastasis to distant sites. Although RB cells do *not* express selectin ligands or beta-2 integrins themselves, ABCG2+ RB stem-like cells *do* express ICAM-1 suggesting a role for leukocyte:RB adhesive interactions as a mechanism that can promotes RB arrest on the endothelium under flow.

ICAM-1 is expressed on a variety of primary tumors, metastases, and normal cells.[5] In the present study, flow cytometry results suggest preferential expression of ICAM-1 on the surface of ABCG2+ RB143 cells. A similar trend in WERI-Rb27 cells was observed (results not shown). This suggests the hypothesis that RB cells, especially ABCG2+ RB cancer stem-like cells, may be recruited to an E-selectin surface by first attaching to activated neutrophils via LFA-1: ICAM-1 binding (Figure 4.5).

The results from the microtube aggregation assay show that aggregate formation is insensitive to the initial ratio of neutrophils and RB cells. One might expect to observe more aggregates as the neutrophil concentration is increased from 2 to 5 million/mL for both RB cell lines. However, no significant increase in the number of aggregates is observed in experiments using RB143 nor WERI-Rb27 cells since all four conditions (RB143 1:2, 1:5; WERI-Rb27 1:2, 1:5) show similar trends in terms of

the distribution of adhering and rolling/flowing aggregates. The significant decrease in the number of RB-neutrophil aggregates captured in the presence of ICAM-1 blocking antibodies suggests that the phenomenon of RB-neutrophil binding is highly ICAM-1 specific. In addition to the sensitivity and specificity, it was found that the majority of RB-neutrophil aggregates were one-to-one binding, i.e., once a neutrophil binds to a RB cell, it is less likely to recruit another RB cell, likewise the RB cells, once bound in one-to-one aggregates, are less likely to bind to a second neutrophil. This may be due to the relocation of receptors to the cell:cell contact area, as observed in neutrophil relocation on the neutrophil surface.[9,13] Furthermore, it was observed that 90% of the bound RB cells are downstream to their anchoring neutrophils, which shares similarities to the secondary recruitment mechanism observed for neutrophil-neutrophil interactions.[29]

Interestingly, in the aggregation assay (Figure 4.3), at least 20% of RB cell and neutrophil aggregates were observed to flow or roll rather than adhere to the E-selectin surface. This suggests a step-wise binding mechanism in which the RB cells and neutrophils first interact and form aggregates in flow, roll together on the surface through the neutrophil sialyl Lewis ($sLe^x$):E-selectin binding, and then firmly adhere to the surface (Figure 4.5). Alternatively, the neutrophils could first adhere to the E-selectin surface and then recruit RB cells. However, the experiments in which activated neutrophils were first perfused through the E-selectin surface with subsequent RB cell introduction showed no aggregate formation. This indicates that neutrophil recruitment of RB cells precedes neutrophil firm adhesion to E-selectin. Since adhesion molecules, such as ICAM-1 expressed on ABCG2+ RB stem-like

cells, are critical for invasion and metastasis, anti-adhesion strategies as a potential adjunct to conventional cancer therapies were proposed. This study provides insight for future experimental designs investigating RB metastasis and developing therapeutic approaches to prevent secondary tumor formation in patients that survive a primary RB tumor.

## 4.5 CONCLUSIONS

In this study, it was discovered that ABCG2+ stem-like RB143 and WERI-Rb27 cells preferentially express ICAM-1, which acts as a bridge linking RB cells to leukocytes in the bloodstream via LFA-1:ICAM-1 interactions. It was found that neutrophil and RB cell aggregate formation is insensitive to initial cell ratio, highly ICAM-1 specific, and preferentially forms one-to-one aggregates (one neutrophil to one RB cell). Furthermore, it was hypothesized that a step-wise binding mechanism in which the neutrophils and RB cells first interact and form aggregates, roll on the E-selectin surface, and firmly adhere to the surface. Results from our work could lead to the design of anti-adhesion therapies that target metastatic cancer cells (especially cancer stem cells) and combat the invasive spread of cancer.

**Figure 4.1:** ABCG2+ RB cells preferentially express ICAM-1. (a) Detection of an ABCG2+/ICAM1+ subpopulation within RB143 cells labeled with FITC-conjugated anti-ABCG2 monoclonal antibody and PE-conjugated anti-CD54 (ICAM-1) monoclonal antibody. The upper right panel consists of isotype control antibodies (background), followed by panels for individual ABCG2 or ICAM-1 fluorescence. The lower right panel demonstrates double labeling and the degree of overlap between ABCG2 and ICAM-1. (b) Double immunofluorescent labeling of ABCG2 (red) and ICAM-1 (green). The same microscopic field is shown in all panels and merged with brightfield to display all cells in the field.

**Figure 4.1: ABCG2+ RB cells preferentially express ICAM-1**

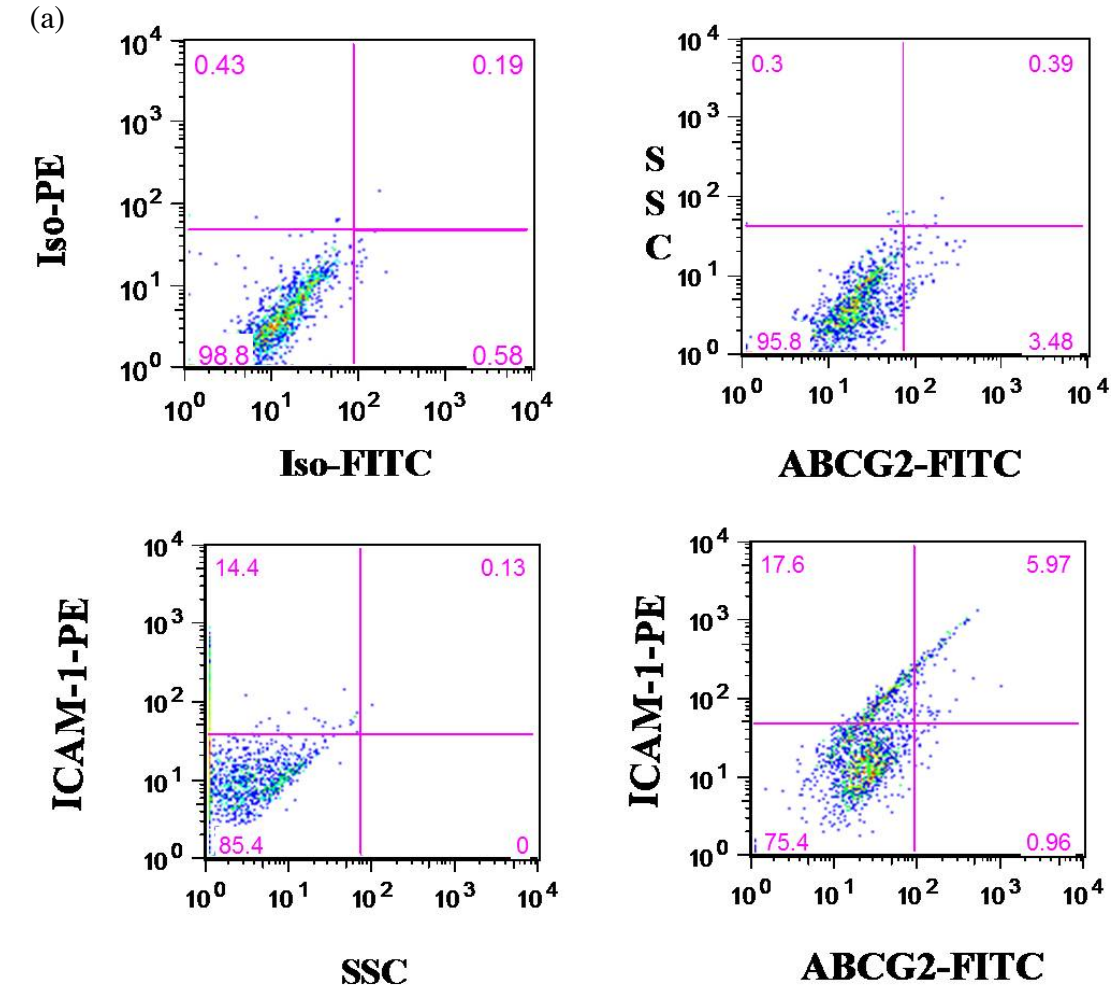


(b)

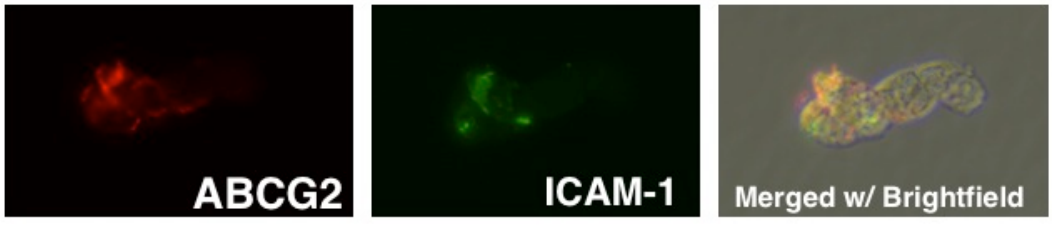

**Figure 4.2:** Aggregate Formation is ICAM-1 Specific and Insensitive to Initial Cell Ratios. RB143 and WERI-Rb27 retinoblastoma cell lines were used in the microtube aggregation assay. For both cell lines, RB cell concentration was held constant at 1 million/mL while neutrophil concentrations were varied from 2 million to 5 million/mL. Antibody blocking experiments were done using monoclonal anti-human ICAM-1 antibody. In the "E-selectin negative" experiments, the microtube surface was only incubated with protein G. In PMN-negative experiments, only RB cells were perfused in the functionalized E-selectin surface. ANOVA and student t tests were used for statistical analyses. * $p < 0.01$; ** $p<0.005$

**Figure 4.2: Aggregate formation is ICAM-1 specific and insensitive to initial cell ratios**

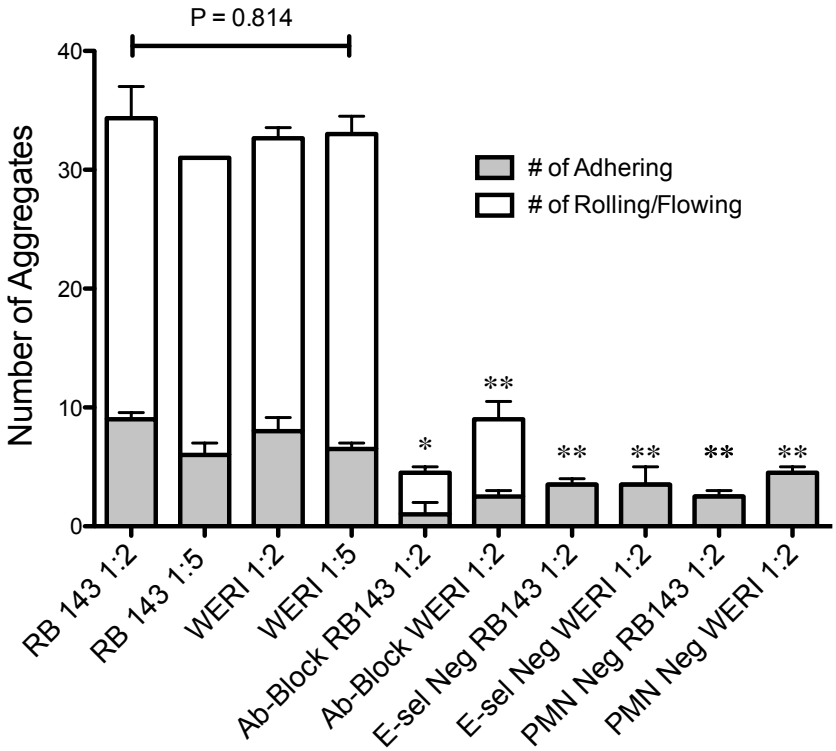

**Figure 4.3:** RB-leukocyte binding events are primarily one-to-one binding. RB143 concentration was held constant at 1 million/mL while neutrophil concentrations were varied from 2 million to 5 million/mL. 1r1p = one RB with one neutrophil observed in aggregates, etc. Student t test was used for statistical analysis. P = 0.885

**Figure 4.3: RB-leukocyte binding events are primarily one-to-one binding**

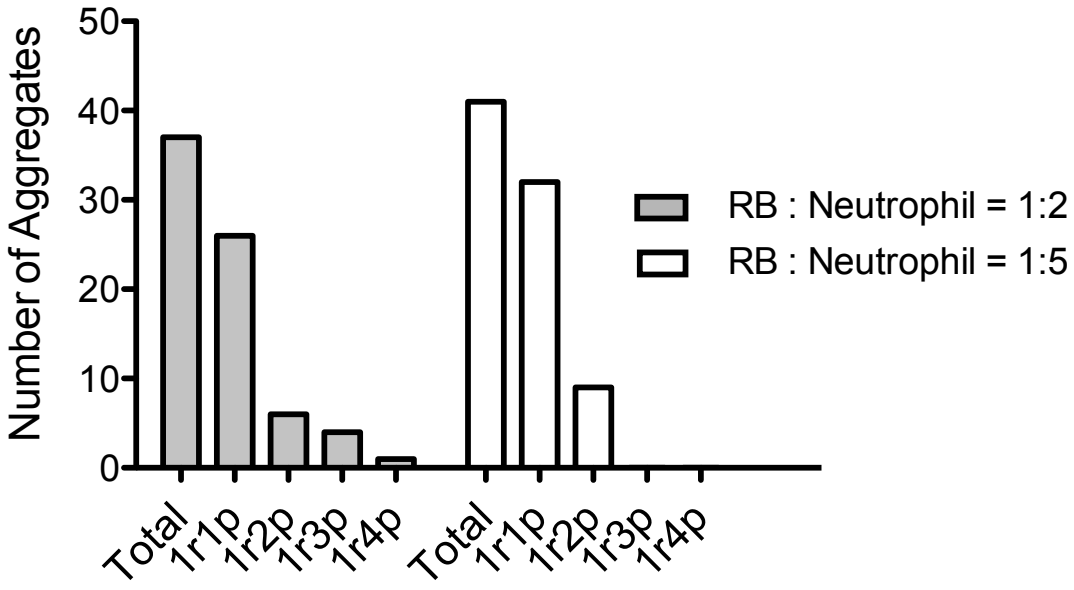

**Figure 4.4:** Bound RB is downstream to its anchoring leukocyte under physiological flow. 40 adhering one-to-one binding events were analyzed in which both the RB and neutrophil were attached to the E-selectin surface. The angle of association between RB cells and neutrophils was calculated by measuring the deviation of RB cells from a vertical line drawn straight upward from the center of the neutrophil. Average distance between the centers of RB cells and neutrophils was found to be 22 μm.

**Figure 4.4: Bound RB is downstream to its anchoring leukocyte under physiological flow**

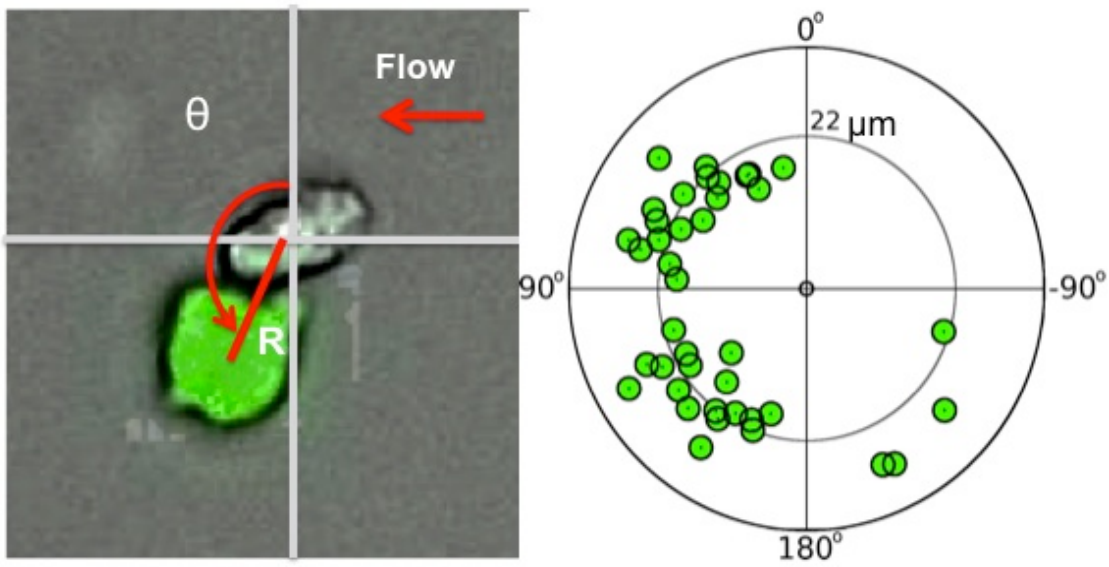

**Figure 4.5:** Hypothesis: RB cells are recruited by leukocytes in the bloodstream via LFA-1:ICAM-1 interactions. This illustration shows a three-step binding mechanism that facilitates the RB-neutrophil aggregate formation. (1) Neutrophils and RB cells are flowing in the microtube; (2) Neutrophils and RB cells interact and form aggregates; (3) The aggregates are firmly arrested to the surface through the neutrophil $sLe^x$:E-selectin binding.

**Figure 4.5: A schematic of RB cells recruited by leukocytes in the bloodstream via LFA-1:ICAM-1 interactions**

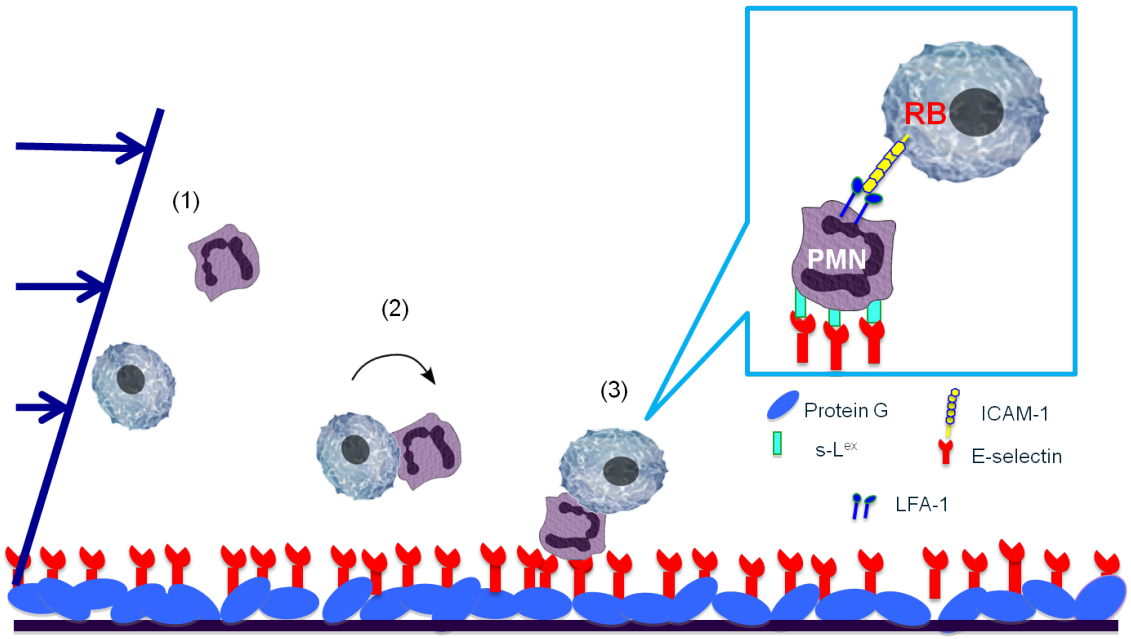

# CHAPTER 5 CHARACTERIZATION OF THE INTERACTIONS OF ENDOTHELIAL ADHESION MOLECULES WITH UNDERGLYCOSYLATED MUC1

## 5.1 THREE TO TANGO: MUC1 AS A LIGAND FOR BOTH E-SELECTIN AND ICAM-1 IN THE BREAST CANCER METASTATIC CASCADE

* This section is adapted from the following publication: Y. Geng, K. Yeh, T. Takatani, and M. R. King. *Front. Oncol.* 2:76, 2012

### 5.1.1 INTRODUCTION

The mucin family of glycoproteins is traditionally associated with the protection of the epithelial layer and provides lubrication of luminal epithelial surfaces. More recently, certain mucins have been identified as markers for metastatic cancers. Of particular importance, the mucin MUC1 is overexpressed in numerous cancers including breast, ovarian, lung, pancreatic, prostate, gastric, and colorectal cancers.[31, 221, 86, 4, 292] where high expression generally correlates with increased mortality rates.[259, 65, 93,139, 168] It is then reasonable to hypothesize that cancer's adaptation and alteration of MUC1 may play a vital role in metastatic progression.

Cancer metastasis through the bloodstream is initiated by the invasion of tumor cells from the primary site into the blood vessel.[186] These circulating tumor cells (CTCs) can then adhere to the endothelial lining, which leads to extravasation and the formation of secondary tumor sites. For CTC adhesion, cells may first establish transient interactions with the activated endothelium which facilitates cell tethering and rolling events.[246, 265, 279] These types of interactions are produced via selectins, a family of adhesion molecules expressed by the endothelium, and carbohydrate moieties, such as sialyl Lewis x ($sLe^x$) or sialyl Lewis a ($sLe^a$), present on the selectin ligands expressed by CTCs.[20, 270] Once the cell has sufficiently reduced its rolling velocity, firm adhesion can be acquired through the interaction of the intracellular cell

adhesion molecule 1 (ICAM-1) on the endothelium and integrins on CTCs. This series of events is commonly referred to as the metastatic adhesion cascade.[202]

MUC1 is not only over-expressed in many cancer types but is also aberrantly underglycosylated. The core structure of the extracellular domain of MUC1 mainly consists of 25-150 repeat units of 20 identical amino acid sequences rich in serines and threonines resulting in a length 5-10 times that of most membrane molecules. Normally, these amino acids would be heavily and richly O-glycosylated however aberrant MUC1 has been shown to express shortened oligosaccharides such as $sLe^x$ and $sLe^a$, where MUC1 has been shown to bind efficiently to E-selectin.[162] Interestingly, high levels of MUC1 carrying $sLe^{x/a}$ correlates to poor prognosis in patients with lung adenocarcinoma.[113] Aberrant MUC1 also has the propensity to expose its core epitope due to underglycosylation where it has become the target of various probes to determine MUC1 expression.[184] Furthermore, ICAM-1 has been shown to recognize and bind to the core epitope of MUC1.[100] Therefore, CTCs may utilize aberrant MUC1 to facilitate tethering and rolling due to the increased length of MUC1 relative to other selectin ligands, and firmly adhere the cell via ICAM-1 interactions.[219]

In this study, we investigate the role of MUC1 in breast cancer cell adhesion under flow with two cell lines: ZR-75-1 which is known to have a high metastatic potential, and MCF7 which is weakly metastatic. The differential adhesion of these two cell lines to the endothelium are studied *in vitro* via micro-renathane tubes coated with varying ratios of E-selectin and ICAM-1 which represent a model of metastasis-prone microvasculature.[72] We hypothesize that the underglycosylated form of MUC1

may serve as a ligand for both E-selectin and ICAM-1, which will allow for efficient interaction between CTCs in transit and the inflamed endothelium.

### 5.1.2 MATERIALS AND METHODS

*Reagents*

Recombinant E-selectin-$IgG_1$ chimera and recombinant ICAM-1-$IgG_1$ chimera were purchased from R&D systems (Minneapolis, MN). Blotting grade blocker non-fat dry milk was obtained from Bio-Rad Laboratories (Hercules, CA) and Protein-G was purchased from EMD Biosciences (San Diego, CA). FITC mouse anti-human CD227 (clone HPMV), FITC Mouse IgG1 k isotype control, purified mouse anti-human CD15s (clone CSLEX), APC rat anti-mouse IgM, and FITC goat anti-mouse IgG/IgM were all purchased from BD Biosciences (San Jose, CA). FITC mouse anti-human CD44v4 was obtained from AbD Serote (Germany). FITC and APC anti-human IgG antibodies were purchased from Invitrogen (Carmarillo, CA). $Ca^{2+}$ and $Mg^{2+}$ free DPBS (Invitrogen, Camarillo, CA, USA), calcium carbonate (Sigma Chemical Co., St. Louis, MO, USA), and low endotoxin (1 ng/mg), essentially globulin-free Bovine Serum Albumin (Sigma Chemical Co., St. Louis, MO, USA) were used to prepare flow buffer for cell adhesion assays.

*Breast Cancer Cell Culture*

Breast cancer cell lines ZR-75-1 and MCF7 were purchased from ATCC and maintained in 10% Fetal Bovine Serum (FBS; Cellgro), 1% penicillin-streptomycin (Invitrogen), and RPMI 1640 medium (ZR-75-1) or eagle's minimal essential medium

with 0.01 mg/mL bovine insulin (MCF7) at 37°C with 5% $CO_2$ in a humidified incubator.

*Flow Cytometry*

Cells were removed from tissue culture flasks prior to antibody incubation using an enzyme-free cell dissociation buffer solution. After washing with 1x DPBS, the cells were resuspended in 1% BSA in DPBS to a final concentration of approximately 250,000 cells in each sample. Antibodies against MUC1 or appropriate isotype controls were added to the cell suspensions and incubated over ice for 45 min. Specifically, mouse anti-human MUC1 mAb clone HPMV (reacts with the peptide core of MUC1) and mouse anti-human MUC1 mAb clone SM3 (recognizes the underglycosylated form of MUC1) were used in this study. Following incubation, cells were washed twice with 500 μL of 1% BSA to remove any unbound antibody. Flow cytometry samples were analyzed using a BD Accuri C6 flow cytometer (Ann Arbor, MI). .

*Soluble ICAM-1 Binding Assay*

Recombinant human ICAM-1-$IgG_1$ chimeric protein (R&D) was fluorescently tagged with Alexa 647 anti-human IgG antibody and incubated with ZR-75-1 and MCF7 cells in 1XDPBS with 2% BSA for 30 min at room temperature. Unbound proteins were washed off with 1XDPBS twice prior to flow cytometry and confocal microscopy imaging.

*Preparation of Combined Protein Surfaces*

Micro-renathane tubing (microtube) with an inner diameter of 300 μm (Braintree Scientific Inc., Braintree, MA, USA) were cut to lengths of 50 cm. Recombinant human E-selectin-$IgG_1$ and ICAM-1-$IgG_1$ chimeric proteins were each dissolved in 1x PBS and mixed in various ratios (E-sel/ICAM-1: 10/0, 7.5/2.5, 5/5, 2.5/7.5, 0/10) to a final protein concentration of 10 μg/mL. The microtube surface was first rinsed with 1x DPBS and then incubated with 10 μg/mL of protein-G solution for 1 h, followed by a 2 h incubation with the premixed E-selectin and ICAM-1 protein solution, then blocked with 5% milk protein in PBS for 1 h. To evaluate the correlation between incubation concentrations and surface coverage, FITC conjugated E-selectin and APC conjugated ICAM-1 were mixed in the ratios described above. Fluorescence images were taken and analyzed using Image J (http://rsbweb.nih.gov/ij/).

*Cell Adhesion Assay*

After surface functionalization as described above, microtubes were secured to the stage of an Olympus IX81 motorized inverted microscope (Olympus America, Melville, NY). A CCD camera (model no: KP-M1AN, Hitachi, Tokyo, Japan) and a DVD recorder (model no: DVD-1000MD, Sony Electronics) were used to record experiments for offline analysis. ZR-75-1 and MCF7 breast cancer cells suspended in flow buffer were perfused through protein coated microtubes using a syringe pump (KDS 230, IITC Life Science, Woodland Hills, CA) at a wall shear stress of 1.0 dyne/$cm^2$.

*Confocal Immunofluorescence Microscopy*

ZR-75-1 and MCF7 cells were removed from tissue culture flasks, washed with 1X DPBS, resuspended with 2% BSA in 1X DPBS, loaded to a pre-assembled cytospin cuvette, and spun at 750 rpm for 3 min in a Shandon Cytospin 3 centrifuge (Harlow Scientific, Arlington, MA). Cytospin slides were than dried and fixed with 4% paraformaldehyde (Electron Microscopy Sciences, Hatfield, PA) prior to antibody labeling. Indirect surface staining for MUC1 was performed using mouse anti-human MUC1 mAb (clone SM3) and Alexa 647 rat anti-mouse mAb as a secondary antibody. For some cytospin slides, nuclear staining with DAPI was performed for 10 min at room temperature prior to imaging. Samples from the soluble ICAM-1 binding assay were deposited on cytospin slides for imaging. A Zeiss 710 laser scanning confocal microscopy at the Cornell University microscopy and imaging core facility was used to collect images at 40X magnification.

*Data Acquisition and Analysis*

‘‘Rolling’’ cells were defined as those observed to translate in the direction of flow with an average velocity less than 50% of the calculated hydrodynamic free stream velocity. The rolling velocity was calculated by measuring the distance a rolling cell traveled over a 30 second interval. Videos of rolling cells were taken at three randomly selected locations along the microtube. “Tethering” cells were defined as cells that were observed to roll intermittently with fluctuating velocity. The quantity of cells rolling, adherent and tethering was determined by recording images at 30 randomly selected locations along the microtube. All errors are reported as standard

error of the mean, and statistical analyses were performed using Prism (GraphPad Software, San Diego, CA).

*Molecular Dynamics*

The crystal structure of SM3 bound to the MUC1 core fragment (1SM360) was obtained from the Protein Data Bank for use as starting coordinates. The MUC1 fragment was equally extended beyond the SM3:MUC1 interaction to include all amino acids of one complete tandem repeat unit (PATSGPAPRTDPASTVGHAP) and the furthest threonine/serine from SM3 was O-glycosylated with the $sLe^x$ carbohydrate group. Using the YASARA (http://yasara.org) package of molecular dynamics (MD) programs, the complex was solvated in a water cube with an initial length of 100 Å to allow for free protein rotation and neutralized to 0.9% NaCl with physiologically neutral pH (7.4). The YAMBER3 self-parameterizing force field[145] was implemented with periodic boundary conditions, the particle mesh Ewald method for electrostatic interactions,[68] and a recommended 7.86 Å force cutoff for long-range interactions. Temperature and pressure were held constant at 300 K and 1 atm, respectively, while the water box was allowed to adjust slightly to constrain the water density to 0.997 g/L. Conformational stresses were then removed via short steepest descent minimizations and simulated annealing was run until sufficient convergences were reached. A free dynamics simulation was then run for 10 ns to obtain the final equilibrated structure.

### 5.1.3 RESULTS

*Differential MUC1 Expression on ZR-75-1 and MCF7 Cells and Their Ability to Bind to ICAM-1 under Static Conditions*

MUC1 core peptide expression was measured for both ZR-75-1 and MCF7 cells via flow cytometry using MUC1 mAb clone HPMV and found to be significantly higher on ZR-75-1 cells (Figure 5.1a). MUC1 mAb clone SM3 was also used to detect the underglycosylated form of MUC1, which has been identified as a tumor associated form of MUC1 181. Although no significant shift was observed, mean fluorescence intensity of sample/isotype for ZR-75-1 cells was observed to be five times higher than MCF7 cells (Figure 5.1b). Furthermore, confocal microscopy images with MUC1 antibody (SM3) labeling showed brighter signals on ZR-75-1 cells (Figure 5.1c). Strong homogenous cytoplasmic staining of MUC1 (SM3) was observed on some ZR-75-1 cells (Figure 5.1c right) but not on MCF7 cells. To assay MUC1:ICAM-1 binding under static conditions, human recombinant ICAM-1 was conjugated with a fluorescently tagged secondary antibody and incubated with both cell types. Flow cytometry and confocal microscopy results both show significantly stronger binding of ICAM-1 to ZR-75-1 cells compared to MCF7 cells (Figure 5.1d).

*E-selectin Ligand and Binding Moiety Expression on ZR-75-1 and MCF7 cells*

The mean fluorescence intensity (MFI) ratios of sample over isotype control for the E-selectin binding moiety $sLe^x$ expression on ZR-75-1 and MCF7 were found to be 8.43 and 8.56, respectively, via flow cytometry (Figure 5.2a). CD44 variant 4 (CD44v4), among the multiple variants of common E-selectin ligand CD44, has been identified as

a major E-selectin ligand for breast cancer cells.[287] CD44v4 expression was measured on ZR-75-1 and MCF7 cells via flow cytometry and no significant difference was observed (Figure 5.2b).

*E-selectin and ICAM-1 Combined Surface*

The initial layer of protein G orients the adhesion molecules to maximally interact with cell surfaces as the cells are perfused through the tubes. As the E-selectin:ICAM-1 concentration ratios were increased, the fluorescence intensity of bound E-selectin in the microtube was found to linearly increase while ICAM-1 fluorescence linearly decreased (Figure 5.2c), verifying the desired protein concentrations on the microtube surfaces.

*MUC1 is Involved in the Cancer Adhesion Cascade in Association with E-Selectin and Its Ligands*

Figures 5.3a and 5.3b divide the cells that interact with the surface into three categories: tethering, rolling, and adherent. ZR-75-1 cells were found to roll quite consistently when E-selectin was present at any concentration on the surface where there was a slight decrease in the percent of rolling cells as the E-selectin concentration decreases (Figure 5.3a). Conversely, the percent of ZR-75-1 tethering cells increased as the E-selectin:ICAM-1 ratio decreased. Interestingly, adherent ZR-75-1 cells were observed only when both E-selectin and ICAM-1 exist on the surface and 7.5:2.5 was found to be the optimal ratio of E-selectin:ICAM-1 that yields the greatest number of adherent cells. However, as the E-selectin:ICAM-1 ratio decreased

so did the percent of adherent cells. On the other hand, MCF7 rolling and tethering showed little sensitivity to varying the E-selectin:ICAM-1 ratios where MCF7 tethering cells only slightly increased as the ratio decreased, as shown in Figure 5.1b. Most notably, no adherent MCF7 cells were observed on the surface for any concentration ratio. For both ZR-75-1 and MCF7 cells, when only ICAM-1 coats the surface no cells interacted adhesively. Anti-MUC1 mAb (clone SM3) was found to block the adhesive interactions on ZR-75-1 cells with the surface, leaving only the tethering and rolling populations (Figure 5.3c).

The cell flux for each cell type (Figures 5.1.4a-c) shows little sensitivity to the combined surface concentration ratios. However, overall the ZR-75-1 cell flux is much greater than both MCF7 and SM3 blocked ZR-75-1 cell fluxes, roughly by a factor of 2. Comparing ZR-75-1 to MCF7 and SM3 blocked ZR-75-1 cells, the cell fluxes inversely correlate with the cell rolling velocities as shown in Figures 5.5a and 5.5b where the ZR-75-1 cell rolling velocities were found slower than MCF7 cell rolling velocities. For example, for surfaces coated with only E-selectin, MCF7 cells rolled at approximately 6-7 μm/s whereas ZR-75-1 cells roll at approximately 2 μm/s. SM3 blockade was found to cause an increase in rolling velocity to approximately 4 μm/s, significantly faster than untreated cells. A structure of SM3 bound to the underglycosylated core epitope of MUC1 is depicted in Figure 5.5c, where SM3 not only blocks ICAM-1 interactions, but is sufficiently bulky compared to $sLe^x$ to inhibit some amount of E-selectin interactions as well. Unlike cell flux, both ZR-75-1 (untreated and blocked) and MCF7 cell rolling velocities were sensitive to the E-selectin concentration where cell rolling velocities increased as the E-selectin

concentration decreased (Figure 5.5a and 5.5b). Furthermore, the MCF7 cell rolling velocity at the lowest E-selectin concentration was double that of the cell rolling velocity at the highest E-selectin concentration which shows a greater sensitivity to E-selectin compared to ZR-75-1 cells.

### 5.1.4 DISCUSSION

The detection and enumeration of circulating tumor cells (CTCs) holds great potential in breast, colorectal, and prostate cancer prognosis, yet the basic biophysics of how these CTCs interact with the endothelium is not fully understood. Similar to leukocyte recruitment to the endothelium, CTC tethering and rolling on the blood vessel wall under hydrodynamic shear stress are also mediated by the selectin family of adhesion molecules.[82] After stable rolling on the endothelium, leukocytes can firmly adhere to the inflamed endothelium via leukocyte beta-2 integrin (Mac-1, LFA-1): ICAM-1 binding.[55, 58,129] Similarly for epithelial-type CTCs, tumor associated MUC1 may play the role of beta-2 integrins on leukocytes by binding ICAM-1 to enable firm adhesion and initiate subsequent events in the metastatic cascade.[216]

Tumor associated MUC1 on breast cancer cells was first identified as a novel adhesion ligand for endothelial ICAM-1 by Regimbald *et al.* via static adhesion assays between MCF7 cells and stimulated HUVEC cells as well as immobilized recombinant ICAM-1.[219] MCF7 cells do not express common ICAM-1 ligands, such as LFA-1, Mac-1, or CD43. However under static conditions, MUC1 was found to interact with ICAM-1, which could mediate firm adhesion of CTCs to the inflamed endothelium. In contrast, we characterized the adhesive role of tumor associated

MUC1 under hydrodynamic shear stress by perfusing both ZR-75-1 (which overexpresses MUC1) and MCF7 cells through functionalized microtubes, more representative of the blood vessel microenvirnoment. Furthermore, the inflamed endothelium was simulated by immobilizing both E-selectin and ICAM-1 with varying ratios on the microtube surface, creating a more physiologically relevant and controllable environment to study the adhesion events of circulating ZR-75-1 and MCF7 cells under flow.

ZR-75-1 cells show a much greater expression of underglycosylated MUC1 compared to MCF7 cells, which significantly affects their adhesion behavior when perfused through the combined surface microtubes. Interestingly, although ZR-75-1 and MCF7 cells have similar expression levels of $sLe^x$, one of the E-selectin binding moieties, ZR-75-1 cells roll on the combined protein surface at a significantly slower rolling velocity, indicating that ZR-75-1 cells establish stronger interactions with E-selectin. Recall that underglycosylated forms of MUC1 also contain shortened oligosaccharides where $sLe^x$ is one of the most common carbohydrates of aberrant MUC1.[31] Therefore MUC1, when appropriately decorated with $sLe^x$ in its underglycosylated form, is expected to extend further from the cell surface compared to other selectin ligands due to its size and is perhaps more able to interact with E-selectin to efficiently mediate tethering and rolling events. The greater rolling velocities of ZR-75-1 cells blocked with SM3 also suggests MUC1 as an important E-selectin ligand because SM3 could inhibit some amount of E-selectin:MUC1 interactions due to the size of SM3 compared to $sLe^x$ (Figure 5.5c). As a result of the slower rolling velocity and greater MUC1 expression, only ZR-75-1 cells firmly

adhered to the combined surface, where firm adhesion is facilitated by MUC1:ICAM-1 interactions. In our study, the observation of firmly adhered cells to the combined surface under shear stress is consistent with the metastatic potential of the ZR-75-1 cell line (highly metastatic) and the MCF7 cell line (weakly metastatic).

In conclusion, we propose a mechanism by which MUC1 can act as a ligand for E-selectin, initiating tethering and rolling events of CTCs on the endothelium, and subsequently serve as an ICAM-1 ligand, mediating firm adhesion of CTCs (Figure 5.6). The synergistic effect of MUC1:E-selectin and MUC1:ICAM-1 may play an important role in breast cancer metastasis through the bloodstream where underglycosylated MUC1 can significantly slow the rolling velocity of CTCs thereby allowing for more frequent occurrence of firm adhesion events and subsequent extravastion. In summary, our results provide new insights into the roles of MUC1 in the metastatic adhesion cascade and suggests future examination into clinical aspects where the underglycosylated form of MUC1 can be targeted since aberrantly underglycosylated MUC1 expression is highly correlated to poor prognosis in breast and colon cancer patients.

**Figure 5.1:** MUC1 expression and ICAM-1/E-selectin binding capabilities of ZR-75-1 and MCF7 cells. (a) Flow cytometry histogram plots of ZR-75-1 and MCF7 labeled with anti-MUC1 mAb clone HPMV, respectively. (b) Quantification of the mean fluorescence intensity (MFI) ratio of sample/isotype for both cell types with anti-MUC1 mAb clone SM3 and HPMV, respectively. Student's t-test was used for statistical analysis and results from both labeling experiments were found to be significantly different for ZR-75-1 and MCF7 cells ($p \leq 0.01$). (c) Left and middle: confocal microscopy images of MCF7 and ZR-75-1 labeled with anti-MUC1 mAb (clone SM3), respectively. Right: strong signal of SM3 anti-MUC1 mAb in the cytoplasmic region of selective ZR-75-1 cells. (d) Left: flow cytometry histogram of fluorescently tagged ICAM-1 labeling on ZR-75-1 and MCF7 cells. Middle and right: confocal microscopy images of MCF7 and ZR-75-1 cells labeled with fluorescently tagged ICAM-1.

**Figure 5.1: MUC1 expression and ICAM-1/E-selectin binding capabilities of ZR-75-1 and MCF7 cells**

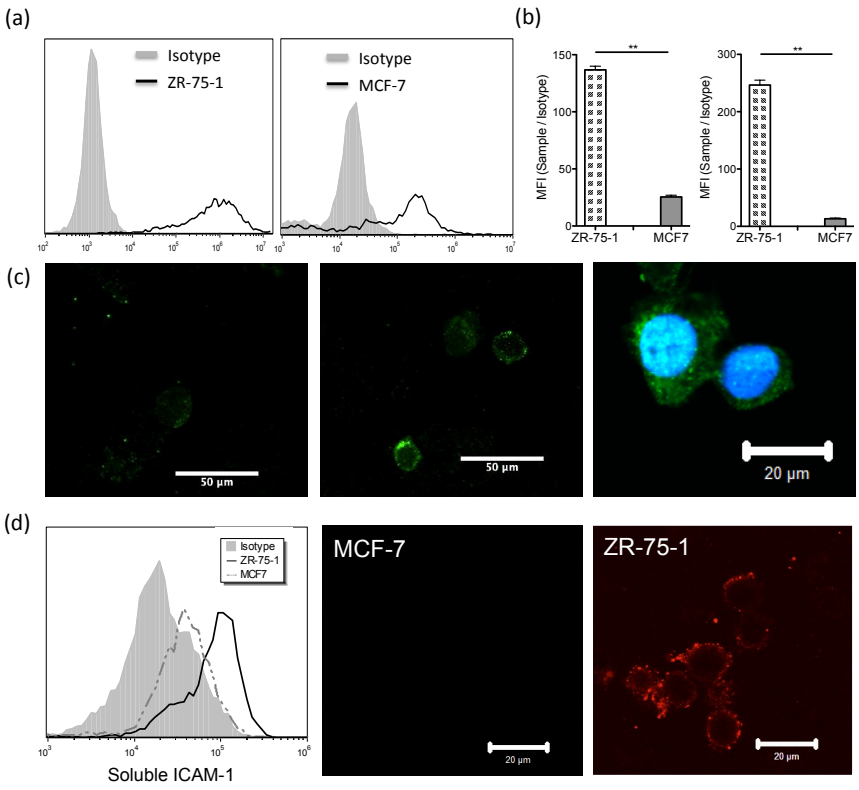

**Figure 5.2:** Characterization of ligand expression and surface functionalization. (a) and (b) Flow cytometry histogram overlays of ZR-75-1 and MCF7 cells labeled with anti-sLe$^x$ (clone CSLEX ) mAb and anti-CD44V4 mAb, respectively. (c) E-selectin and ICAM-1 fluorescence intensities as concentration ratios vary during surface preparation. The $r^2$ values for E-selectin and ICAM-1 fluorescence intensity trend lines were found to be 0.986 and 0.995, respectively.

**Figure 5.2: Characterization of ligand expression and surface functionalization**

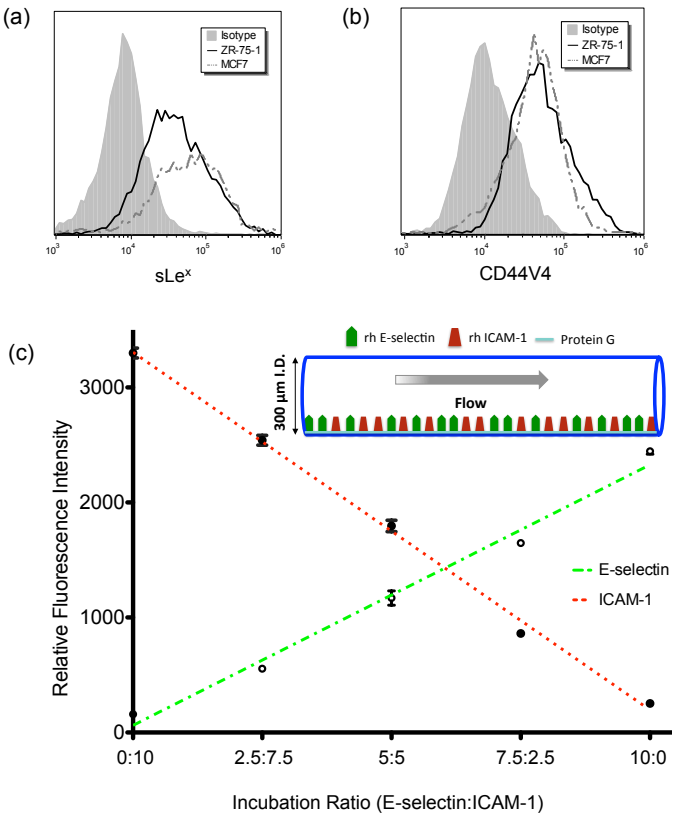

**Figure 5.3:** Adhesion phenotypes on combined protein surface under physiological flow of (a) ZR-75-1, (b) MCF7, and (c) SM3 blocked ZR-75-1 cells. Two-way ANOVA was used for statistical analysis and results from all conditions were found to be significantly different ($p \leq 0.001$).

**Figure 5.3: Adhesion phenotypes of ZR-75-1 and MCF7 cells on combined protein surfaces**

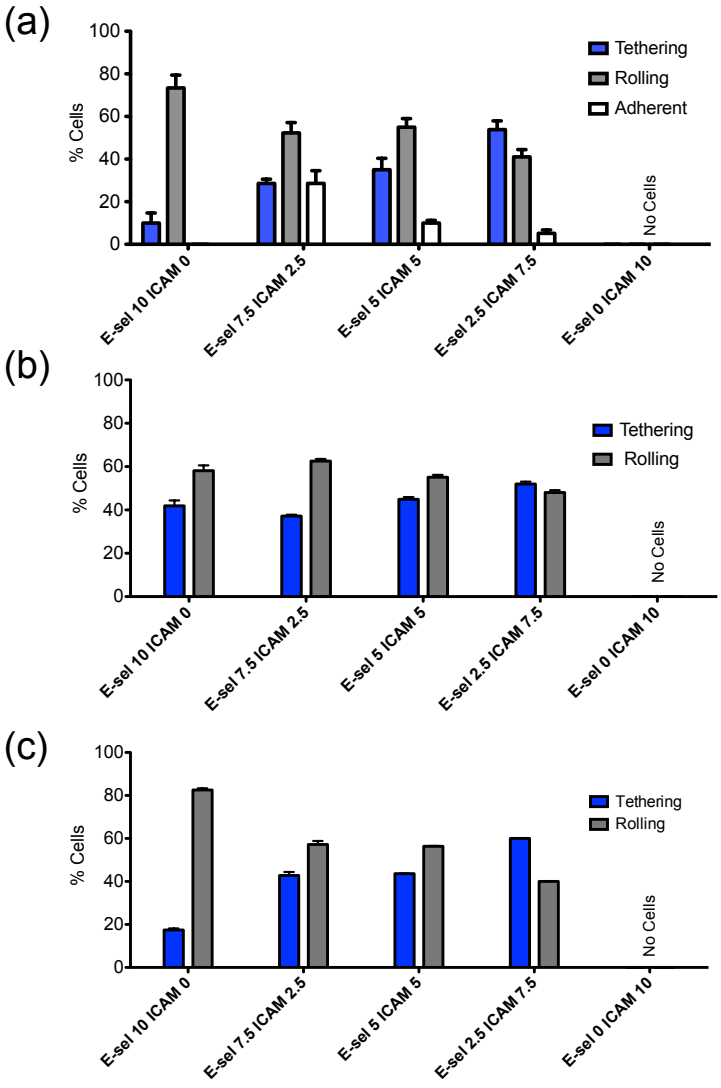

**Figure 5.4:** Quantification of average number of cells captured on the surfaces with varying ratios of E-selectin and ICAM-1 for (a) ZR-75-1, (b) MCF7, and (c) SM3 blocked ZR-75-1 cells. One-way ANOVA was used for statistical analysis. For all three experiments, results from all conditions were found to be significantly different with p values of 0.0008, 0.0093, and 0.0016 for ZR-75-1, MCF7, and SM3 blocked ZR-75-1, respectively. ** $p \leq 0.01$ *** $p \leq 0.001$

**Figure 5.4: Quantification of average number of cells captured on the combined surfaces with varying ratios of E-selectin and ICAM-1**

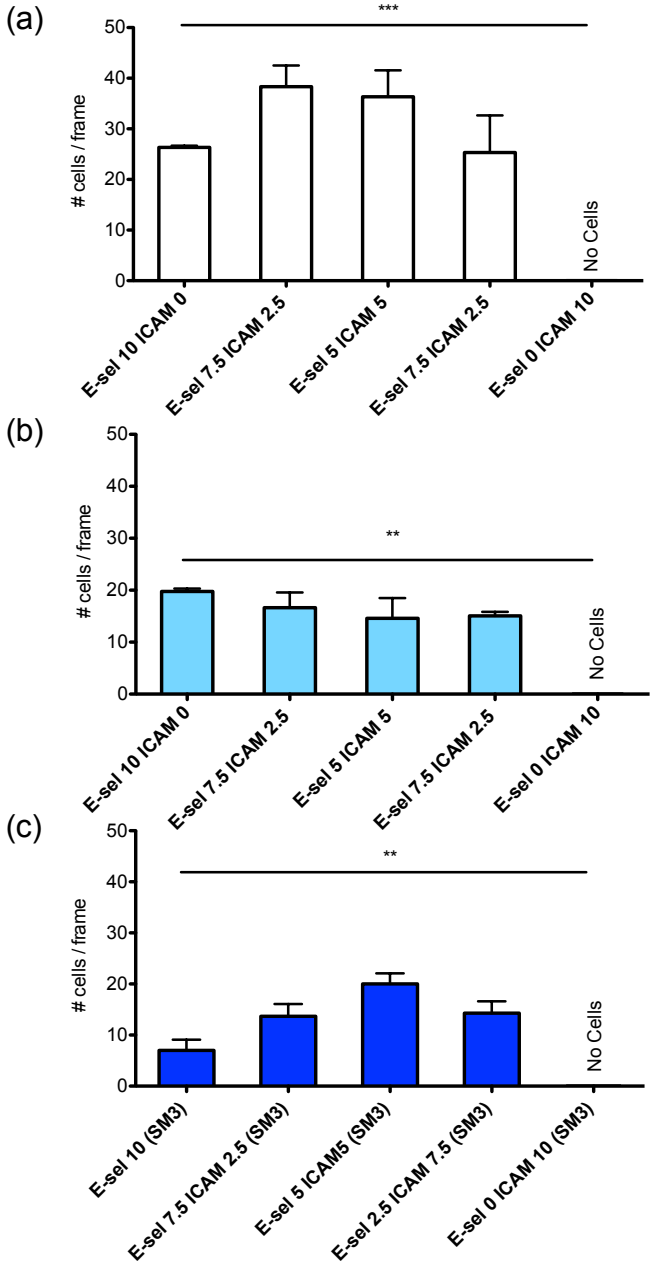

**Figure 5.5:** Adhesion profile of SM3 blocked ZR-75-1 and MCF7 cells. (a) and (b) Rolling velocities of ZR-75-1 (untreated and blocked) and MCF7 cells on combined and E-selectin surfaces with varying incubation concentrations under flow, respectively. (c) Equilibrated structure of SM3 (gray) bound to the core epitope of one repeat unit of MUC1 (red) singly O-glycosylated with $sLe^x$ (blue) on a threonine residue. Below is the amino acid sequence of a MUC1 repeat unit where the bracket indicates the interaction site of SM3 and the blue arrow indicates the chosen O-glycosylated amino acid. Student's t-test and ANOVA were used for statistical analysis. * $p \leq 0.05$ *** $p \leq 0.001$ NS: non-significant

**Figure 5.5: Adhesion profile of SM3 blocked ZR-75-1 and MCF7 cells**

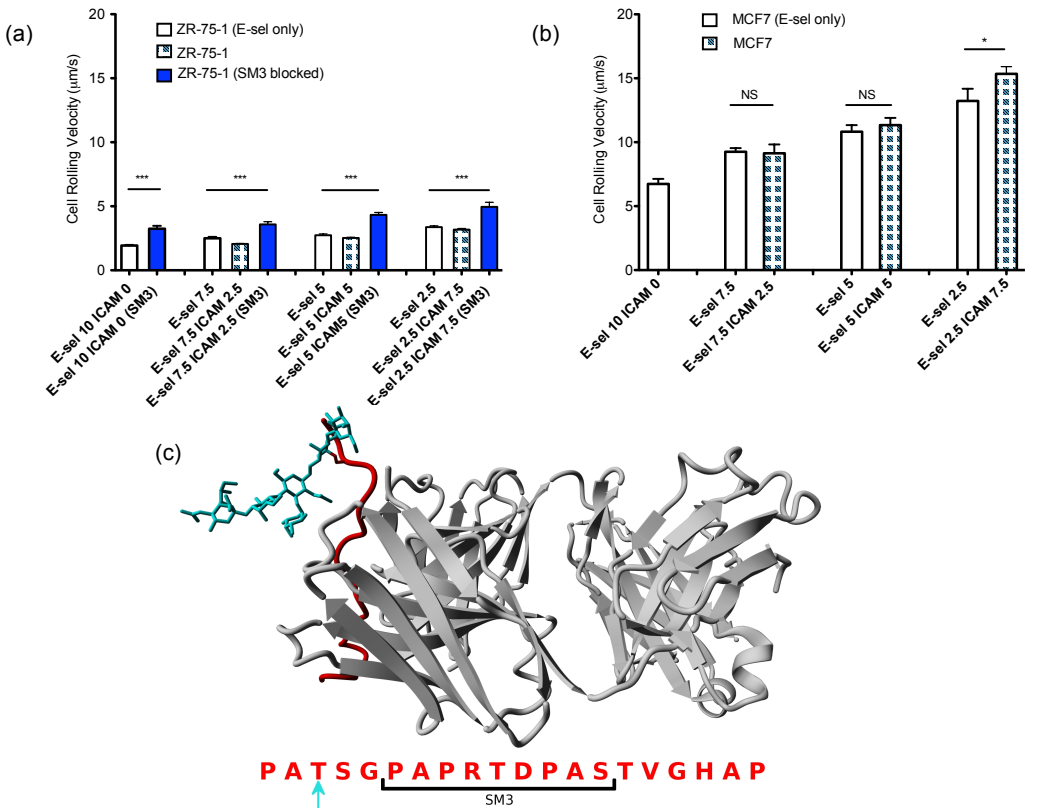

**Figure 5.6:** Proposed mechanism by which MUC1 can act as a ligand for E-selectin, initiating tethering and rolling events of CTCs on the endothelium, and subsequently serve as an ICAM-1 ligand, mediating firm adhesion of CTCs.

**Figure 5.6: A schematic of MUC1 as a ligand for both E-selectin and ICAM-1**

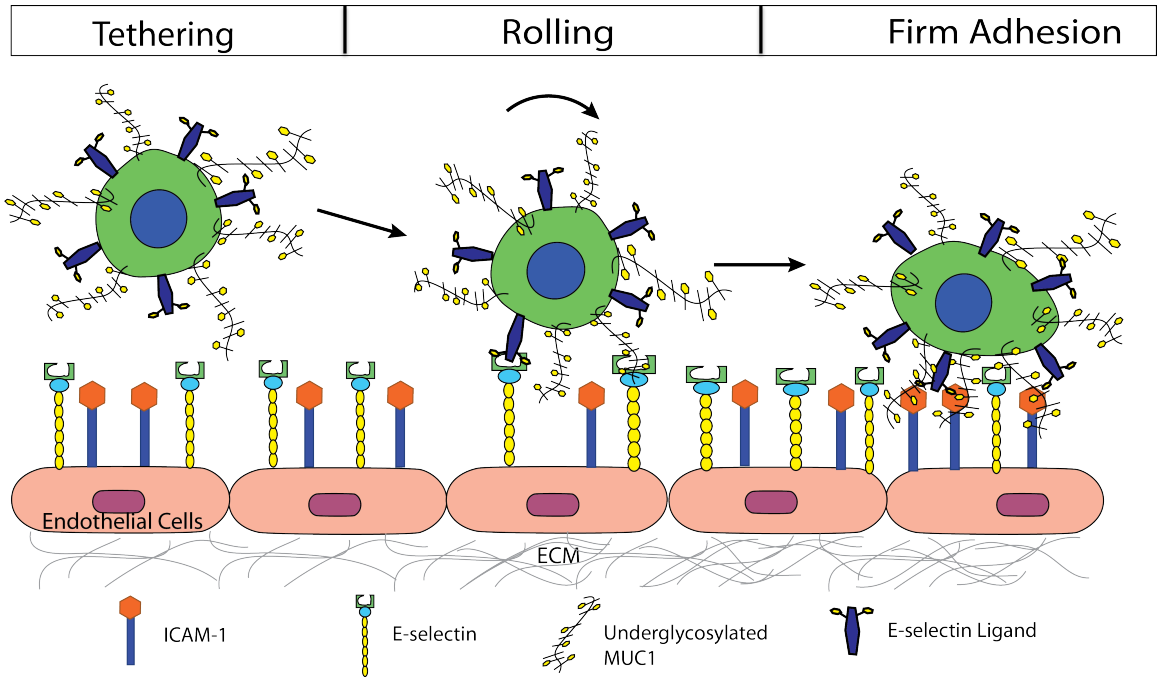

## 5.2 TARGETING UNDERGLYCOSYLATED MUC1 FOR THE SELECTIVE CAPTURE OF HIGHLY METASTATIC BREAST CANCER CELLS UNDER FLOW

*This section is adapted from the following publication: Y. Geng, T. Takatani, K. Yeh, J. W. Hsu, and M. R. King. *Cellular and Molecular Bioengineering*. 6:148-159, 2013

### 5.2.1 INTRODUCTION

Leukocyte recruitment to the inflamed endothelium and cancer metastasis through the bloodstream via circulating tumor cells (CTCs) have been proposed to share a similar stepwise mechanism that allows for cell adhesion and extravasation.[82, 186, 202, 239, 243] Referred to as adhesion cascades (leukocyte and CTC), cells first tether and roll on the blood vessel wall via transient interactions between P- and E-selectin present on the inflamed endothelium[34, 243] and carbohydrate moieties, such sialyl Lewis X ($sLe^x$) or sialyl Lewis a ($sLe^a$) found on leukocytes and CTCs.[240, 241] Sufficiently slow cell rolling permits firm cell adhesion events mediated by endothelial intercellular adhesion molecule-1 (ICAM-1) at locations of transendothelial migration.[18, 72] Work by our group has capitalized on these selectin:carbohydrate based interactions to capture CTCs as well as hematopoietic stem and progenitor cells with the ability to maintain cell viability.[110, 111, 194, 195] Further differentiation between CTCs and contaminating leukocytes will allow isolation processes to be further optimized with respect to both yield and purity.

Three cell adhesion molecules constitute the members of the selectin family. E-selectin, primarily expressed by inflamed endothelial cells, has been extensively

studied for its role in leukocyte recruitment in response to vascular injury[157] as well as CTC adhesion.[82, 120] P-selectin is a granule protein expressed by both platelets and endothelial cells, and therefore has been linked to the adhesion of platelets,[99] leukocytes,[173] and cancer cells[126] to the endothelium. L-selectin differs in that it is expressed by lymphocytes and leukocytes, not endothelial cells, and therefore is not normally considered in the context of cancer cell adhesion. All selectins contain the epidermal growth factor and lectin domains where the carbohydrate moieties can bind via calcium dependent interactions.[175] These carbohydrate moieties are attached to O-glycosylated proteins on the cell surface, referred to as selectin ligands, and in the context of cell adhesion to the vascular wall, both the metastatic and leukocyte adhesion cascades rely on similar selectin ligands to facilitate initial tethering and rolling events.[23, 268]

Leukocytes express three main selectin ligands: P-selectin glycoprotein ligand 1 (PSGL-1), E-selectin ligand (ESL-1), and CD44.[103] CTCs, on the other hand, not only potentially express these three selectin ligands[56, 261] but also a myriad of other selectin ligands such as CD24, CD43, CEA, and PCLP.[2, 260, 261, 288] Recently two novel E-selectin ligands, mainly present on breast cancer cells, have been postulated: Mac-2BP[237] and MUC1.[69, 288, 289] Interestingly, the underglycosylated form of MUC1 (uMUC1) has been shown to be upregulated in various breast cancer cells43, 184 and clinically, high uMUC1 expression is correlated to poor prognosis and increased metastases.[267] Moreover, the core of MUC1 has also been shown to be an ICAM-1 ligand.[100] Motivated by these findings, we recently elucidated the synergistic role of uMUC1 as both E-selectin and ICAM-1 ligands during the CTC adhesion cascade.[84]

Although selectin ligands can potentially bind to all three selectins via calcium:carbohydrate dependent binding, selectin ligands often preferentially bind to particular selectins. Hidalgo *et al*. attempted to clarify the specific functions of each selectin ligand during the leukocyte adhesion cascade.[103] PSGL-1, which preferentially binds to P- and L-selectin,[241] was found responsible for the initial capture and tethering of leukocytes. ESL-1, which preferentially binds to E-selectin,[249] generated rolling cells from tethering events. Lastly, CD44 interactions with E-selectin have been found to control cell rolling velocity.[103] L-selectin (present on leukocytes) is polarized after leukocyte firm adhesion where further possible interactions with PSGL-1 on other leukocytes in the bloodstream can occur. It is also possible for L-selectin to interact with E-selectin on the endothelium to further enhance cell capture.[291] Our group has exploited this selectin preference while studying the efficiency of halloysite nanotubes on CTC capture,[110, 111] where P-selectin was utilized when cells expressed PSGL-1 and E-selectin was used otherwise. We have also found that pathologically decreasing extracellular pH can enhance PSGL-1 binding to P- and L-selectin, while having no effect on E-selectin:PSGL-1 binding.[35] Taken together, the use of different selectins can offer another axis of control to more efficiently and selectively capture CTCs.

In our previous study of MUC1, we examined the adhesion profiles of ZR-75-1 and MCF7 cells on combined surfaces of E-selectin and ICAM-1.[84] We found that whereas both cell lines exhibited high levels of MUC1, only ZR-75-1 cells exhibited uMUC1 which lead to slower rolling velocities (facilitated by E-selectin) and the existence of firm adhesion events (facilitated by ICAM-1) which strongly suggested

that the uMUC1 glycoprotein significantly participates in the adhesion of metastatic cancer cells to the inflamed endothelium. To extend the E-selectin/ICAM-1 combined surface study in the context of cell adhesion facilitated by uMUC1, we first utilize the ZR-75-1 and T47D cell lines, which both have been shown to express high levels of uMUC1, to further characterize the differential adhesion of uMUC1 to E-selectin coated surfaces. We then explore the preferential binding of uMUC1 to E-, P-, and L-selectin via experimental rolling assays under shear stress and molecular dynamics (MD) simulations. Since uMUC1 is only expressed by CTCs in the bloodstream, we further hypothesize that utilizing a combined E-selectin and SM3 (antibody that specifically binds to uMUC1) surface may provide a novel approach to target CTCs for capture or treatment, where the E-selectin:uMUC1 interactions facilitate cell rolling and the SM3:uMUC1 interactions selectively capture rolling CTCs.

### 5.2.2 MATERIALS AND METHODS

*Reagents*

Recombinant human E-selectin-IgG chimera was purchased from R&D systems (Minneapolis, MN). Blotting grade blocker non-fat dry milk was purchased from Bio-Rad Laboratories (Hercules, CA) and Protein-G was purchased from EMD Biosciences (San Diego, CA). FITC mouse anti-human CD227 (clone HPMV), FITC Mouse IgG1 k isotype control, purified mouse anti-human CD15s (clone CSLEX), APC rat anti-mouse IgM, FITC mouse anti-human CD44, and FITC goat anti-mouse IgG/IgM were all purchased from BD Biosciences (San Jose, CA). Mouse anti-human MUC1 mAb clone SM3 (recognizing the underglycosylated form of MUC1) was

purchased from Abcam (Cambridge, MA). Mouse anti-human CA19-9 ($sLe^a$) was purchased from Santa Cruz Biotechnology (Santa Cruz, CA). APC anti-human IgG antibodies were purchased from Invitrogen (Carmarillo, CA). $Ca^{2+}$ and $Mg^{2+}$ free DPBS (Invitrogen, Camarillo, CA, USA), calcium carbonate (Sigma Chemical Co., St. Louis, MO, USA), and low endotoxin (1 ng/mg), essentially globulin-free Bovine Serum Albumin (Sigma Chemical Co., St. Louis, MO, USA) were used to prepare flow buffer for cell adhesion assays. CELLview™ glass bottom dishes from Greiner Bio-one were used to plate cells for confocal microscopy experiments.

*Breast Cancer Cell Culture*

Breast cancer cell lines ZR-75-1 and T47D were purchased from ATCC and maintained in 10% Fetal Bovine Serum (FBS; Cellgro), 1% penicillin-streptomycin (Invitrogen), and RPMI 1640 medium at 37°C with 5% $CO_2$ in a humidified incubator.

*Flow Cytometry*

Cells were removed from tissue culture flasks prior to antibody incubation using an enzyme-free cell dissociation buffer solution. After washing with 1x DPBS, the cells were resuspended in 1% BSA in DPBS to a final concentration of approximately 250,000 cells per sample. Antibodies against MUC1 or appropriate isotype controls were added to the cell suspensions and incubated over ice for 45 min. Specifically, mouse anti-human MUC1 mAb clone HPMV (reacts with the peptide core of MUC1) and mouse anti-human MUC1 mAb clone SM3 (recognizing the underglycosylated form of MUC1) were used in this study. Antibodies against CD44, $sLe^a$, and $sLe^x$

were also used in this study to quantify the ligand and glycan expression on both cell types. Following incubation, cells were washed twice with 500 μL of 1% BSA to remove any unbound antibody. Flow cytometry samples were analyzed using a BD Accuri C6 flow cytometer (Ann Arbor, MI).

*Confocal Immunofluorescence Microscopy*

ZR-75-1 and T47D cells were plated in CELLview$^{TM}$ glass bottom dishes overnight prior to imaging. Surface staining for MUC1, uMUC1 and sialyl lewis x was performed using mouse anti-human MUC1 mAb (clone SM3) and Alexa 647 rat anti-mouse mAb as a secondary antibody as described in Ref. 84. Cells were also incubated with conjugated human recombinant E-selectin chimera for 30 min at room temperature (RT). A Zeiss 710 laser scanning confocal microscopy at the Cornell University microscopy and imaging core facility was used to collect images at 40X magnification.

*Preparation of Immobilized Protein Surfaces*

Polyurethane microtubes with an inner diameter of 300 μm (Braintree Scientific Inc., Braintree, MA, USA) were cut to a length of 50 cm. Recombinant human E-selectin-IgG chimeric protein was dissolved in 1X PBS to a final concentration of 5 μg/mL. The microtube surface was first rinsed with 75% ethanol and then 1X PBS. The surface was subsequently incubated with 10 μg/mL protein-G solution for 1.5 h, followed by a 2 h incubation with selectin chimera then blocked with 5% milk protein in PBS for 1 h. Control tubes were blocked with 5 % milk protein in PBS for 1 h.

*Flow-Based Adhesion Assay*

Microtubes functionalized with E-selectin/Fc chimera (described above) were taped onto a piece of thin glass in the viewing area of the Olympus IX81 inverted microscope (Olympus America Inc., Melville, NY, USA). A CCD camera (model no: KP-M1AN, Hitachi, Tokyo, Japan) and a DVD recorder (model no: DVD-1000MD, Sony Electronics) were used to record experiments for offline analysis. ZR-75-1 and T47D breast cancer cells suspended in flow buffer containing calcium were perfused through the microtubes using a syringe pump (KDS 230, IITC Life Science, Woodland Hills, CA) at a wall shear stress of 1.0 dyne/cm$^2$.

*Neuraminidase Treatment*

For certain experiments, ZR-75-1 and T47D cells were treated with 0.1 U/mL Vibrio Cholerae Neuraminidase (Roche Applied Science, Indianapolis, IN) for 45 min at 37°C to cleave the terminal sialic acid residues. After enzyme treatment cells were washed and perfused through the functionalized microtubes.

*siRNA Transfection*

Cells were transfected with MUC1 siRNA 20 nM (QIAGEN) for 12 hr. Total RNA was isolated from transfected cells using TRIzol (Life Technologies). A real-time PCR was carried out using oligo dT first strand primers, MUC1 specific primers ((5′TGCATCAGGCTCAGCTTCTA 3′ and 5′ GAAATGGCACATCACTCACG3′, IDT Integrated DNA Technologies), and SYBR Green PCR Kit (QIAGEN). MUC1

expression was normalized against GAPDH.

**P***olymorphonuclear Neutrophil (PMN) and Buffy Coat Isolation*

Human peripheral blood was collected from healthy adult donors after informed consent by venipuncture into BD Vacutainer tubes, approved by the Cornell University Institutional Review Board for Human Participants. PMN isolation was performed following a protocol described previously.[83] Briefly, PMNs were isolated by centrifugation at 500g for 50 min using 1-Step Polymorphs (Accurate Chemical and Scientific Corporation, Westbury, NY, USA). The PMN layer was extracted and washed twice in $Ca^{2+}$ and $Mg^{2+}$ free HBSS to remove the polymorph residue, and any remaining red blood cells were lysed hypotonically with 1:6 and 4X PBS. PMNs were then resuspended at various concentrations of HBSS containing 0.5% HSA, 2 mM $Ca^{2+}$, and 10 mM HEPES, buffered to 7.4. Similarly, buffy coat layer isolation was performed using Ficoll density gradient and washed with HBSS.

*Cancer Cell Capture from Spiked Buffy Coat*

ZR-75-1 cells were fluorescently labeled with Cell Tracker Green (Invitrogen), a live cell dye, for 30 min at 37°C. 100,000 or 50,000 of the labeled ZR-75-1 cells were then spiked into 1 mL of normal buffy coat and perfused through protein coated microtubes in two separate experiments. Capture efficiency was calculated using the estimated total number of cells in the microtube from 20 images recorded at random locations along the length of the microtube based on a previously published calibration.[111]

*Data Acquisition and Analaysis*

‘‘Rolling’’ cells were defined as those observed to translate in the direction of flow with an average velocity less than 50% of the calculated hydrodynamic free stream velocity. The rolling velocity was calculated by measuring the distance a rolling cell traveled over a 30 second interval. Videos of rolling cells were taken at three randomly selected locations along the microtube. For capture experiments, adherent cells were counted after perfusion with cell-free buffer for 5 min. The quantities of cells rolling and adhering were determined by recording images at 20 randomly selected locations along the microtube. All errors are reported as standard error of the mean, and statistical analyses were performed using Prism (GraphPad Software, San Diego, CA).

*Molecular Dynamics Simulations*

Free dynamics simulations were performed using the YASARA (http://yasara.org) package of molecular dynamics (MD) programs with the YAMBER3 self-parameterizing force field[145] and no external force field parameters. All simulations held the temperature and pressure constant at 300 K and 1 atm, respectively, while utilizing periodic boundary conditions, the particle mesh Ewald method for electrostatic interactions,[67] equilibrium pH (7.4), and the recommended 7.86 Å force cutoff for long-range interactions. Complexes were solvated in a water box and neutralized by adding $Ca^{2+}$ and $Cl^-$ ions to a concentration of ~50 mM calcium where the water boxes were defined as cubes with lengths measuring approximately 85 Å to allow for free protein rotation. The water boxes were also allowed to adjust slightly to

constrain the water density to 0.997 g/L. Conformational stresses were removed via short steepest descent minimizations followed by simulated annealing until sufficient convergences were reached. Free dynamics simulations were then run for 20 ns time periods.

The lectin and epidermal growth factor crystal structures of P-selectin bound to PSGL-1 (1G1S [241]), E-selectin bound to $sLe^x$ (1G1T[241]), and L-selectin (3CFW) were obtained from the Protein Data Bank for use as starting atomic coordinates. Predicted uMUC1 bound to P-selectin was obtained by altering the PSGL-1 amino acid sequence of the P-selectin:PSGL-1 complex (1G1S subunit A) to the uMUC 1 sequence where two amino acids were included beyond the O-glycosylated site for consistency with the PSGL-1 crystal structure. Extra amino acids were extended to include the entire 20 unit uMUC1 sequence (PDTRPAPGSTAPPAHGVTSA). In separate trials, residues S9, T10, and T18 were O-glycosylated with the carbohydrate moiety where $sLe^x$ was coordinately bound to the calcium of P-selectin. To obtain starting E-selectin:uMUC1 and L-selectin:uMUC1 complexes, the E-selectin (1G1T) and L-selectin (3CFW) crystal structures were aligned on the various P-selectin:uMUC1 complexes via the MUSTANG algorithm.[140]

### 5.2.3 RESULTS AND DISCUSSION

*Selectin Ligand Expression*

The surface expression of common selectin ligands and their carbohydrate binding moieties was first characterized. Both T47D and ZR-75-1 cells were found to express some amount of CD44 (Figure 5.7A&E) while neither expressed PSGL-1 (data not

shown, also suggested by Shirure *et al.*[237]). These two cells lines differed in their expression of the important selectin-binding moieties $sLe^a$ and $sLe^x$. T47D cells exhibited very little $sLe^a$ (Figure 5.7B) and no $sLe^x$ (Figure 5.7C) while ZR-75-1 cells showed significant expression of both $sLe^a$ and $sLe^x$ (Figures 5.7F&G). The differential expression of these selectin binding moieties resulted in a greater preference of ZR-75-1 over T47D cells in soluble E-selectin binding assays, as revealed by confocal microscopy (Figures 5.7D&H). T47D cells, however, showed weak staining of bound E-selectin which may be due to the minimal surface expression of $sLe^a$.

In previous research to examine the adhesive capabilities of uMUC1, we utilized the ZR-75-1 and MCF7 cells lines due to their high expression of the MUC1 glycoprotein.[84] It was found that while both cell lines expressed MUC1, ZR-75-1 cells expressed significantly more MUC1 as indicated by SM3 antibody staining. The SM3 antibody has been shown to bind to the MUC1 core epitope corresponding to the underglycosylated form of MUC1 (uMUC1).[60] We hypothesized that the metastatic potential of ZR-75-1 cells (highly metastatic) and MCF7 cells (weakly metastatic) correlate with the expression of uMUC1. In this study, we tested the MUC1 expression of T47D cells (weakly metastatic) compared to ZR-75-1 cells. Interestingly, both cell lines highly express MUC1 as revealed by the CD227 antibody (Figures 5.8A&E) and exhibited high expression of uMUC1 as revealed by SM3 labeling and flow cytometry (Figures 5.8C&G). Furthermore, both cell lines showed strong homogeneous surface staining of MUC1 (Figures 5.8B&F) and uMUC1 (Figures 5.8D&H) via confocal microscopy where ZR-75-1 cells showed greater

staining for both antibodies, indicating relatively higher MUC1 and uMUC1 expression over T47D cells. While MCF7 and ZR-75-1 cells differentially expressed uMUC1, T47D and ZR-75-1 cells varied only in their expression of the carbohydrate binding moieties $sLe^x$ and $sLe^a$.

*Cell Rolling Assay*

Lack of $sLe^x$ expression generally suggests a lack of selectin adhesive interactions under flow conditions. However, T47D cells interacted with the E-selectin surface (consistent with confocal staining by soluble E-selectin and likely due to $sLe^a$) which facilitated rolling events, albeit extremely fast cell rolling velocities, > 15 μm/s, and lower numbers of interacting cells, < 15 cells/frame, for an E-selectin concentration of 5 μg/mL (Figures 5.9A&B). Increasing the E-selectin concentration to 10 ug/mL significantly decreased the cell rolling velocities to ~5 μm/s and slightly increased the number of interacting cells to ~18 cells/frame indicating that cell interactions were indeed E-selectin dependent. Furthermore, perfusing cells with uMUC1 blocked with SM3 through microtubes with 5 μg/mL E-selectin concentration resulted in no significant change in cell rolling velocities or number of interacting cells, suggesting that the E-selectin binding moiety responsible for these weak interactions was most likely not presented by MUC1. Thus, the hypothesized correspondence between uMUC1 expression and metastatic potential must be amended to include the expression of $sLe^x$, since T47D cells (weakly metastatic) express uMUC1 but not $sLe^x$.

ZR-75-1 cells, on the other hand, showed greater interactions with the E-

selectin coated microtubes yielding slower cell rolling velocities of ~3 μm/s and greater numbers of interacting cells, nearly 39 cells/frame, for the 5μg/mL concentration of E-selectin (Figures 5.9A&B), consistent with the evident expression of $sLe^x$ on the cell surface. Doubling the E-selectin concentration statistically decreased the cell rolling velocities to ~2 μm/s while only slightly increasing the number of interacting cells to around 40 cells/frame. SM3 blocking of ZR-75-1 cells nearly doubled the cell rolling velocity and dramatically decreased the number of interacting cells to about 6 cells/frame. This demonstrates the interruption of the E-selectin:uMUC1 interaction as first described in previous work.[84] Inhibiting $sLe^x$ moieties from the cell surface via neuraminidase treatment significantly increased cell rolling velocities to > 7 μm/s and decreased the number of interacting cells to ~13 cells/frame, further demonstrating the importance of the $sLe^x$ binding moiety. Finally, knocking down MUC1 via siRNA transfection yielded an effect similar to SM3 blocking where cell rolling velocities significantly increased to 4.3 μm/s and the number of interacting cells decreased to ~13 cells/frame. After siRNA treatment, as indicated in Figures 5.2.3C and 5.2.3D, both mRNA and protein levels of MUC1 were reduced by at least 50% compared to the control ZR-75-1 cells.

Interestingly, perfusing ZR-75-1 cells through P-selectin coated microtubes produced around 25 interacting cells/frame (Figure 5.9A), however, no cells were found rolling or firmly adhered to the surface (Figure 5.9B). This interaction was abolished after siRNA knockdown of uMUC1. Therefore, the uMUC1:P-selectin interaction facilitated tethering events where cells experienced momentary arrest to the surface followed by rapid release of the cells into the flow buffer. Furthermore,

perfusing ZR-75-1 cells through combined E- and P-selectin coated microtubes resulted in around 50 interacting cells/frame, significantly more than E-selectin only surfaces (Figure 5.9A), where cell rolling velocities increased nearly double compared to E-selectin-only surfaces (Figure 5.9B). This further indicates the specific role of P-selectin for cell tethering rather than cell rolling. Perfusing cells through L-selectin coated microtubes did not produce any interacting cells indicating that the uMUC1:L-selectin interaction is too weak to influence cell motion.

*Molecular Dynamic Simulations*

To further explore the differential interactions between the uMUC1 glycoprotein and each selectin, MD simulations were used to dock several O-glycosylated variants of uMUC1 to E-, P-, and L-selectin. Figure 4 shows E-selectin:uMUC1 complexes where the S9 (Figures 5.10A&B), T10 (Figures 5.10C&D), and T18 (Figures 5.10E&F) amino acid sites of the uMUC1 core epitope were O-glycosylated with a $sLe^x$ moeity. Sites T3 and S19 sites were not tested because these sites should not be in a glycosylated form as suggested by SM3 binding.[60] Each variant of uMUC1 binding indicated a different degree of residue contact. In the majority of cases, residues R108 and K112 experienced hydrogen bonding interactions, where both residues interacted with the core epitope of uMUC1 exclusively and not $sLe^x$. On the other hand, residue R97 only interacted with the $sLe^x$ forming hydrogen bonds in Figures 5.10A, D, and E. In a single case (Figure 5.10E, site T18) all three residues formed contacts and since the PSGL-1 glycoprotein is considered a P-selectin specific ligand due to enhanced interactions facilitated by the R85 and H114 residues of P-selectin,[241] these

MD results suggest that the uMUC1 glycoprotein can be regarded as an E-selectin specific ligand.

Figure 5.11 depicts the uMUC1 interactions with P-selectin (top) and L-selectin (bottom), where one of each S9 (Figure 5.2.5A&B), T10 (Figures 5.11C&D), and T18 (Figures5.11E&F) glycosylated site is shown for clarity. In the case of P-selectin, residues R85, H108, and K112 formed hydrogen bonding contacts to the uMUC1 core epitope. For L-selectin, only residues R97 and K111 formed contacts where both residues contacted $sLe^x$ and not the uMUC1 core epitope. Again, glycosylating the T18 site of uMUC1 yielded the most interactions for both P-selectin and L-selectin (Figures 5.11E&F, respectively). In comparison with E-selectin, P-selectin lacked residue R97 to form contacts with $sLe^x$ whereas L-selectin lacked residues R108 and K112 to form contacts with the uMUC1 core epitope. Thus, to qualitatively interpret the experimental rolling assays, E-selectin facilitates cell rolling due to its ability to contact both the uMUC1 core epitope and $sLe^x$. P-selectin effectively tethers cells due to its ability to contact the uMUC1 core epitope but was unable to produce cell rolling possibly because of insufficient binding with $sLe^x$. Lastly, L-selectin initiated no interacting cells due to its inability to interact specifically with uMUC1. These data suggest that uMUC1 can be considered both E- and P-selectin specific ligands where each selectin facilitates different roles in the metastatic adhesion cascade, whereas L-selectin most likely plays no part in functional uMUC1 binding.

*Capturing Breast Cancer Cells Using uMUC1 mAb*

Applying these insights into the selective adhesion of the uMUC1 glycoprotein, a combined E-selectin and SM3 surface was prepared to capture cancer cells. It was found that SM3 bound minimally to PMNs (Figure 5.12A) via flow cytometry, with the mean fluorescence intensity index significantly lower compared to ZR-75-1 cells (Figure 5.12B). Perfusing ZR-75-1 cells through a microtube coated with only E-selectin resulted in nearly 50 rolling cells/frame (Figure 5.12C) with no adherent cells on the surface. Coating the microtube surface with both E-selectin and SM3 did not change the number of rolling cells, but allowed for firm adhesion events facilitated by uMUC1:SM3 interactions where subsequent perfusion of buffer resulted in over an average of 17 captured cells per frame. The ratio of firm adhesion events to total number of cells found on the protein coated surface was comparable to the ratio for the E-selectin/ICAM-1 combined surface as studied previously.[84] Perfusing isolated PMNs over the same E-selectin/SM3 combined surface resulted in over 50 rolling events per frame with no adherent cells. Furthermore, since ICAM-1 also facilitates firm adhesion events with leukocytes, the E-selectin/SM3 combined surface may provide a more selective method to separate CTCs from whole blood.

Processing normal buffy coat spiked with Cell Tracker labeled ZR-75-1 cells through microtubes coated with E-selectin only or E-selectin with SM3 antibody resulted in capture efficiencies of 0.4% and 26.7%, respectively (Figure 5.12D). Here, 'captured' cells refers to the number of firmly adherent cells. Cells that were effectively captured by this combined surface strategy must express both the $sLe^x$ glycan and the uMUC1 glycoprotein. The $sLe^x$ glycan facilitates the initial tethering and rolling events due to its interactions with surface E-selectin when presented by

uMUC1 or other E-selectin ligands such as CD44. Cells that initiate stable cell rolling can then form firm adhesion events due to the interaction of uMUC1 and the surface SM3. Therefore, uMUC1 and $sLe^x$ expression is essential for cell capture, whether or not the $sLe^x$ is found on uMUC1. However, our current and previous results indicated that $sLe^x$ terminated uMUC1 is an E-selectin specific ligand that effectively contributes to cell rolling. Moreover, of the three cell lines studied here and previously, only the highly metastatic ZR-75-1 cells expressed both $sLe^x$ and uMUC1 where uMUC1 was found to be decorated with $sLe^x$. The capture percentage of non-cancer cells was not presented in this study due to high variance of blood cell count between donor buffy coats. Furthermore, due to the high degree of ZR-75-1 cell aggregation, the spiking cell concentration performed in this study was much higher than clinical values as well as concentrations used in our previous studies using clinically-motivated devices.[110, 111] Although at the proof-of-concept stage, the combined E-selectin/SM3 surface described in this study shows potential for selectively capturing CTCs expressing uMUC1.

### 5.2.4 CONCLUSIONS

In previous work, we examined two cell lines (MCF7 and ZR-75-1) that exhibited variants of the MUC1 glycoprotein where both cell lines expressed MUC1, however only ZR-75-1 expressed the underglycosylated form uMUC1. We had previously found that uMUC1 has the ability to interact with E-selectin and ICAM-1 and, for these two cell lines, the metastatic potential corresponded with uMUC1 expression since ZR-75-1 cells are highly metastatic and MCF7 cells are weakly metastatic.[14]

Here, we further explored the function of uMUC1 during the metastatic adhesion cascade by extending the study to the T47D cell line (weakly metastatic). It was found by examining various E-selectin ligands that T47D and ZR-75-1 cells differed only in their expression of the E-selectin binding moiety $sLe^x$ where T47D cells lacked this expression. Without sufficient $sLe^x$, T47D cells showed little interaction with E-selectin coated microtubes, resulting in extremely fast rolling velocities and low numbers of interacting cells. Thus, for these three cell lines, the metastatic potential seems to correlate with the expression of uMUC1 as well as $sLe^x$.

ZR-75-1 cell interactions with E-selectin, however, were highly dependent on uMUC1 expression where cell velocities significantly decreased when uMUC1 was blocked with either the SM3 antibody or uMUC1 siRNA knockdown. Moreover, uMUC1 interactions with P-selectin exclusively facilitated cell tethering events on P-selectin-only and E- and P-selectin combined surfaces whereas L-selectin surfaces produced no cell interactions. Utilizing MD simulations, E-selectin was shown to interact with uMUC1 via three distinct residue contacts to both the uMUC1 core epitope and $sLe^x$. On the other hand, P-selectin possessed three distinct contacts that interacted with only the uMUC1 core epitope and L-selectin only interacted with $sLe^x$. These MD data suggest that specific interactions with both the core epitope and $sLe^x$ is required to produce cell rolling events whereas interactions with just the core epitope produce tethering events and interactions with only the carbohydrate unit do not produce any cell interactions.

Based on these observations, we propose a combined surface of E-selectin and SM3 to preferentially capture cells exhibiting uMUC1. It was found that the E-

selectin/SM3 microtubes captured approximately 26% of the number of interacting cancer cells. Since PMNs are not targeted by the SM3 mAb, it is expected that this E-selectin/SM3 surface strategy may offer a novel and viable method to selectively isolate cancer cells from whole blood.

**Figure 5.7:** Ligand expression and E-selectin binding capability of T47D and ZR-75-1 cells. Flow cytometry histogram plots of T47D (in red) and ZR-75-1 (in blue) cells labeled with anti-CD44 mAb (A and E), anti-sLe$^a$ mAb (B and F), and anti-sLe$^x$ (clone CSLEX, C and G), respectively. Isotype controls are represented by solid gray peaks in each plot. D and H: Confocal microscopy images of T47D and ZR-75-1 cells labeled with pre-conjugated recombinant human E-selectin/Fc (shown in green) and DAPI nucleic acid stain (shown in blue), respectively. Scale bar: 50 μm

**Figure 5.7: Ligand expression and E-selectin binding characterization of T47D and ZR-75-1 cells**

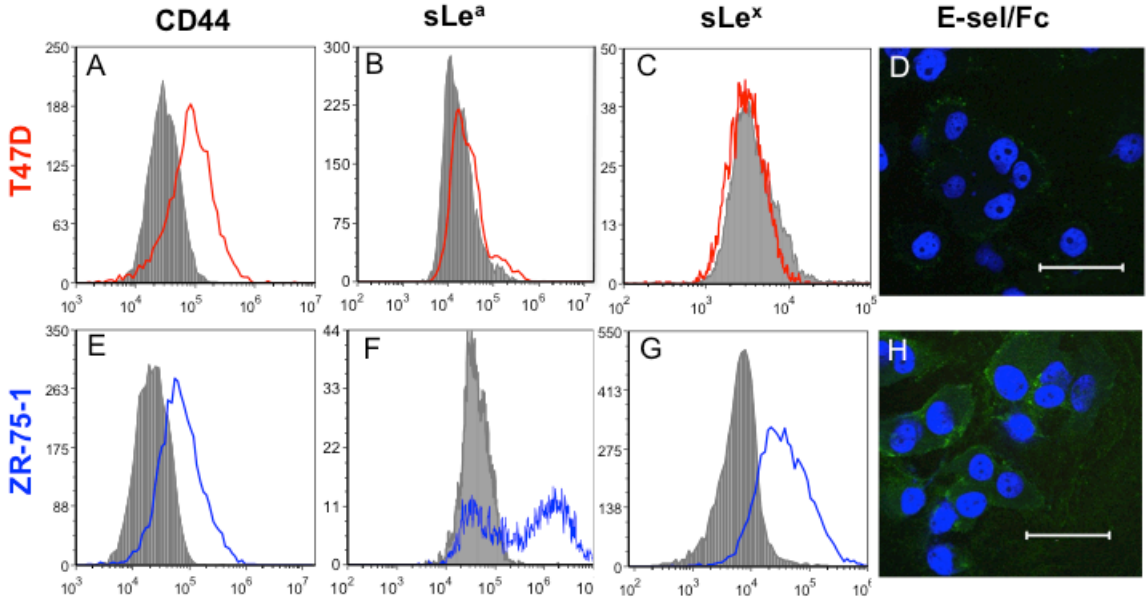

**Figure 5.8:** MUC1 expression of T47D and ZR-75-1 cells. Flow cytometry histogram plots of T47D (in red) and ZR-75-1 (in blue) cells labeled with anti-MUC1 (CD227) mAb (clone HPMV, A and E) and anti-uMUC1 mAb (clone SM3, C and G). B and F: Confocal microscopy images of T47D and ZR-75-1 cells labeled with anti-CD227 mAb (green) and DAPI nucleic acid stain (blue), respectively. D and H: Confocal microscopy images of T47D and ZR-75-1 cells labeled with anti-uMUC1 mAb, respectively. I and J: Co-staining of CD227 mAb (green) and $sLe^x$ (red) on ZR-75-1 cells. Scale bar: 50 μm

**Figure 5.8: MUC1 expression of T47D and ZR-75-1 cells**

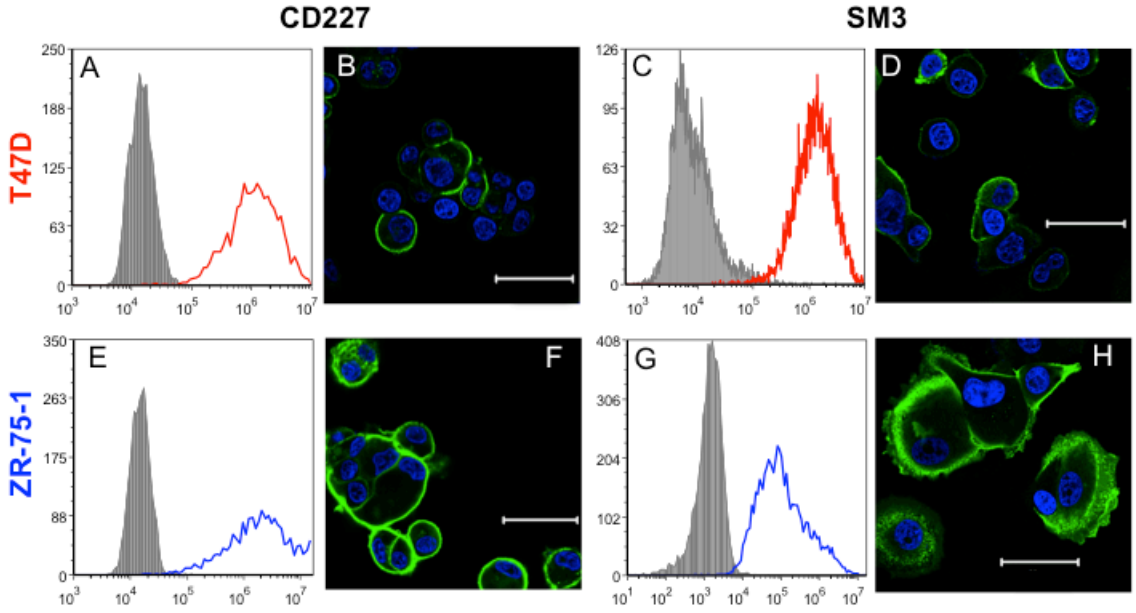

**Figure 5.9:** Adhesion profile of T47D and ZR-75-1 cells on E-, P-, and L-selectin coated surfaces. Adhesion phenotype of T47D (in red) and ZR-75-1 (in blue) cells represented by their rolling velocity on E-selectin coated surface (A) and average number of cells observed on the surface (B). E-sel, P-sel, and L-sel indicate the surface proteins E-selectin, P-selectin, and L-selectin, respectively. Numbers following the surface protein abbreviations denote the surface protein concentration in μg/mL, for example 'E-sel5' signifies the surface protein E-selectin at a concentration of 5 μg/mL was utilized. Combined surfaces utilizing both E- and P-selectin were utilized with constant E-selectin concentrations (5 μg/mL) and varying P-selectin concentrations (10 and 25 μg/mL) and are denoted as 'E-sel5 P-sel10' and 'E-sel5 P-sel25', respectively. Text in parentheses following the surface protein indicators denote specific treatments of either ZR-75-1 or T47D cells where (SM3 Blocked) and (Neuraminidase) indicates that cells were incubated with either anti-SM3 neutralizing antibody or neuraminidase, respectively. (siRNA) indicates that cells were transfected with MUC1 siRNA. Lack of parentheses indicates that no treatments were performed. Student's t test was performed for all results compared to E-sel5 within each cell line. Combined surfaces E-sel5 P-sel10 and E-sel5 P-sel25 for the ZR-75-1 cell line were also paired. All significances are $p<0.001$, unless otherwise indicated by ** ($p<0.01$), * ($p<0.05$), or NS (not significant). C: Quantification of MUC1 mRNA level knockdown efficiency via qPCR. D: Quantification of cell surface MUC1 protein level knockdown efficiency via flow cytometry (mean fluorescence intensity index was plotted).

**Figure 5.9: Adhesion profiles of T47D and ZR-75-1 cells on E-, P-, and L-selectin coated surfaces**

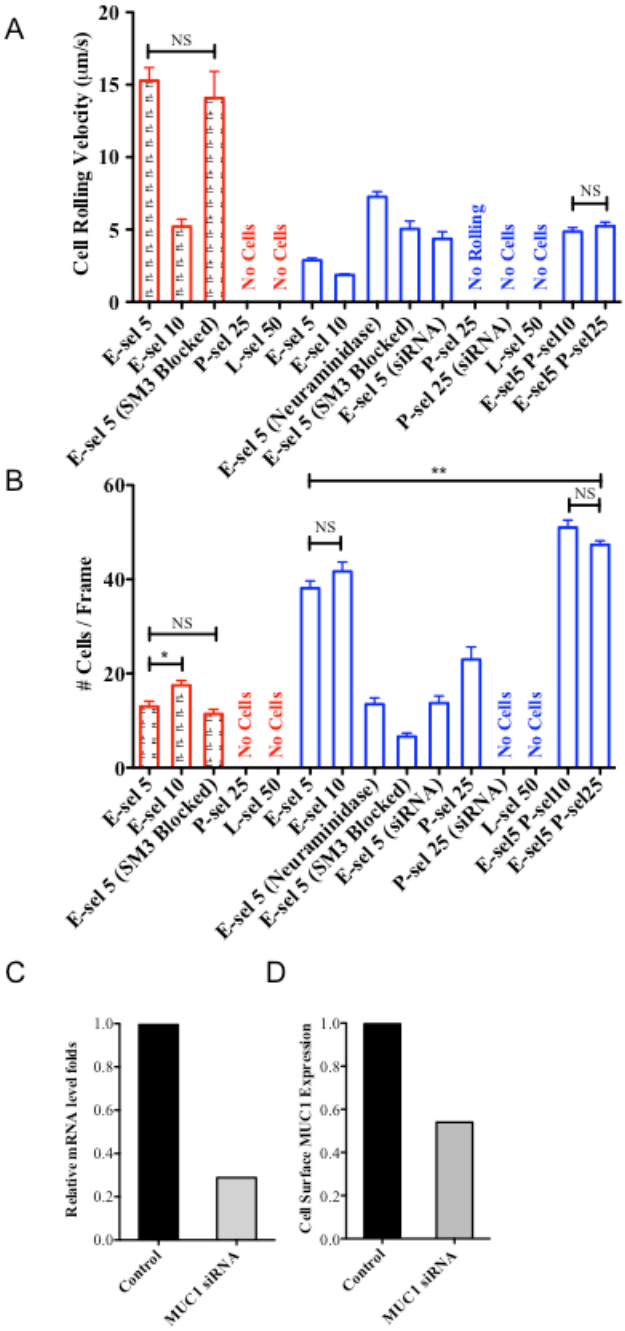

**Figure 5.10:** Equilibrated uMUC1 (magenta) and $sLe^x$ (orange) structures bound to E-selectin (green). With respect to the uMUC1 sequence, PDTRPAPGSTAPPAHGVTSA, the top and bottom rows correspond with the 'reverse' and 'forward' sequence, respectively. uMUC1 residues S9 (A and B), T10 (C and D), and T18 (E and F) are glycosylated as indicated by the uMUC1 sequence and the orange arrow. The atoms of select E-selectin amino acids (R97, R108, and K112) are depicted to show varying degrees of contacting residues.

**Figure 5.10: Equilibrated uMUC1 and sialyl lewis x structures bound to E-selectin**

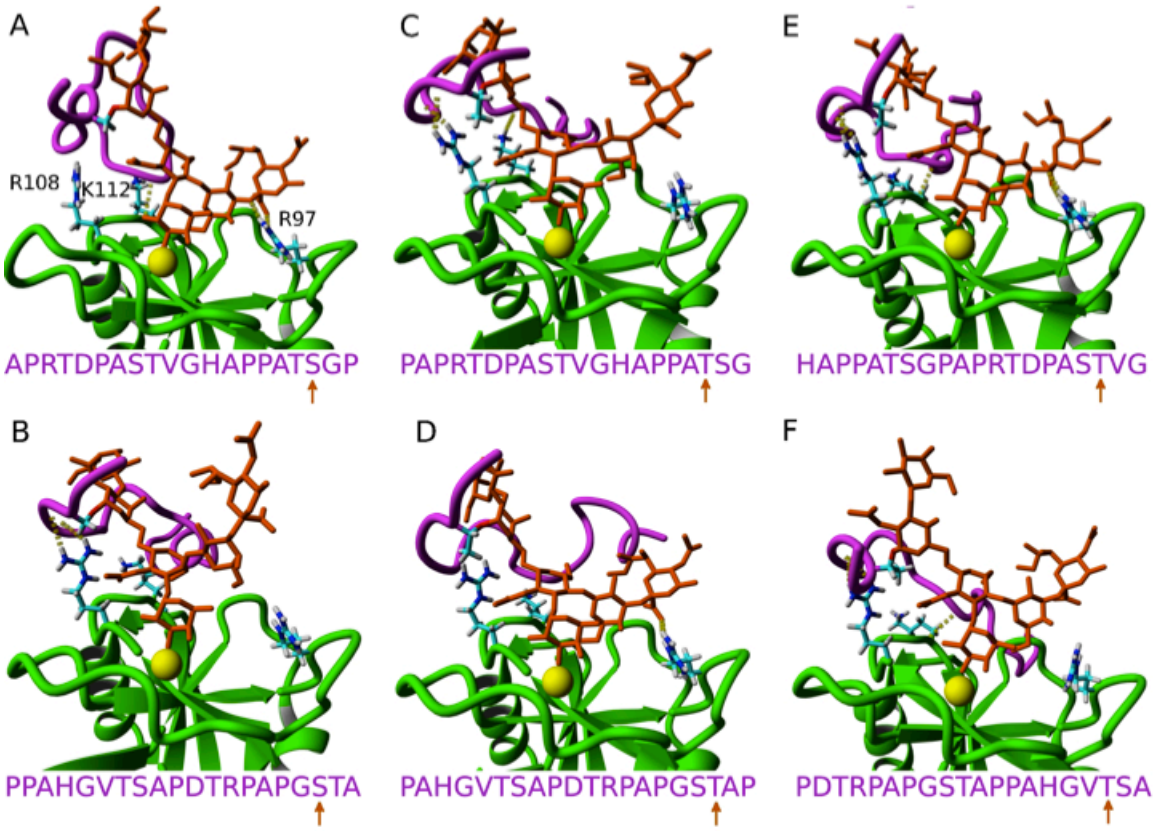

**Figure 5.11:** Equilibrated uMUC1 (magenta) and $sLe^x$ (orange) structures bound to P-selectin (gray, top row) and L-selectin (blue, bottom row). With respect to the uMUC1 sequence, PDTRPAPGSTAPPAHGVTSA, all interactions correspond with the 'reverse' sequence. uMUC1 residues S9 (A and B), T10 (C and D), and T18 (E and F) are glycosylated as indicated by the uMUC1 sequence and the orange arrow. The atoms of select P-selectin amino acids (R85, H108, and K112) and L-selectin amino acids (R97 and K111) are depicted to show varying degrees of contacting residues.

**Figure 5.11: Equilibrated uMUC1 and sialyl lewis x structures bound to P-selectin and L-selectin**

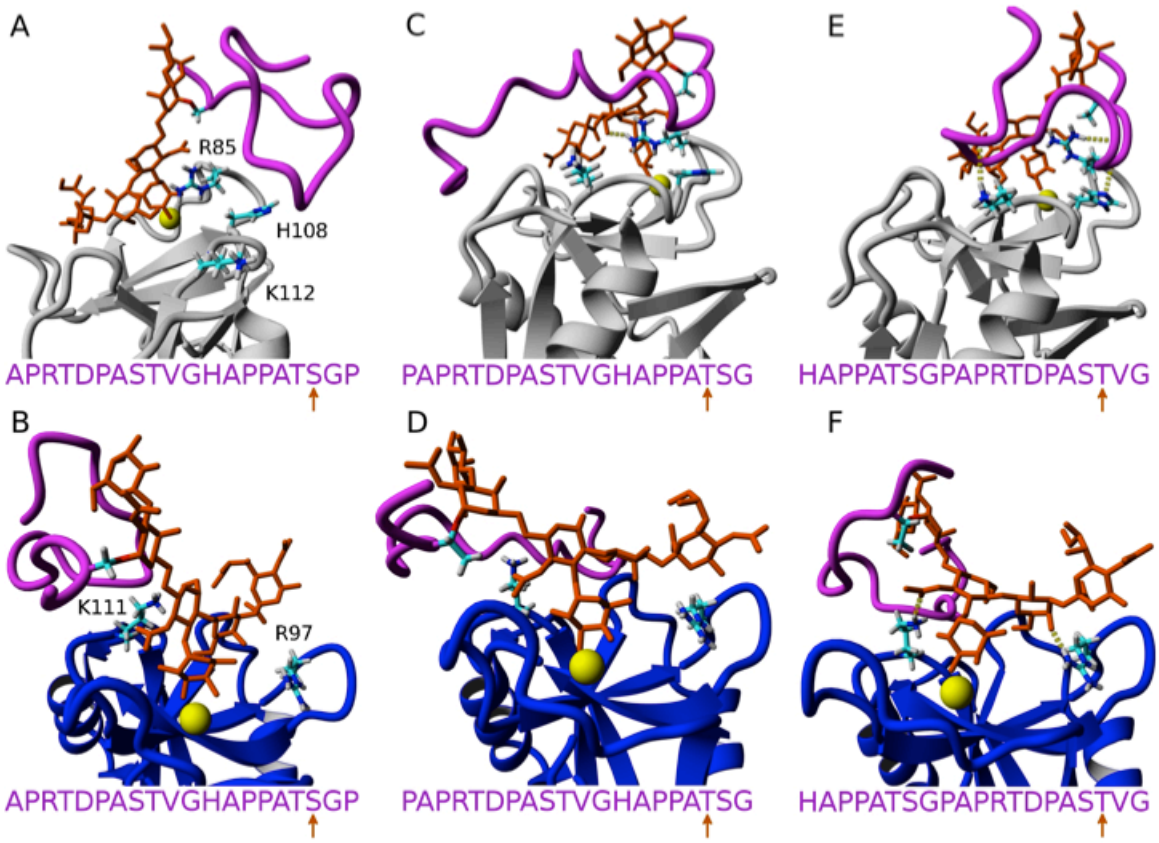

**Figure 5.12:** Capture efficiency of uMUC1 expressing cells in normal buffy coat. A: Flow cytometry histogram plot of isolated polymorphonuclear neutrophils (PMNs) labeled with anti-uMUC1 mAb (clone SM3, in blue) and isotype control (in grey). B: Mean fluorescence intensity quantification of uMUC1 expression of ZR-75-1 cells (in black) and PMNs (in grey). C: Average total number of ZR-75-1 cells (left and middle bar sets) and PMNs (right bar set) observed on surfaces coated with E-selectin at a concentration of 5 μg/mL (E-sel5) and the combination of E-selectin and SM3 at concentrations of 5 and 50 μg/mL, respectively (E-sel5 SM3 50). Columns in gray indicate the average number of cells (either ZR-75-1 or PMNs) while perfusing with cell solution and columns in white indicate the average number cells quantified after washing the surfaces with flow buffer for 5 min. Student's t test was performed for both comparisons. *** $p<0.001$ ** $p<0.01$ * $p<0.05$ NS: not significant. D: Numbers of captured ZR-75-1 cells from cancer cell spiked buffy coat on surfaces coated with E-selectin (5.0 μg/mL) and the combination of E-selectin (5.0 μg/mL) and SM3 (50 μg/mL). Two separate experiments were performed with 100,000 cells (24,176 captured) and 50,000 cells (14,587 captured), resulting in 24.2% and 29.1% yield, respectively.

**Figure 5.12: Capture efficiency of uMUC1 expressing cells in normal buffy coat**

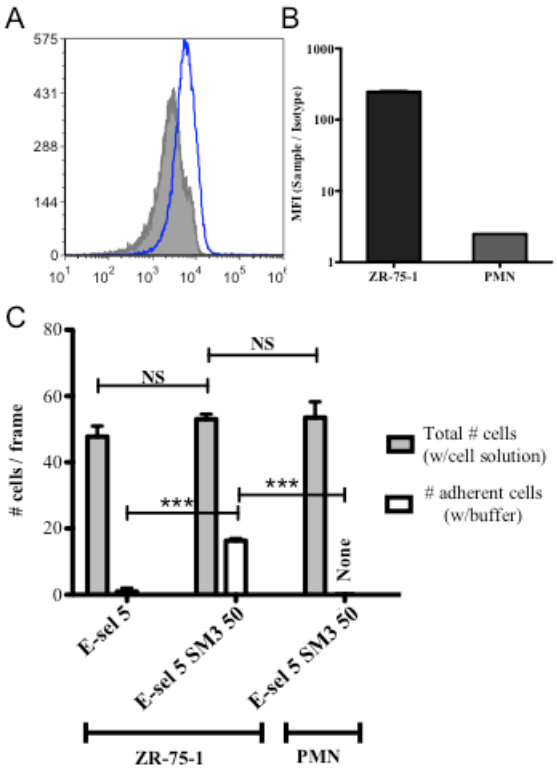


D

| | E-sel 5 | E-sel 5 + SM3 50 |
|---|---|---|
| # Captured Cells | 180 | 24176/14587 |
| % Captured Cells | 0.4 | 24.2/29.1 |

# CHAPTER 6 CONCLUDING REMARKS

## 6.1 INTRODUCTION

Hydrodynamic shear force plays an important role in the leukocyte adhesion cascade that involves the tethering and rolling of cells along the endothelial layer, their firm adhesion or arrest, and their extravasation or escape from the circulatory system by inducing passive deformation, or cell flattening, and microvilli stretching, as well as regulating the expression, distribution, and conformation of adhesion molecules on leukocytes and the endothelial layer.

Similarly, the dissemination of CTCs from the primary tumor sites is believed to involve tethering, rolling, and firm adhesion steps before their eventual extravasation which leads to secondary tumor sites (metastasis). Of particular importance to both the leukocyte adhesion cascade and the extravasation of CTCs, glycoproteins are involved in all three steps (capture, rolling, and firm adhesion) and consist of a variety of important selectin ligands. Moreover, these selectin ligands are differentially expressed by varying cancer cell types where the specific ligand expression (well-established, novel, or non-existent) and their ability to interact with E-selectin can determine the mechanistic pathway for CTC adhesion to the inflamed endothelium.

## 6.2 DICUSSION

The colon cancer cell line COLO 205, interestingly grows simultaneously in both adherent and suspended states in culture, consistently reaching an equilibrium 7:3 (adherent:suspended) ratio. The adherent state demonstrates cell-cell interactions in small aggregates whereas the suspended state consists mostly of single cells. Loss of

epithelial markers such as junctional- and cell-cell adhesion proteins is an important characteristic in the EMT, a critical step necessary for metastasis. Manipulation of the EMT markers β-catenin and E-cadherin expression, either by siRNA knockdown of β-catenin or incubation with E-cadherin antibody-coated microbeads, shifts the equilibrium ratio to 9:1. Interestingly, human plasma supplemented media shifts the equilibrium ratio in the opposite direction to 1:9, favoring the suspended state. In the context of metastasis, the suspended COLO 205 population represents a more invasive phenotype. Suspended cells expressed 60% more $sLe^x$ and 80% more $sLe^a$ than adherent cells which resulted in significantly slower rolling velocities on E-selectin coated microtubes. Moreover when cells were cultured in human plasma, the expression of phosphorylated β-catenin increased, shifting the majority of cells into the suspended population where $sLe^x$ and E-selectin ligand CD44 expression both increased as well. The dynamic COLO 205 population switch presents unique differences in the phenotype of their subpopulations and could serve as a good model for studying cell heterogeneity and the EMT process *in vitro*.

Furthermore, E-selectin mediated cell sorting of COLO 205 and MDA-MB-231 cell lines on functionalized microbubble and PDMS surfaces was achieved due to the differential E-selectin adhesion of COLO 205 and MDA-MB-231 cells. The toxicity of the anti-cancer drug, doxorubicin, on COLO 205 cells in spheroids was tested and compared to cells in 2D culture. COLO 205 spheroids cultured in flow showed a threefold increase in resistance to doxorubicin compared to COLO 205 monolayer cells cultured under static conditions, consistent with the resistance observed previously in other MCTS models. The advantages presented by our

microfluidic system, such as the ability to control the size uniformity of the spheroids and to perform real-time imaging on cells in the growth platform, show potential for high throughput drug screening development.

Despite their high metastatic potential, human breast carcinoma cells MDA-MB-231 lack interactions with E-selectin functionalized surfaces under physiological shear stresses. Interestingly, the pro-inflammatory cytokines IL-6 and TNF-a, which play an important role in potentiating the inflammatory cascade, are significantly elevated in metastatic breast cancer (BCa) patients. We hypothesized that human plasma, 3-D tumor spheroid culture, and cytokine-supplemented culture media could induce a phenotypic switch that allows BCa cells to interact with E-selectin coated surfaces under physiological flow. Flow cytometry, immunofluorescence imaging, and flow-based cell adhesion assay were utilized to investigate the phenotypic changes of MDA-MB-231 cells with various treatments. Our results indicated that plasma, IL-6, and TNF-a promote breast cancer cell growth as aggregates and induced adhesive recruitment of BCa cells on E-selectin coated surfaces under flow. 3-D tumor spheroid culture exhibited the most significant increases in the interactions between BCa and E-selectin coated surfaces by upregulating CD44V4 and sLex expression. Furthermore, we showed that IL-6 and TNF-α concentrations in blood may regulate the recruitment of BCa cells to the inflamed endothelium. Finally, we proposed a mechanism that could explain the invasiveness of 'triple-negative' breast cancer cell line MDA-MB-231 via a positive feedback loop of IL-6 secretion and maintenance. Taken together, our results suggest that therapeutic approaches targeting cytokine receptors and adhesion molecules on cancer cells may potentially reduce metastatic load and

improve current cancer treatments.

Retinoblastoma (RB) is a rare retinal cancer of childhood. RB survivors tend to develop additional tumors later in life, although the physical mechanisms of RB metastatic spread are largely unknown. Yet, human RB cell lines RB143 and WERI-Rb27 do not express selectin ligands or beta-2 integrins and cannot directly interact with inflamed endothelium. In this study, we showed that RB cells express ICAM-1, a beta-2 integrin ligand that correlates with metastasis and was preferentially co-expressed on RB cells that also express ABCG2, a stem cell marker associated with chemoresistance and metastasis. Based on the presence of ICAM-1+ RB cells, we tested the hypothesis that RB cells could be recruited to an E-selectin surface via attachment to activated PMNs. We characterized the dynamic adhesion between RB cells and PMNs within E-selectin coated microtubes under a physiological range of wall shear stress values (0.2–5 dyn/cm2). We showed that activated PMNs were necessary for the recruitment of RB cells through ICAM-1:LFA-1 binding. Results from this work may lead to new strategies that target the metastatic spread of tumor cells via CTC:leukocyte aggregation.

Lastly, the aberrantly underglycosylated mucin MUC1 has been shown to both abundantly express selectin binding moieties (sialyl Lewis x and a) and to consistently expose its core epitope. Flow cytometry was initially used to determine MUC1 expression on ZR-75-1 and MCF7 cells, while immunofluorescence microscopy was used to confirm the aberrant form of MUC1 and MUC1:ICAM-1 interactions. Each cell line was then perfused through combined E-selectin and ICAM-1 coated microtubes, as a model of the microvascular endothelium. ZR-75-1 and MCF7 were

found to express abundant and low levels of underglycosylated MUC1, respectively. The rolling/adhesion profiles showed that ZR-75-1 cells, when compared to MCF7 cells, interacted with E-selectin more efficiently resulting in sufficiently slow rolling velocities to form MUC1:ICAM-1 interactions thereby facilitating firm adhesion. Interestingly, the observed differential adhesion was consistent with the relative metastatic potential of the ZR-75-1 (highly metastatic) and MCF7 (weakly metastatic) cell lines.

To further characterize the novel E-selectin ligand, uMUC1, the T47D cell line was subsequently verified to highly express uMUC1 utilizing flow cytometry and confocal microscopy. However it was found that only ZR-75-1 cells expressed the E-selectin binding moiety $sLe^x$. Furthermore, perfusing T47D cells through E-selectin coated microtubes resulted in fast rolling velocities and low numbers of interacting cells and that blocking uMUC1 with the SM3 antibody had no effect. ZR-75-1 cells, on the other hand, were highly dependent on the E-selectin:uMUC1 interaction as exemplified by significant increases in cell rolling velocities and decreases in the number of interacting cells when blocking with SM3 or when uMUC1 expression was knocked down via siRNA transfection. Whereas uMUC1 interactions with E-selectin supported cell rolling, P-selectin: uMUC1 interactions exclusively facilitated cell tethering, while L-selectin surfaces supported no cell adhesive interactions. These experimental observations were consistent with molecular dynamics simulations of uMUC1 bound to E-, P-, and L-selectin where the degree of residue contact correlated with the differential adhesion of uMUC1 to each selectin. Finally, an E-selectin and SM3 combined surface coating captured approximately 30% of the total number of

interacting cancer cells comparable to the number of adhered cells when utilizing E-selectin and ICAM-1 combined surfaces. The E-selectin/SM3 surface strategy may offer a viable method to selectively capture cancer cells from whole blood samples.

## 6.3 FUTURE WORK

To extend the studies discussed in this thesis, relevant animal models can be designed to validate the in vitro cell line based results. For the retinoblastoma study, ICAM-1 siRNA transfected and control RB143 cells can be injected into NOD-SCID mice and monitored for tumor development. It was hypothesized that ICAM-1:LFA-1 facilitated the aggregate formation between RB cells and circulating leukocytes, allowing RB cells to follow the metastatic cascade through the blood stream. ICAM-1 siRNA transfected RB143 cells are expected to show significantly less metastatic lesions compared to control RB cells due to the lack of the RB:leukocyte aggregation. Similarly, 3D tumor spheroid grown and monolayer grown MDA-MB-231, adherent and suspended COLO 205 cells, and MUC1 siRNA transfected and control ZR-75-1 cells can be evaluated for their metastatic potentials using animal models.

Utilizing the selectin-based cell capturing devices may have applications besides CTC isolation. Circulating fetal cells in maternal blood during pregnancy were first observed by Schomorl in 1893. Reliable prenatal diagnosis of fetal aneuploidy and single gene disorders currently involves invasive procedures such as chorionic villus sampling (CVS) and amniocentesis. These invasive tests are each associated with a low, but finite risk of one fetal loss in every 100 to 175 sampling procedures.

The detection of fetal cells and fetal DNA circulating in maternal blood has encouraged the development of noninvasive prenatal screening and diagnosis. Current technologies focusing on fetal cells isolation include cell size and density, optical, magnetic, adhesion, and electrical based separation techniques. Many of these techniques destroy fetal cells as part of the isolation process which does not allow *in vitro* expansion of the isolated fetal cells for future characterization. Moreover, theses technologies fail to provide sufficient enrichment of the circulating fetal cells needed to proceed further with genetic testing. A novel generation of Non-Invasive Prenatal Testing based on the sequencing of free fetal DNA, is emerging to overcome fetal cell isolation pitfalls. However, these techniques are costly and limited to screening purposes.

Utilizing flow cytometry and confocal microscopy, fetal cell lines labeled with trophoblast markers EpCAM (TROP-1) and HLA-G indicated that while JAR expressed abundant EpCAM (Figure 6.1A and B) and moderate HLA-G, HTR-8/Svneo showed minimal expression of both markers. Interestingly, both cell lines were found to express $sLe^x$, an essential glycan decorating common E-selectin ligands. JAR cells were found to roll stably on E-selectin coated surfaces at $4.36 \pm 0.38$ μm/s under 1 dyn/cm$^2$ shear stress. Significant capture of JAR cells was observed when spiked into normal buffy coat (Figure 6.1C). EpCAM-positive cells were found in maternal buffy coat (Figure 6.1D) and FISH analysis was performed for chromosome Y detection. These results show the effectiveness of a microfluidic device coated with halloysite nanotubes and functionalized with E-selectin and anti-EpCAM antibody to capture viable trophoblast cell lines JAR and HTR-8/SVneo and EpCAM-positive

fetal cells from maternal blood. This biomimetic approach allows a smooth capture of circulating fetal cells which indicates great potential as a novel non-invasive prenatal screening/diagnosis platform to replace CVS and amniocentesis and offers a much greater breadth of application for selectin-based cell capturing devices.

**Figure 6.1:** Characterization of trophoblast cell line JAR and isolation of EpCAM-positive fetal cells. (A) JAR cells highly express EpCAM (Yellow:isotype; Green: sample). (B) JAR cells labeled with anti-EpCAM mAb. (C) Fluorescently labeled JAR cells in normal buffy coat captured on the functionalized surface. (D) EpCAM-positive fetal cell isolated from maternal blood.

**Figure 6.1: Characterization of trophoblast cell line JAR and isolation of EpCAM-positive fetal cells**

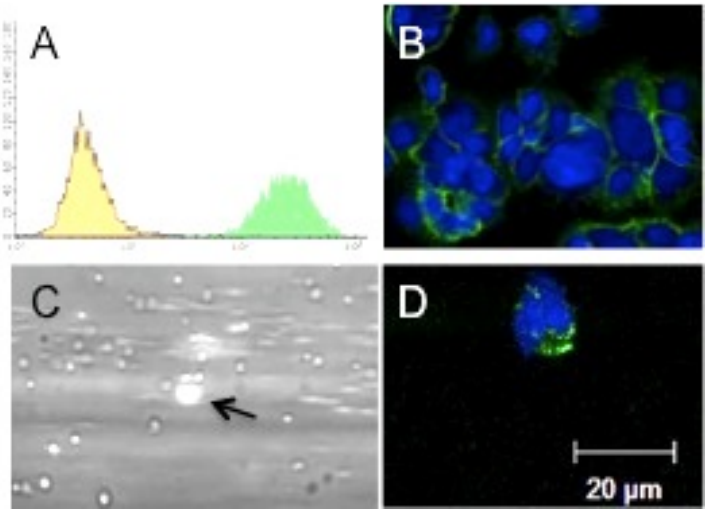

**REFERENCES**:

1Agastin, S., U. B. T. Giang, Y. Geng, L. A. DeLouise and M. R. King. Continuously perfused microbubble array for 3d tumor spheroid model. *Biomicrofluidics* 5(2):2011.

2Aigner, S., C. L. Ramos, A. Hafezi-Moghadam, M. B. Lawrence, J. Friederichs, P. Altevogt and K. Ley. Cd24 mediates rolling of breast carcinoma cells on p-selectin. *Faseb Journal* 12(12):1241-51, 1998.

3Aigner, S., Z. M. Sthoeger, M. Fogel, E. Weber, J. Zarn, M. Ruppert, Y. Zeller, D. Vestweber, R. Stahel, M. Sammar and P. Altevogt. Cd24, a mucin-type glycoprotein, is a ligand for p-selectin on human tumor cells. *Blood* 89(9):3385-95, 1997.

4Ajioka, Y., L. J. Allison and J. R. Jass. Significance of muc1 and muc2 mucin expression in colorectal cancer. *J. Clin. Pathol.* 49(7):560-64, 1996.

5Albertsson, P. A., U. Nannmark and B. R. Johansson. Melanoma cell destruction in the microvasculature of perfused hearts is reduced by pretreatment with vitamin-e. *Clin. Exp. Metastasis* 13(4):269-76, 1995.

6Alon, R., D. A. Hammer and T. A. Springer. Lifetime of the p-selectin-carbohydrate bond and its response to tensile force in hydrodynamic flow. *Nature* 374(6522):539-42, 1995.

7Alves, C. S., M. M. Burdick, S. N. Thomas, P. Pawar and K. Konstantopoulos. The dual role of cd44 as a functional p-selectin ligand and fibrin receptor in colon carcinoma cell adhesion. *Am J Physiol Cell Physiol* 294(4):C907-16, 2008.

8Alves, C. S., S. Yakovlev, L. Medved and K. Konstantopoulos. Biomolecular characterization of cd44-fibrin(ogen) binding: Distinct molecular requirements mediate binding of standard and variant isoforms of cd44 to immobilized fibrin(ogen).

*J Biol Chem* 284(2):1177-89, 2009.

9Apweiler, R., H. Hermjakob and N. Sharon. On the frequency of protein glycosylation, as deduced from analysis of the swiss-prot database. *Biochim. Biophys. Acta-Gen. Subj.* 1473(1):4-8, 1999.

10Baisse, B., H. Bouzourene, E. P. Saraga, F. T. Bosman and J. Benhattar. Intratumor genetic heterogeneity in advanced human colorectal adenocarcinoma. *Int J Cancer* 93(3):346-52, 2001.

11Barbone, D., T. M. Yang, J. R. Morgan, G. Gaudino and V. C. Broaddus. Mammalian target of rapamycin contributes to the acquired apoptotic resistance of human mesothelioma multicellular spheroids. *J Biol Chem* 283(19):13021-30, 2008.

12Bates, R. C. and A. M. Mercurio. Tumor necrosis factor-α stimulates the epithelial-to-mesenchymal transition of human colonic organoids. *Molecular Biology of the Cell* 14(5):1790-800, 2003.

13Becker, D. J. and J. B. Lowe. Fucose: Biosynthesis and biological function in mammals. *Glycobiology* 13(7):41R-53R, 2003.

14Bell, G. Models for the specific adhesion of cells to cells. *Science* 200(4342):618-27, 1978.

15Ben-Baruch, A. Host microenvironment in breast cancer development: Inflammatory cells, cytokines and chemokines in breast cancer progression: Reciprocal tumor-microenvironment interactions. 1465-542X (Electronic)):

16Berberoglu, U., E. Yildirim and O. Celen. Serum levels of tumor necrosis factor alpha correlate with response to neoadjuvant chemotherapy in locally advanced breast cancer. *International Journal of Biological Markers* 19(2):130-34, 2004.

17Berg, E. L., L. M. McEvoy, C. Berlin, R. F. Bargatze and E. C. Butcher. L-selectin-mediated lymphocyte rolling on madcam-1. *Nature* 366(6456):695-98, 1993.

18Bhatia, S. K., M. R. King and D. A. Hammer. The state diagram for cell adhesion mediated by two receptors. *Biophysical Journal* 84(4):2671-90, 2003.

19Bissell, M. J. and M. H. Barcellos-Hoff. The influence of extracellular matrix on gene expression: Is structure the message? *J Cell Sci Suppl* 8(327-43, 1987.

20Borsig, L., R. Wong, R. O. Hynes, N. M. Varki and A. Varki. Synergistic effects of l- and p-selectin in facilitating tumor metastasis can involve non-mucin ligands and implicate leukocytes as enhancers of metastasis. *Proceedings of the National Academy of Sciences of the United States of America* 99(4):2193-98, 2002.

21Brabletz, T., A. Jung, S. Reu, M. Porzner, F. Hlubek, L. A. Kunz-Schughart, R. Knuechel and T. Kirchner. Variable beta-catenin expression in colorectal cancers indicates tumor progression driven by the tumor environment. *Proceedings of the National Academy of Sciences of the United States of America* 98(18):10356-61, 2001.

22Brady, J. F. and G. Bossis. Stokesian dynamics. *Annual Review of Fluid Mechanics* 20(111-57, 1988.

23Brandley, B. K., M. Kiso, S. Abbas, P. Nikrad, O. Srivasatava, C. Foxall, Y. Oda and A. Hasegawa. Structure-function studies on selectin carbohydrate ligands. Modifications to fucose, sialic acid and sulphate as a sialic acid replacement. *Glycobiology* 3(6):633-41, 1993.

24Brayman, M., A. Thathiah and D. D. Carson. Muc1: A multifunctional cell surface component of reproductive tissue epithelia. *Reproductive biology and endocrinology : RB&E* 2(4, 2004.

25Brockhausen, I. Pathways of o-glycan biosynthesis in cancer cells. *Biochim. Biophys. Acta-Gen. Subj.* 1473(1):67-95, 1999.

26Brooks, D. E. The biorheology of tumor-cells. *Biorheology* 21(1-2):85-91, 1984.

27Brooks, S. A. and D. M. S. Hall. Investigations into the potential role of aberrant n-acetylgalactosamine glycans in tumour cell interactions with basement membrane components. *Clin. Exp. Metastasis* 19(6):487-93, 2002.

28Buisine, M. P., L. Devisme, P. Degand, M. C. Dieu, B. Gosselin, M. C. Copin, J. P. Aubert and N. Porchet. Developmental mucin gene expression in the gastroduodenal tract and accessory digestive glands. Ii. Duodenum and liver, gallbladder, and pancreas. *J. Histochem. Cytochem.* 48(12):1667-76, 2000.

29Burchell, J., S. Gendler, J. Taylorpapadimitriou, A. Girling, A. Lewis, R. Millis and D. Lamport. Development and characterization of breast-cancer reactive monoclonal-antibodies directed to the core protein of the human-milk mucin. *Cancer Research* 47(20):5476-82, 1987.

30Burdick, M., J. McCaffery, Y. Kim, B. Bochner and K. Konstantopoulos. Colon carcinoma cell glycolipids, integrins, and other glycoproteins mediate adhesion to huvecs under flow. *Am J Physiol Cell Physiol* 284(4):C977-87, 2003.

31Burdick, M. D., A. Harris, C. J. Reid, T. Iwamura and M. A. Hollingsworth. Oligosaccharides expressed an muc1 produced by pancreatic and colon tumor cell lines. *Journal of Biological Chemistry* 272(39):24198-202, 1997.

32Burdick, M. M., B. S. Bochner, B. E. Collins, R. L. Schnaar and K. Konstantopoulos. Glycolipids support e-selectin-specific strong cell tethering under flow. *Biochem. Biophys. Res. Commun.* 284(1):42-49, 2001.

33Burdick, M. M., J. M. McCaffery, Y. S. Kim, B. S. Bochner and K. Konstantopoulos. Colon carcinoma cell glycolipids, integrins, and other glycoproteins mediate adhesion to huvecs under flow. *Am. J. Physiol.-Cell Physiol.* 284(4):C977-C87, 2003.

34Butcher, E. C. Leukocyte-endothelial cell recognition - 3 (or more) steps to specificity and diversity. *Cell* 67(6):1033-36, 1991.

35Cao, T. M., T. Takatani and M. R. King. Effect of extracellular ph on selectin adhesion: Theory and experiment. *Biophysical Journal* 104(2):292-99, 2013.

36Caputo, K. E. and D. A. Hammer. Effect of microvillus deformability on leukocyte adhesion explored using adhesive dynamics simulations. *Biophysical Journal* 89(1):187-200, 2005.

37Carlsson, J. and J. M. Yuhas. Liquid-overlay culture of cellular spheroids. *Recent Results Cancer Res* 95(1-23, 1984.

38Carraway, K. L. and S. R. Hull. O-glycosylation pathway for mucin-type glycoproteins. *Bioessays* 10(4):117-21, 1989.

39Chandrasekaran, S., Y. Geng, L. A. DeLouise and M. R. King. Effect of homotypic and heterotypic interaction in 3d on the e-selectin mediated adhesive properties of breast cancer cell lines. *Biomaterials* 33(35):9037-48, 2012.

40Chandrasekaran, S., U. B. Giang, M. R. King and L. A. DeLouise. Microenvironment induced spheroid to sheeting transition of immortalized human keratinocytes (hacat) cultured in microbubbles formed in polydimethylsiloxane. *Biomaterials* 32(29):7159-68, 2011.

41Chang, K. C., D. F. J. Tees and D. A. Hammer. The state diagram for cell adhesion

under flow: Leukocyte rolling and firm adhesion. *Proc. Natl. Acad. Sci. U. S. A.* 97(21):11262-67, 2000.

42Chang, S. F., C. A. Chang, D. Y. Lee, P. L. Lee, Y. M. Yeh, C. R. Yeh, C. K. Cheng, S. Chien and J. J. Chiu. Tumor cell cycle arrest induced by shear stress: Roles of integrins and smad. *Proc Natl Acad Sci U S A* 105(10):3927-32, 2008.

43Chu, J. S. and K. J. Chang. Mucin expression in mucinous carcinoma and other invasive carcinomas of the breast. *Cancer Lett* 142(1):121-7, 1999.

44Condeelis, J. and J. W. Pollard. Macrophages: Obligate partners for tumor cell migration, invasion, and metastasis. *Cell* 124(2):263-6, 2006.

45Coussens, L. M. and Z. Werb. Inflammation and cancer. *Nature* 420(6917):860-7, 2002.

46Damiano, E. R., J. Westheider, A. Tozeren and K. Ley. Variation in the velocity, deformation, and adhesion energy density of leukocytes rolling within venules. *Circulation Research* 79(6):1122-30, 1996.

47Daniel, J. M. and A. B. Reynolds. Tyrosine phosphorylation and cadherin/catenin function. *Bioessays* 19(10):883-91, 1997.

48Davril, M., S. Degroote, P. Humbert, C. Galabert, V. Dumur, J. J. Lafitte, G. Lamblin and P. Roussel. The sialylation of bronchial mucins secreted by patients suffering from cystic fibrosis or from chronic bronchitis is related to the severity of airway infection. *Glycobiology* 9(3):311-21, 1999.

49de Vries, T., R. M. A. Knegtel, E. H. Holmes and B. A. Macher. Fucosyltransferases: Structure/function studies. *Glycobiology* 11(10):119R-28R, 2001.

50Deng, B., X. Yang, J. Liu, F. He, Z. Zhu and C. Zhang. Focal adhesion kinase

mediates tgf-β1-induced renal tubular epithelial-to-mesenchymal transition in vitro. *Molecular and Cellular Biochemistry* 340(1):21-29, 2010.

51Deng, X. S., S. Wang, A. Deng, B. Liu, S. M. Edgerton, S. E. Lind, R. Wahdan-Alaswad and A. D. Thor. Metformin targets stat3 to inhibit cell growth and induce apoptosis in triple-negative breast cancers. *Cell Cycle* 11(2):367-76, 2012.

52Dennis, J. W., M. Granovsky and C. E. Warren. Glycoprotein glycosylation and cancer progression. *Biochim. Biophys. Acta-Gen. Subj.* 1473(1):21-34, 1999.

53Desoize, B., D. Gimonet and J. C. Jardiller. Cell culture as spheroids: An approach to multicellular resistance. *Anticancer Res* 18(6A):4147-58, 1998.

54Desoize, B. and J. Jardillier. Multicellular resistance: A paradigm for clinical resistance? *Crit Rev Oncol Hematol* 36(2-3):193-207, 2000.

55Diamond, M. S., D. E. Staunton, A. R. Defougerolles, S. A. Stacker, J. Garciaaguilar, M. L. Hibbs and T. A. Springer. Icam-1 (cd54) - a counter-receptor for mac-1 (cd11b cd18). *Journal of Cell Biology* 111(6):3129-39, 1990.

56Dimitroff, C. J., L. Descheny, N. Trujillo, R. Kim, V. Nguyen, W. Huang, K. J. Pienta, J. L. Kutok and M. A. Rubin. Identification of leukocyte e-selectin ligands, p-selectin glycoprotein ligand-1 and e-selectin ligand-1, on human metastatic prostate tumor cells. *Cancer Res.* 65(13):5750-60, 2005.

57Dimitroff, C. J., J. Y. Lee, S. Rafii, R. C. Fuhlbrigge and R. Sackstein. Cd44 is a major e-selectin ligand on human hematopoietic progenitor cells. *Journal of Cell Biology* 153(6):1277-86, 2001.

58Ding, Z. M., J. E. Babensee, S. I. Simon, H. F. Lu, J. L. Perrard, D. C. Bullard, X. Y. Dai, S. K. Bromley, M. L. Dustin, M. L. Entman, C. W. Smith and C. M.

Ballantyne. Relative contribution of lfa-1 and mac-1 to neutrophil adhesion and migration. *Journal of Immunology* 163(9):5029-38, 1999.

59dit Faute, M. A., L. Laurent, D. Ploton, M. F. Poupon, J. C. Jardillier and H. Bobichon. Distinctive alterations of invasiveness, drug resistance and cell-cell organization in 3d-cultures of mcf-7, a human breast cancer cell line, and its multidrug resistant variant. *Clin Exp Metastasis* 19(2):161-8, 2002.

60Dokurno, P., P. A. Bates, H. A. Band, L. M. D. Stewart, J. M. Lally, J. M. Burchell, J. Taylor-Papadimitriou, D. Snary, M. J. E. Sternberg and P. S. Freemont. Crystal structure at 1.95 angstrom resolution of the breast tumour-specific antibody sm3 complexed with its peptide epitope reveals novel hypervariable loop recognition. *Journal of Molecular Biology* 284(3):713-28, 1998.

61Dong, C., J. Cao, E. J. Struble and H. W. Lipowsky. Mechanics of leukocyte deformation and adhesion to endothelium in shear flow. *Ann. Biomed. Eng.* 27(3):298-312, 1999.

62Dong, C. and X. X. Lei. Biomechanics of cell rolling: Shear flow, cell-surface adhesion, and cell deformability. *J. Biomech.* 33(1):35-43, 2000.

63Dong, C., R. Skalak, K. L. P. Sung, G. W. Schmidschonbein and S. Chien. Passive deformation analysis of human-leukocytes. *Journal of Biomechanical Engineering-Transactions of the Asme* 110(1):27-36, 1988.

64Dubessy, C., J. M. Merlin, C. Marchal and F. Guillemin. Spheroids in radiobiology and photodynamic therapy. *Crit Rev Oncol Hematol* 36(2-3):179-92, 2000.

65Duncan, T. J., N. F. S. Watson, A. H. Al-Attar, J. H. Scholefield and L. G. Durrant. The role of muc1 and muc3 in the biology and prognosis of colorectal cancer. *World*

*journal of surgical oncology* 5(31, 2007.

66Edelman, M. J., P. Potter, K. G. Mahaffey, R. Frink and R. B. Leidich. The potential for reintroduction of tumor cells during intraoperative blood salvage: Reduction of risk with use of the rc-400 leukocyte depletion filter. *Urology* 47(2):179-81, 1996.

67Essmann, U., L. Perera, M. Berkowitz, T. Darden, H. Lee and L. Pedersen. A smooth particle mesh ewald method. *The Journal of Chemical Physics* 103(19):8577-93, 1995.

68Essmann, U., L. Perera, M. L. Berkowitz, T. Darden, H. Lee and L. G. Pedersen. A smooth particle mesh ewald method. *J. Chem. Phys.* 103(19):8577-93, 1995.

69Fernandez-Rodriguez, J., O. Dwir, R. Alon and G. C. Hansson. Tumor cell muc1 and cd43 are glycosylated differently with sialyl-lewis a and x epitopes and show variable interactions with e-selectin under physiological flow conditions. *Glycoconj J* 18(11-12):925-30, 2001.

70Fidler, I. J. The relationship of embolic homogeneity, number, size and viability to the incidence of experimental metastasis. *European Journal of Cancer (1965)* 9(3):223-27, 1973.

71Finger, E. B., R. E. Bruehl, D. F. Bainton and T. A. Springer. A differential role for cell shape in neutrophil tethering and rolling on endothelial selectins under flow. *Journal of Immunology* 157(11):5085-96, 1996.

72Finzel, A., A. Reininger, P. Bode and L. Wurzinger. Icam-1 supports adhesion of human small-cell lung carcinoma to endothelial cells. *Clinical and Experimental Metastasis* 21(3):185-89, 2004.

73Friederichs, J., Y. Zeller, A. Hafezi-Moghadam, H. J. Grone, K. Ley and P. Altevogt. The cd24/p-selectin binding pathway initiates lung arrest of human a125 adenocarcinoma cells. *Cancer Research* 60(23):6714-22, 2000.

74Fruhauf, N. R., O. Dumpich, C. P. Kaudel, S. Kasimir-Bauer and K. J. Oldhafer. Filtration of malignant cells: Tumour cell depletion in an ex vivo model using a leukocyte adhesion filter. *Perfusion-Uk* 16(51-55, 2001.

75Fukuda, J., Y. Sakai and K. Nakazawa. Novel hepatocyte culture system developed using microfabrication and collagen/polyethylene glycol microcontact printing. *Biomaterials* 27(7):1061-70, 2006.

76Fuster, M. M. and J. D. Esko. The sweet and sour of cancer: Glycans as novel therapeutic targets. *Nat. Rev. Cancer* 5(7):526-42, 2005.

77Gallegos, B., E. Perez-Campos, R. Martinez, P. Leyva, M. Martinez, R. Hernandez, S. Pina, C. Hernandez, E. Zenteno and P. Hernandez. O-glycosylation expression in fibroadenoma. *Prep. Biochem. Biotechnol.* 40(1):1-12, 2010.

78Gay, L. J. and B. Felding-Habermann. Contribution of platelets to tumour metastasis. *Nat. Rev. Cancer* 11(2):123-34, 2011.

79Gendler, S. J. Muc1, the renaissance molecule. *J. Mammary Gland Biol. Neoplasia* 6(3):339-53, 2001.

80Gendler, S. J. and A. P. Spicer. Epithelial mucin genes. *Annu Rev Physiol* 57(607-34, 1995.

81Geng, Y., S. Chandrasekaran, J.-W. Hsu, M. Gidwani, A. D. Hughes and M. R. King. Phenotypic switch in blood: Effects of pro-inflammatory cytokines on breast cancer cell aggregation and adhesion. *PLoS ONE* 8(1):e54959, 2013.

82Geng, Y., J. R. Marshall and M. R. King. Glycomechanics of the metastatic cascade: Tumor cell-endothelial cell interactions in the circulation. *Ann Biomed Eng* 40(4):790-805, 2012.

83Geng, Y., S. Narasipura, G. M. Seigel and M. R. King. Vascular recruitment of human retinoblastoma cells by multi-cellular adhesive interactions with circulating leukocytes. *Cellular and Molecular Bioengineering* 3(4):361-68, 2010.

84Geng, Y., K. Yeh, T. Takatani and M. R. King. Three to tango: Muc1 as a ligand for both e-selectin and icam-1 in the breast cancer metastatic cascade. *Front Oncol* 2(76, 2012.

85Giang, U. B., D. Lee, M. R. King and L. A. DeLouise. Microfabrication of cavities in polydimethylsiloxane using drie silicon molds. *Lab Chip* 7(12):1660-2, 2007.

86Girling, A., J. Bartkova, J. Burchell, S. Gendler, C. Gillett and J. Taylorpapadimitriou. A core protein epitope of the polymorphic epithelial mucin detected by the monoclonal-antibody sm-3 is selectively exposed in a range of primary carcinomas. *International Journal of Cancer* 43(6):1072-76, 1989.

87Glinsky, G. V. and V. V. Glinsky. Apoptosis and metastasis: A superior resistance of metastatic cancer cells to programmed cell death. *Cancer Letters* 101(1):43-51, 1996.

88Goetz, D. J., M. E. ElSabban, D. A. Hammer and B. U. Pauli. Lu-ecam-1-mediated adhesion of melanoma cells to endothelium under conditions of flow. *International Journal of Cancer* 65(2):192-99, 1996.

89Goswami, K., H. Nandeesha, B. Koner and D. Nandakumar. A comparative study of serum protein-bound sialic acid in benign and malignant prostatic growth: Possible

role of oxidative stress in sialic acid homeostasis. *Prostate Cancer and Prostatic Diseases* 10(4):356-59, 2007.

90Grivennikov, S. I., F. R. Greten and M. Karin. Immunity, inflammation, and cancer. *Cell* 140(6):883-99, 2010.

91Groux-degroote, S., M.-A. Krzewinski-recchi, A. Cazet, A. Vincent, S. Lehoux, J.-J. Lafitte, I. van seuningen and P. Delannoy. Il-6 and il-8 increase the expression of glycosyltransferases and sulfotransferases involved in the biosynthesis of sialylated and/or sulfated lewisx epitopes in the human bronchial mucosa. *Biochem J* 410(1):213-23, 2008.

92Guan, F., K. Handa and S. Hakomori. Specific glycosphingolipids mediate epithelial-to-mesenchymal transition of human and mouse epithelial cell lines. *Proc Natl Acad Sci U S A* 106(18):7461-6, 2009.

93Guddo, F., A. Giatromanolaki, M. I. Koukourakis, C. Reina, A. M. Vignola, G. Chlouverakis, J. Hilkens, K. C. Gatter, A. L. Harris and G. Bonsignore. Muc1 (episialin) expression in non-small cell lung cancer is independent of egfr and c-erbb-2 expression and correlates with poor survival in node positive patients. *Journal of Clinical Pathology* 51(9):667-71, 1998.

94Hakomori, S. I. Cell adhesion/recognition and signal transduction through glycosphingolipid microdomain. *Glycoconj J* 17(3 -4):143-51, 2000.

95Hammer, D. A. Leukocyte adhesion: What's the catch? *Curr. Biol.* 15(3):R96-R99, 2005.

96Hammer, D. A. and S. M. Apte. Simulation of cell rolling and adhesion on surfaces in shear-flow - general results and analysis of selectin-mediated neutrophil adhesion.

*Biophysical Journal* 63(1):35-57, 1992.

97Hanisch, F. A. O-glycosylation of the mucin type. *Biol. Chem.* 382(2):143-49, 2001.

98Hanley, W. D., M. M. Burdick, K. Konstantopoulos and R. Sackstein. Cd44 on ls174t colon carcinoma cells possesses e-selectin ligand activity. *Cancer Res.* 65(13):5812-17, 2005.

99Harrison, P. and E. M. Cramer. Platelet alpha-granules. *Blood Rev* 7(1):52-62, 1993.

100Hayashi, T., T. Takahashi, S. Motoya, T. Ishida, F. Itoh, M. Adachi, Y. Hinoda and K. Imai. Muc1 mucin core protein binds to the domain 1 of icam-1. *Digestion* 63 Suppl 1(87-92, 2001.

101Hentzen, E. R., S. Neelamegham, G. S. Kansas, J. A. Benanti, L. V. McIntire, C. W. Smith and S. I. Simon. Sequential binding of cd11a/cd18 and cd11b/cd18 defines neutrophil capture and stable adhesion to intercellular adhesion molecule-1. *Blood* 95(3):911-20, 2000.

102Heuberger, J. and W. Birchmeier. Interplay of cadherin-mediated cell adhesion and canonical wnt signaling. *Cold Spring Harb Perspect Biol* 2(2):a002915,

103Hidalgo, A., A. J. Peired, M. K. Wild, D. Vestweber and P. S. Frenette. Complete identification of e-selectin ligands on neutrophils reveals distinct functions of psgl-1, esl-1, and cd44. *Immunity* 26(4):477-89, 2007.

104Hirschhaeuser, F., H. Menne, C. Dittfeld, J. West, W. Mueller-Klieser and L. A. Kunz-Schughart. Multicellular tumor spheroids: An underestimated tool is catching up again. *Journal of Biotechnology* 148(1):3-15, 2010.

105Ho, W. J., E. A. Pham, J. W. Kim, C. W. Ng, J. H. Kim, D. T. Kamei and B. M. Wu. Incorporation of multicellular spheroids into 3-d polymeric scaffolds provides an improved tumor model for screening anticancer drugs. *Cancer Sci* 101(12):2637-43,

106Ho, W. J., E. A. Pham, J. W. Kim, C. W. Ng, J. H. Kim, D. T. Kamei and B. M. Wu. Incorporation of multicellular spheroids into 3-d polymeric scaffolds provides an improved tumor model for screening anticancer drugs. *Cancer Sci* 101(12):2637-43, 2010.

107Hollingsworth, M. A. and B. J. Swanson. Mucins in cancer: Protection and control of the cell surface. *Nat. Rev. Cancer* 4(1):45-60, 2004.

108Hou, J.-M., M. Krebs, T. Ward, K. Morris, R. Sloane, F. Blackhall and C. Dive. Circulating tumor cells, enumeration and beyond. *Cancers* 2(2):1236-50, 2010.

109Huang, Z. and M. R. King. An immobilized nanoparticle-based platform for efficient gene knockdown of targeted cells in the circulation. *Gene Ther.* 16(10):1271-82, 2009.

110Hughes, A. D., J. Mattison, J. D. Powderly, B. T. Greene and M. R. King. Rapid isolation of viable circulating tumor cells from patient blood samples. *J Vis Exp* 64):e4248, 2012.

111Hughes, A. D., J. Mattison, L. T. Western, J. D. Powderly, B. T. Greene and M. R. King. Microtube device for selectin-mediated capture of viable circulating tumor cells from blood. *Clin Chem* 58(5):846-53, 2012.

112Ilyas, M., I. P. Tomlinson, A. Rowan, M. Pignatelli and W. F. Bodmer. Beta-catenin mutations in cell lines established from human colorectal cancers. *Proc Natl Acad Sci U S A* 94(19):10330-4, 1997.

113Inata, J., N. Hattori, A. Yokoyama, S. Ohshimo, M. Doi, N. Ishikawa, H. Hamada and N. Kohno. Circulating kl-6/muc1 mucin carrying sialyl lewis(a) oligosaccharide is an independent prognostic factor in patients with lung adenocarcinoma. *International Journal of Cancer* 120(12):2643-49, 2007.

114Jadhav, S., B. S. Bochner and K. Konstantopoulos. Hydrodynamic shear regulates the kinetics and receptor specificity of polymorphonuclear leukocyte-colon carcinoma cell adhesive interactions. *Journal of Immunology* 167(10):5986-93, 2001.

115Jadhav, S., C. D. Eggleton and K. Konstantopoulos. A 3-d computational model predicts that cell deformation affects selectin-mediated leukocyte rolling. *Biophysical Journal* 88(1):96-104, 2005.

116Jadhav, S. and K. Konstantopoulos. Fluid shear- and time-dependent modulation of molecular interactions between pmns and colon carcinomas. *Am. J. Physiol.-Cell Physiol.* 283(4):C1133-C43, 2002.

117Jeanes, A., C. J. Gottardi and A. S. Yap. Cadherins and cancer: How does cadherin dysfunction promote tumor progression? *Oncogene* 27(55):6920-9, 2008.

118Jin, Q., C. Verdier, P. Singh, N. Aubry, R. Chotard-Ghodsnia and A. Duperray. Migration and deformation of leukocytes in pressure driven flows. *Mech. Res. Commun.* 34(5-6):411-22, 2007.

119Johnson, F. E., M. Zhou, B. T. Collins and J. S. Huang. Mechanical deformation induces proliferation of human colorectal carcinoma cells. *Int. J. Oncol.* 16(3):617-22, 2000.

120Kannagi, R., M. Izawa, T. Koike, K. Miyazaki and N. Kimura. Carbohydrate-mediated cell adhesion in cancer metastasis and angiogenesis. *Cancer Sci.* 95(5):377-

84, 2004.

121Kansas, G. S. Selectins and their ligands: Current concepts and controversies. *Blood* 88(9):3259-87, 1996.

122Keller, G. M. In vitro differentiation of embryonic stem cells. *Curr Opin Cell Biol* 7(6):862-9, 1995.

123Kelly, C. P., J. C. Okeane, J. Orellana, P. C. Schroy, S. Yang, J. T. Lamont and H. R. Brady. Human colon cancer-cells express icam-1 invivo and support lfa-1-dependent lymphocyte adhesion invitro. *American Journal of Physiology* 263(6):G864-G70, 1992.

124Khismatullin, D. B. and G. A. Truskey. A 3d numerical study of the effect of channel height on leukocyte deformation and adhesion in parallel-plate flow chambers. *Microvascular Research* 68(3):188-202, 2004.

125Kim, Y. J., L. Borsig, H. L. Han, N. M. Varki and A. Varki. Distinct selectin ligands on colon carcinoma mucins can mediate pathological interactions among platelets, leukocytes, and endothelium. *American Journal of Pathology* 155(2):461-72, 1999.

126Kim, Y. J., L. Borsig, N. M. Varki and A. Varki. P-selectin deficiency attenuates tumor growth and metastasis. *Proc Natl Acad Sci U S A* 95(16):9325-30, 1998.

127Kim, Y. J., L. Borsig, N. M. Varki and A. Varki. P-selectin deficiency attenuates tumor growth and metastasis. *Proc. Natl. Acad. Sci. U. S. A.* 95(16):9325-30, 1998.

128Kim, Y. S., J. Gum and I. Brockhausen. Mucin glycoproteins in neoplasia. *Glycoconjugate J.* 13(5):693-707, 1996.

129

130King, M. R., D. Bansal, M. B. Kim and I. H. Sarelius. The effect of hematocrit and leukocyte adherence on flow direction in the microcirculation. *Ann. Biomed. Eng.* 32(6):803-14, 2004.

131King, M. R. and D. A. Hammer. Multiparticle adhesive dynamics: Hydrodynamic recruitment of rolling leukocytes. *Proc. Natl. Acad. Sci. U. S. A.* 98(26):14919-24, 2001.

132King, M. R. and D. A. Hammer. Multiparticle adhesive dynamics. Interactions between stably rolling cells. *Biophysical Journal* 81(2):799-813, 2001.

133King, M. R., V. Heinrich, E. Evans and D. A. Hammer. Nano-to-micro scale dynamics of p-selectin detachment from leukocyte interfaces. Iii. Numerical simulation of tethering under flow. *Biophysical Journal* 88(3):1676-83, 2005.

134King, M. R., M. B. Kim, I. H. Sarelius and D. A. Hammer. Hydrodynamic interactions between rolling leukocytes in vivo. *Microcirculation* 10(5):401-09, 2003.

135King, M. R., S. D. Rodgers and D. A. Hammer. Hydrodynamic collisions suppress fluctuations in the rolling velocity of adhesive blood cells. *Langmuir* 17(14):4139-43, 2001.

136King, M. R., A. D. Ruscio, M. B. Kim and I. H. Sarelius. Interactions between stably rolling leukocytes in vivo. *Physics of Fluids* 17(3):2005.

137King, M. R., R. Sumagin, C. E. Green and S. I. Simon. Rolling dynamics of a neutrophil with redistributed l-selectin. *Math. Biosci.* 194(1):71-79, 2005.

138King, M. R., L. T. Western, K. Rana and J. L. Liesveld. Biomolecular surfaces for the capture and reprogramming of circulating tumor cells. *J. Bionic Eng.* 6(4):311-17, 2009.

139Kocer, B., A. Soran, G. Kiyak, S. Erdogan, A. Eroglu, B. Bozkurt, C. Solak and O. Cengiz. Prognostic significance of mucin expression in gastric carcinoma. *Digestive Diseases and Sciences* 49(6):954-64, 2004.

140Konagurthu, A. S., J. C. Whisstock, P. J. Stuckey and A. M. Lesk. Mustang: A multiple structural alignment algorithm. *Proteins* 64(3):559-74, 2006.

141Konstantopoulos, K. and S. N. Thomas. Cancer cells in transit: The vascular interactions of tumor cells. *Annual Review of Biomedical Engineering* 11(177-202, 2009.

142Korn, C. B. and U. S. Schwarz. Dynamic states of cells adhering in shear flow: From slipping to rolling. *Physical Review E* 77(4):2008.

143Kozlowski, L., I. Zakrzewska, P. Tokajuk and M. Z. Wojtukiewicz. Concentration of interleukin-6 (il-6), interleukin-8 (il-8) and interleukin-10 (il-10) in blood serum of breast cancer patients. *Roczniki Akademii Medycznej w Bialymstoku (1995)* 48(82-4, 2003.

144Krasik, E. F., K. E. Caputo and D. A. Hammer. Adhesive dynamics simulation of neutrophil arrest with stochastic activation. *Biophysical Journal* 95(4):1716-28, 2008.

145Krieger, E., T. Darden, S. B. Nabuurs, A. Finkelstein and G. Vriend. Making optimal use of empirical energy functions: Force-field parameterization in crystal space. *Proteins* 57(4):678-83, 2004.

146L√§ubli, H. and L. Borsig. Selectins promote tumor metastasis. *Seminars in Cancer Biology* 20(3):169-77, 2010.

147Lagow, E. L. and D. D. Carson. Synergistic stimulation of muc1 expression in normal breast epithelia and breast cancer cells by interferon-gamma and tumor

necrosis factor-alpha. *J Cell Biochem* 86(4):759-72, 2002.

148Laskowska, A., B. Dolińiska-Krajewska, M. Zabel and M. Ugorski. Sialosyl le(a)-carrying gangliosides present on the surface of colon carcinoma cells are not directly involved in adhesion to e-selectin. *Eur J Cell Biol* 80(12):784-91, 2001.

149Lawrence, M. B. and T. A. Springer. Leukocytes roll on a selectin at physiological flow-rates - distinction from and prerequisite for adhesion through integrins. *Cell* 65(5):859-73, 1991.

150Lawrence, M. B. and T. A. Springer. Neutrophils roll on e-selectin. *Journal of Immunology* 151(11):6338-46, 1993.

151Lee, D., K. E. Caputo, D. A. Hammer and M. R. King. Adhesive dynamics simulations of the mechanical shedding of l-selectin from the neutrophil surface. *J. Theor. Biol.* 260(1):27-30, 2009.

152Lee, D. and M. R. King. Shear-induced capping of l-selectin on the neutrophil surface during centrifugation. *J. Immunol. Methods* 328(1-2):97-105, 2007.

153Lee, D., J. B. Schultz, P. A. Knauf and M. R. King. Mechanical shedding of l-selectin from the neutrophil surface during rolling on sialyl lewis x under flow. *Journal of Biological Chemistry* 282(7):4812-20, 2007.

154Lee, M. J., H. S. Lee, W. H. Kim, Y. Choi and M. H. Yang. Expression of mucins and cytokeratins in primary carcinomas of the digestive system. *Mod. Pathol.* 16(5):403-10, 2003.

155Lee, S. O., W. Lou, M. Hou, F. de Miguel, L. Gerber and A. C. Gao. Interleukin-6 promotes androgen-independent growth in lncap human prostate cancer cells. *Clin Cancer Res* 9(1):370-6, 2003.

156Lehmann, B. D., J. A. Bauer, X. Chen, M. E. Sanders, A. B. Chakravarthy, Y. Shyr and J. A. Pietenpol. Identification of human triple-negative breast cancer subtypes and preclinical models for selection of targeted therapies. *J Clin Invest* 121(7):2750-67, 2011.

157Ley, K., C. Laudanna, M. I. Cybulsky and S. Nourshargh. Getting to the site of inflammation: The leukocyte adhesion cascade updated. *Nature Reviews Immunology* 7(9):678-89, 2007.

158Li, J. and M. R. King. Adhesion receptors as therapeutic targets for circulating tumor cells. *Front Oncol* 2(79, 2012.

159Liang, S., M. Hoskins, P. Khanna, R. F. Kunz and C. Dong. Effects of the tumor-leukocyte microenvironment on melanoma-neutrophil adhesion to the endothelium in a shear flow. *Cell. Mol. Bioeng.* 1(2-3):189-200, 2008.

160Liang, S., M. J. Slattery, D. Wagner, S. I. Simon and C. Dong. Hydrodynamic shear rate regulates melanoma-leukocyte aggregation, melanoma adhesion to the endothelium, and subsequent extravasation. *Ann. Biomed. Eng.* 36(4):661-71, 2008.

161Lichtenstein, A. Stimulation of the respiratory burst of murine peritoneal inflammatory neutrophils by conjugation with tumor-cells. *Cancer Research* 47(9):2211-17, 1987.

162Lloyd, K. O., J. Burchell, V. Kudryashov, B. W. T. Yin and J. TaylorPapadimitriou. Comparison of o-linked carbohydrate chains in muc-1 mucin from normal breast epithelial cell lines and breast carcinoma cell lines - demonstration of simpler and fewer glycan chains in tumor cells. *Journal of Biological Chemistry* 271(52):33325-34, 1996.

163Lou, J. Z., T. Yago, A. G. Klopocki, P. Mehta, W. Chen, V. I. Zarnitsyna, N. V. Bovin, C. Zhu and R. P. McEver. Flow-enhanced adhesion regulated by a selectin interdomain hinge. *Journal of Cell Biology* 174(7):1107-17, 2006.

164Lowe, J. B. Glycosylation in the control of selectin counter-receptor structure and function. *Immunological Reviews* 186(19-36, 2002.

165Luque-Ramirez, M. and H. F. Escobar-Morreale. Treatment of polycystic ovary syndrome (pcos) with metformin ameliorates insulin resistance in parallel with the decrease of serum interleukin-6 concentrations. *Horm Metab Res* 42(11):815-20, 2010.

166Lyon, D. E., N. L. McCain, J. Walter and C. Schubert. Cytokine comparisons between women with breast cancer and women with a negative breast biopsy. *Nurs Res* 57(1):51-8, 2008.

167Ma, B., J. L. Simala-Grant and D. E. Taylor. Fucosylation in prokaryotes and eukaryotes. *Glycobiology* 16(12):158R-84R, 2006.

168MacLean, G. D., M. A. Reddish and B. M. Longenecker. Prognostic significance of preimmunotherapy serum ca27.29 (muc-1) mucin level after active specific immunotherapy of metastatic adenocarcinoma patients. *Journal of Immunotherapy* 20(1):70-78, 1997.

169Marui, N., M. K. Offermann, R. Swerlick, C. Kunsch, C. A. Rosen, M. Ahmad, R. W. Alexander and R. M. Medford. Vascular cell adhesion molecule-1 (vcam-1) gene transcription and expression are regulated through an antioxidant-sensitive mechanism in human vascular endothelial cells. *The Journal of Clinical Investigation* 92(4):1866-74, 1993.

170Maruo, Y., A. Gochi, A. Kaihara, H. Shimamura, T. Yamada, N. Tanaka and K. Orita. Icam-1 expression and the soluble icam-1 level for evaluating the metastatic potential of gastric cancer. *International Journal of Cancer* 100(4):486-90, 2002.

171Masaki, Y., M. Oka, Y. Ogura, T. Ueno, K. Nishihara, A. Tangoku, M. Takahashi, M. Yamamoto and T. Irimura. Sialylated muc1 mucin expression in normal pancreas, benign pancreatic lesions, and pancreatic ductal adenocarcinoma. *Hepato-Gastroenterol*. 46(28):2240-45, 1999.

172Matta, A., R. Ralhan, L. V. DeSouza and K. W. Siu. Mass spectrometry-based clinical proteomics: Head-and-neck cancer biomarkers and drug-targets discovery. *Mass Spectrom Rev* 29(6):945-61, 2010.

173Mayadas, T. N., R. C. Johnson, H. Rayburn, R. O. Hynes and D. D. Wagner. Leukocyte rolling and extravasation are severely compromised in p-selectin-deficient mice. *Cell* 74(3):541-54, 1993.

174McCarty, O. J., S. A. Mousa, P. F. Bray and K. Konstantopoulos. Immobilized platelets support human colon carcinoma cell tethering, rolling, and firm adhesion under dynamic flow conditions. *Blood* 96(5):1789-97, 2000.

175McEver, R. P. Role of selectins in leukocyte adhesion to platelets and endothelium. *Ann N Y Acad Sci* 714(185-9, 1994.

176McEver, R. P. Selectins: Lectins that initiate cell adhesion under flow. *Curr. Opin. Cell Biol*. 14(5):581-86, 2002.

177McIntyre, T. M., S. M. Prescott, A. S. Weyrich and G. A. Zimmerman. Cell-cell interactions: Leukocyte-endothelial interactions. *Curr. Opin. Hematol*. 10(2):150-58, 2003.

178Mellor, H. R., D. J. Ferguson and R. Callaghan. A model of quiescent tumour microregions for evaluating multicellular resistance to chemotherapeutic drugs. *Br J Cancer* 93(3):302-9, 2005.

179Micalizzi, D. S., S. M. Farabaugh and H. L. Ford. Epithelial-mesenchymal transition in cancer: Parallels between normal development and tumor progression. *J Mammary Gland Biol Neoplasia* 15(2):117-34, 2010.

180Minn, A. J., Y. B. Kang, I. Serganova, G. P. Gupta, D. D. Giri, M. Doubrovin, V. Ponomarev, W. L. Gerald, R. Blasberg and J. Massague. Distinct organ-specific metastatic potential of individual breast cancer cells and primary tumors. *Journal of Clinical Investigation* 115(1):44-55, 2005.

181Mommers, E. C. M., A. M. Leonhart, S. von Mensdorff-Pouilly, D. J. Schol, J. Hilgers, C. J. L. M. Meijer, J. P. A. Baak and P. J. van Diest. Aberrant expression of muc1 mucin in ductal hyperplasia and ductal carcinoma in situ of the breast. *International Journal of Cancer* 84(5):466-69, 1999.

182Mong, T. K. K., H. K. Lee, S. G. Duron and C. H. Wong. Reactivity-based one-pot total synthesis of fucose gm(1) oligosaccharide: A sialylated antigenic epitope of small-cell lung cancer. *Proc. Natl. Acad. Sci. U. S. A.* 100(3):797-802, 2003.

183Monzavi-Karbassi, B., J. S. Stanley, L. Hennings, F. Jousheghany, C. Artaud, S. Shaaf and T. Kieber-Emmons. Chondroitin sulfate glycosaminoglycans as major p-selectin ligands on metastatic breast cancer cell lines. *International Journal of Cancer* 120(6):1179-91, 2007.

184Moore, A., Z. Medarova, A. Potthast and G. Dai. In vivo targeting of underglycosylated muc-1 tumor antigen using a multimodal imaging probe. *Cancer*

*Res*. 64(5):1821-27, 2004.

185Moore, K. L., S. F. Eaton, D. E. Lyons, H. S. Lichenstein, R. D. Cummings and R. P. McEver. The p-selectin glycoprotein ligand from human neutrophils displays sialylated, fucosylated, o-linked poly-n-acetyllactosamine. *Journal of Biological Chemistry* 269(37):23318-27, 1994.

186Moss, M. A. and K. W. Anderson. Adhesion of cancer cells to endothelial monolayers: A study of initial attachment versus firm adhesion. *Journal of Adhesion* 74(1-4):19-40, 2000.

187Mueller-Klieser, W. Three-dimensional cell cultures: From molecular mechanisms to clinical applications. *Am J Physiol* 273(4 Pt 1):C1109-23, 1997.

188Muir, C. P., M. A. Adams and C. H. Graham. Nitric oxide attenuates resistance to doxorubicin in three-dimensional aggregates of human breast carcinoma cells. *Breast Cancer Res Treat* 96(2):169-76, 2006.

189Muller, A., B. Homey, H. Soto, N. Ge, D. Catron, M. E. Buchanan, T. McClanahan, E. Murphy, W. Yuan, S. N. Wagner, J. L. Barrera, A. Mohar, E. Verastegui and A. Zlotnik. Involvement of chemokine receptors in breast cancer metastasis. *Nature* 410(6824):50-56, 2001.

190Muthukumaran, N., K. E. Miletti-Gonzalez, A. K. Ravindranath and L. Rodriguez-Rodriguez. Tumor necrosis factor-alpha differentially modulates cd44 expression in ovarian cancer cells. *Mol Cancer Res* 4(8):511-20, 2006.

191Myung, J. H., K. A. Gajjar, R. M. Pearson, C. A. Launiere, D. T. Eddington and S. Hong. Direct measurements on cd24-mediated rolling of human breast cancer mcf-7 cells on e-selectin. *Analytical Chemistry* 83(3):1078-83, 2011.

192Nagrath, S., L. V. Sequist, S. Maheswaran, D. W. Bell, D. Irimia, L. Ulkus, M. R. Smith, E. L. Kwak, S. Digumarthy, A. Muzikansky, P. Ryan, U. J. Balis, R. G. Tompkins, D. A. Haber and M. Toner. Isolation of rare circulating tumour cells in cancer patients by microchip technology. *Nature* 450(7173):1235-U10, 2007.

193Nakazawa, K., Y. Izumi and R. Mori. Morphological and functional studies of rat hepatocytes on a hydrophobic or hydrophilic polydimethylsiloxane surface. *Acta Biomater* 5(2):613-20, 2009.

194Narasipura, S. D., J. C. Wojciechowski, N. Charles, J. L. Liesveld and M. R. King. P-selectin-coated microtube for enrichment of cd34(+) hematopoietic stem and progenitor cells from human bone marrow hematology. *Clinical Chemistry* 54(1):77-85, 2008.

195Narasipura, S. D., J. C. Wojclechowski, B. M. Duffy, J. L. Liesveld and M. R. King. Purification of cd45+ hematopoietic cells directly from human bone marrow using a flow-based p-selectin-coated microtube. *American Journal of Hematology* 83(8):627-29, 2008.

196Narita, T., N. Kawakami-Kimura, N. Matsuura, H. Funahashi and R. Kannagi. Adhesion of human breast cancer cells to vascular endothelium mediated by sialyl lewis<sup>x</sup>/e-selectin. *Breast Cancer* 3(1):19-23, 1996.

197Nelson, W. J. and R. Nusse. Convergence of wnt, beta-catenin, and cadherin pathways. *Science* 303(5663):1483-7, 2004.

198Nicolson, G. L. Paracrine and autocrine growth mechanisms in tumor-metastasis to specific sites with particular emphasis on brain and lung metastasis. *Cancer and Metastasis Reviews* 12(3-4):325-43, 1993.

199Norgard, K. E., K. L. Moore, S. Diaz, N. L. Stults, S. Ushiyama, R. P. McEver, R. D. Cummings and A. Varki. Characterization of a specific ligand for p-selectin on myeloid cells - a minor glycoprotein with sialylated o-linked oligosaccharides. *Journal of Biological Chemistry* 268(17):12764-74, 1993.

200Oda, T., Y. Kanai, T. Oyama, K. Yoshiura, Y. Shimoyama, W. Birchmeier, T. Sugimura and S. Hirohashi. E-cadherin gene mutations in human gastric carcinoma cell lines. *Proc Natl Acad Sci U S A* 91(5):1858-62, 1994.

201Ohtsubo, K. and J. D. Marth. Glycosylation in cellular mechanisms of health and disease. *Cell* 126(5):855-67, 2006.

202Orr, F. W., H. H. Wang, R. M. Lafrenie, S. Scherbarth and D. M. Nance. Interactions between cancer cells and the endothelium in metastasis. *Journal of Pathology* 190(3):310-29, 2000.

203Oyama, T., Y. Kanai, A. Ochiai, S. Akimoto, T. Oda, K. Yanagihara, A. Nagafuchi, S. Tsukita, S. Shibamoto, F. Ito and et al. A truncated beta-catenin disrupts the interaction between e-cadherin and alpha-catenin: A cause of loss of intercellular adhesiveness in human cancer cell lines. *Cancer Res* 54(23):6282-7, 1994.

204Pandit, T. S., W. Kennette, L. Mackenzie, G. Zhang, W. Al-Katib, J. Andrews, S. A. Vantyghem, D. G. Ormond, A. L. Allan, D. I. Rodenhiser, A. F. Chambers and A. B. Tuck. Lymphatic metastasis of breast cancer cells is associated with differential gene expression profiles that predict cancer stem cell-like properties and the ability to survive, establish and grow in a foreign environment. *Int J Oncol* 35(2):297-308, 2009.

205Papadopoulou, S., A. Scorilas, N. Arnogianaki, B. Papapanayiotou, A.

Tzimogiani, N. Agnantis and M. Talieri. Expression of gelatinase-a (mmp-2) in human colon cancer and normal colon mucosa. *Tumour Biol* 22(6):383-9, 2001.

206Park, E. Y. H., M. J. Smith, E. S. Stropp, K. R. Snapp, J. A. DiVietro, W. F. Walker, D. W. Schmidtke, S. L. Diamond and M. B. Lawrence. Comparison of psgl-1 microbead and neutrophil rolling: Microvillus elongation stabilizes p-selectin bond clusters. *Biophysical Journal* 82(4):1835-47, 2002.

207Paterlini-Brechot, P. and N. L. Benali. Circulating tumor cells (ctc) detection: Clinical impact and future directions. *Cancer Letters* 253(2):180-204, 2007.

208Patsos, G., V. Hebbe-Viton, C. Robbe-Masselot, D. Masselot, R. S. Martin, R. Greenwood, C. Paraskeva, A. Klein, M. Graessmann, J. C. Michalski, T. Gallagher and A. Corfield. O-glycan inhibitors generate aryl-glycans, induce apoptosis and lead to growth inhibition in colorectal cancer cell lines. *Glycobiology* 19(4):382-98, 2009.

209Perseghin, P., M. Vigano, G. Rocco, C. DellaPona, A. Buscemi and A. Rizzi. Effectiveness of leukocyte filters in reducing tumor cell contamination after intraoperative blood salvage in lung cancer patients. *Vox Sanguinis* 72(4):221-24, 1997.

210Phan, U. T., T. T Waldron and T. A. Springer. Remodeling of the lectin-egf-like domain interface in p- and l-selectin increases adhesiveness and shear resistance under hydrodynamic force. *Nat. Immunol.* 7(8):883-89, 2006.

211Poste, G. and I. J. Fidler. The pathogenesis of cancer metastasis. *Nature* 283(5743):139-46, 1980.

212Pouyani, T. and B. Seed. Psgl-1 recognition of p-selectin is controlled by a tyrosine sulfation consensus at the psgl-1 amino-terminus. *Cell* 83(2):333-43, 1995.

213Puri, K. D., E. B. Finger, G. Gaudernack and T. A. Springer. Sialomucin cd34 is the major l-selectin ligand in human tonsil high endothelial venules. *Journal of Cell Biology* 131(1):261-70, 1995.

214Queen, M. M., R. E. Ryan, R. G. Holzer, C. R. Keller-Peck and C. L. Jorcyk. Breast cancer cells stimulate neutrophils to produce oncostatin m: Potential implications for tumor progression. *Cancer Research* 65(19):8896-904, 2005.

215Rachagani, S., M. P. Torres, N. Moniaux and S. K. Batra. Current status of mucins in the diagnosis and therapy of cancer. *Biofactors* 35(6):509-27, 2009.

216Rahn, J., J. Chow, G. Horne, B. Mah, J. Emerman, P. Hoffman and J. Hugh. Muc1 mediates transendothelial migration <i>in vitro</i> by ligating endothelial cell icam-1. 6):475-83, 2005.

217Ramaswamy, S., K. N. Ross, E. S. Lander and T. R. Golub. A molecular signature of metastasis in primary solid tumors. *Nat Genet* 33(1):49-54, 2003.

218Rana, K., J. L. Liesveld and M. R. King. Delivery of apoptotic signal to rolling cancer cells: A novel biomimetic technique using immobilized trail and e-selectin. *Biotechnol Bioeng* 102(6):1692-702, 2009.

219Regimbald, L. H., L. M. Pilarski, B. M. Longenecker, M. A. Reddish, G. Zimmermann and J. C. Hugh. The breast mucin muc1 as a novel adhesion ligand for endothelial intercellular adhesion molecule 1 in breast cancer. *Cancer Res*. 56(18):4244-49, 1996.

220Reis, C. A., H. Osorio, L. Silva, C. Gomes and L. David. Alterations in glycosylation as biomarkers for cancer detection. *J. Clin. Pathol*. 63(4):322-29, 2010.

221Retz, M., J. Lehmann, C. Roder, B. Plotz, J. Harder, J. Eggers, J. Pauluschke, H.

Kalthoff and M. Stockle. Differential mucin muc7 gene expression in invasive bladder carcinoma in contrast to uniform muc1 and muc2 gene expression in both normal urothelium and bladder carcinoma. *Cancer Res*. 58(24):5662-66, 1998.

222Riethdorf, S., H. Fritsche, V. Muller, T. Rau, C. Schindibeck, B. Rack, W. Janni, C. Coith, K. Beck, F. Janicke, S. Jackson, T. Gornet, M. Cristofanilli and K. Pantel. Detection of circulating tumor cells in peripheral blood of patients with metastatic breast cancer: A validation study of the cellsearch system. *Clin. Cancer Res*. 13(3):920-28, 2007.

223Ringel, J. and M. Lohr. The muc gene family: Their role in diagnosis and early detection of pancreatic cancer. *Molecular cancer* 2(9, 2003.

224Rodriguez-Enriquez, S., J. C. Gallardo-Perez, A. Aviles-Salas, A. Marin-Hernandez, L. Carreno-Fuentes, V. Maldonado-Lagunas and R. Moreno-Sanchez. Energy metabolism transition in multi-cellular human tumor spheroids. *J Cell Physiol* 216(1):189-97, 2008.

225Rosette, C., R. B. Roth, P. Oeth, A. Braun, S. Kammerer, J. Ekblom and M. F. Denissenko. Role of icam1 in invasion of human breast cancer cells. *Carcinogenesis* 26(5):943-50, 2005.

226Sakai, Y. and K. Nakazawa. Technique for the control of spheroid diameter using microfabricated chips. *Acta Biomater* 3(6):1033-40, 2007.

227Santibanez, J. F., J. Kocic, A. Fabra, A. Cano and M. Quintanilla. Rac1 modulates tgf-beta 1-mediated epithelial cell plasticity and mmp9 production in transformed keratinocytes. *Febs Letters* 584(11):2305-10, 2010.

228Sarrio, D., S. M. Rodriguez-Pinilla, D. Hardisson, A. Cano, G. Moreno-Bueno and

J. Palacios. Epithelial-mesenchymal transition in breast cancer relates to the basal-like phenotype. *Cancer Res* 68(4):989-97, 2008.

229Schaff, U., P. E. Mattila, S. I. Simon and B. Walcheck. Neutrophil adhesion to e-selectin under shear promotes the redistribution and co-clustering of adam17 and its proteolytic substrate l-selectin. *Journal of Leukocyte Biology* 83(1):99-105, 2008.

230Scheel, C., E. N. Eaton, S. H. Li, C. L. Chaffer, F. Reinhardt, K. J. Kah, G. Bell, W. Guo, J. Rubin, A. L. Richardson and R. A. Weinberg. Paracrine and autocrine signals induce and maintain mesenchymal and stem cell states in the breast. *Cell* 145(6):926-40, 2011.

231Schmidtke, D. W. and S. L. Diamond. Direct observation of membrane tethers formed during neutrophil attachment to platelets or p-selectin under physiological flow. *Journal of Cell Biology* 149(3):719-29, 2000.

232Schwachofer, J. H. Multicellular tumor spheroids in radiotherapy research (review). *Anticancer Res* 10(4):963-9, 1990.

233Semple, T. U., L. A. Quinn, L. K. Woods and G. E. Moore. Tumor and lymphoid cell lines from a patient with carcinoma of the colon for a cytotoxicity model. *Cancer Res* 38(5):1345-55, 1978.

234Shao, J. Y., H. P. Ting-Beall and R. M. Hochmuth. Static and dynamic lengths of neutrophil microvilli. *Proc. Natl. Acad. Sci. U. S. A.* 95(12):6797-802, 1998.

235Shieh, A. C. Biomechanical forces shape the tumor microenvironment. *Ann Biomed Eng*

236Shimodaira, K., J. Nakayama, N. Nakamura, O. Hasebe, T. Katsuyama and M. Fukuda. Carcinoma-associated expression of core 2 beta-1,6-n-

acetylglucosaminyltransferase gene in human colorectal cancer: Role of o-glycans in tumor progression. *Cancer Research* 57(23):5201-06, 1997.

237Shirure, V. S., N. M. Reynolds and M. M. Burdick. Mac-2 binding protein is a novel e-selectin ligand expressed by breast cancer cells. *PLoS One* 7(9):e44529, 2012.

238Slattery, M. J. and C. Dong. Neutrophils influence melanoma adhesion and migration under flow conditions. *International Journal of Cancer* 106(5):713-22, 2003.

239Smith, C. W. Possible steps involved in the transition to stationary adhesion of rolling neutrophils: A brief review. *Microcirculation* 7(6):385-94, 2000.

240Snook, J. H. and W. H. Guilford. The effects of load on e-selectin bond rupture and bond formation. *Cell. Mol. Bioeng.* 3(2):128-38, 2010.

241Somers, W. S., J. Tang, G. D. Shaw and R. T. Camphausen. Insights into the molecular basis of leukocyte tethering and rolling revealed by structures of p- and e-selectin bound to sle(x) and psgl-1. *Cell* 103(3):467-79, 2000.

242Spassov, D. S., C. H. Wong, N. Sergina, D. Ahuja, M. Fried, D. Sheppard and M. M. Moasser. Phosphorylation of trask by src kinases inhibits integrin clustering and functions in exclusion with focal adhesion signaling. *Mol Cell Biol*

243Springer, T. A. Traffic signals for lymphocyte recirculation and leukocyte emigration: The multistep paradigm. *Cell* 76(2):301-14, 1994.

244Springer, T. A. Traffic signals on endothelium for lymphocyte recirculation and leukocyte emigration. *Annu. Rev. Physiol.* 57(827-72, 1995.

245Spurrier, B., P. Honkanen, A. Holway, K. Kumamoto, M. Terashima, S. Takenoshita, G. Wakabayashi, J. Austin and S. Nishizuka. Protein and lysate array

technologies in cancer research. *Biotechnol Adv* 26(4):361-9, 2008.

246St Hill, C. A. Interactions between endothelial selectins and cancer cells regulate metastasis. *Frontiers in Bioscience-Landmark* 16(3233-51, 2011.

247Steeber, D. A. and T. F. Tedder. Adhesion molecule cascades direct lymphocyte recirculation and leukocyte migration during inflammation. *Immunol. Res.* 22(2-3):299-317, 2000.

248Steegmaier, M., J. E. Blanks, E. Borges and D. Vestweber. P-selectin glycoprotein ligand-1 mediates rolling of mouse bone marrow-derived mast cells on p-selectin but not efficiently on e-selectin. *Eur. J. Immunol.* 27(6):1339-45, 1997.

249Steegmaier, M., A. Levinovitz, S. Isenmann, E. Borges, M. Lenter, H. P. Kocher, B. Kleuser and D. Vestweber. The e-selectin-ligand esl-1 is a variant of a receptor for fibroblast growth factor. *Nature* 373(6515):615-20, 1995.

250Steegmaier, M., A. Levinovitz, S. Isenmann, E. Borges, M. Lenter, H. P. Kocher, B. Kleuser and D. Vestweber. The e-selectin-ligand esl-1 is a variant of a receptor for fibroblast growth-factor. *Nature* 373(6515):615-20, 1995.

251Stockler, M., N. R. Wilcken, D. Ghersi and R. J. Simes. Systematic reviews of chemotherapy and endocrine therapy in metastatic breast cancer. *Cancer Treat Rev* 26(3):151-68, 2000.

252Sullivan, N. J., A. K. Sasser, A. E. Axel, F. Vesuna, V. Raman, N. Ramirez, T. M. Oberyszyn and B. M. Hall. Interleukin-6 induces an epithelial-mesenchymal transition phenotype in human breast cancer cells. *Oncogene* 28(33):2940-7, 2009.

253Sutherland, R. M., H. A. Eddy, B. Bareham, K. Reich and D. Vanantwerp. Resistance to adriamycin in multicellular spheroids. *Int J Radiat Oncol Biol Phys*

5(8):1225-30, 1979.

254Sutherland, R. M., J. A. McCredie and W. R. Inch. Growth of multicell spheroids in tissue culture as a model of nodular carcinomas. *J Natl Cancer Inst* 46(1):113-20, 1971.

255Takeichi, M. Cadherin cell adhesion receptors as a morphogenetic regulator. *Science* 251(5000):1451-5, 1991.

256Tassi, E., R. T. Henke, E. T. Bowden, M. R. Swift, D. P. Kodack, A. H. Kuo, A. Maitra and A. Wellstein. Expression of a fibroblast growth factor-binding protein during the development of adenocarcinoma of the pancreas and colon. *Cancer Res* 66(2):1191-8, 2006.

257Taylor-Papadimitriou, J., J. M. Burchell, T. Plunkett, R. Graham, I. Correa, D. Miles and M. Smith. Muc1 and the immunobiology of cancer. *J. Mammary Gland Biol. Neoplasia* 7(2):209-21, 2002.

258Terada, T., T. Ohta, M. Sasaki, Y. Nakanuma and Y. S. Kim. Expression of muc apomucins in normal pancreas and pancreatic tumours. *Journal of Pathology* 180(2):160-65, 1996.

259Tewes, M., B. Aktas, A. Welt, S. Mueller, S. Hauch, R. Kimmig and S. Kasimir-Bauer. Molecular profiling and predictive value of circulating tumor cells in patients with metastatic breast cancer: An option for monitoring response to breast cancer related therapies. *Breast Cancer Research and Treatment* 115(3):581-90, 2009.

260Thomas, S. N., R. L. Schnaar and K. Konstantopoulos. Podocalyxin-like protein is an e-/l-selectin ligand on colon carcinoma cells: Comparative biochemical properties of selectin ligands in host and tumor cells. *American Journal of Physiology-Cell*

*Physiology* 296(3):C505-C13, 2009.

261Thomas, S. N., F. Zhu, R. L. Schnaar, C. S. Alves and K. Konstantopoulos. Carcinoembryonic antigen and cd44 variant isoforms cooperate to mediate colon carcinoma cell adhesion to e- and l-selectin in shear flow. *Journal of Biological Chemistry* 283(23):15647-55, 2008.

262Thorlacius, H., J. Prieto, J. Raud, N. Gautam, M. Patarroyo, P. Hedqvist and L. Lindbom. Tumor cell arrest in the microcirculation: Lack of evidence for a leukocyte-like rolling adhesive interaction with vascular endothelium in vivo. *Clin Immunol Immunopathol* 83(1):68-76, 1997.

263Timmins, N. E. and L. K. Nielsen. Generation of multicellular tumor spheroids by the hanging-drop method. *Methods Mol Med* 140(141-51, 2007.

264Tomlinson, J., J. L. Wang, S. H. Barsky, M. C. Lee, J. Bischoff and M. Nguyen. Human colon cancer cells express multiple glycoprotein ligands for e-selectin. *Int. J. Oncol.* 16(2):347-53, 2000.

265Tremblay, P. L., J. Huot and F. A. Auger. Mechanisms by which e-selectin regulates diapedesis of colon cancer cells under flow conditions. *Cancer Res.* 68(13):5167-76, 2008.

266Ut-Binh T. Giang, M. R. K., Lisa A. DeLouise. Microfabrication of bubbular cavities in pdms for cell sorting and microcell culture applications. *Journal of Bionic Engineering* 5(4):308-16, 2008.

267Van Der Vegt, B., M. A. J. De Roos, J. L. Peterse, C. Patriarca, J. Hilkens, G. H. De Bock and J. Wesseling. The expression pattern of muc1 (ema) is related to tumour characteristics and clinical outcome of invasive ductal breast carcinoma.

*Histopathology* 51(3):322-35, 2007.

268Varki, A. Selectin ligands. *Proceedings of the National Academy of Sciences of the United States of America* 91(16):7390-97, 1994.

269Varki, A. Selectin ligands: Will the real ones please stand up? *Journal of Clinical Investigation* 100(11):S31-S35, 1997.

270Varki, N. M. and A. Varki. Diversity in cell surface sialic acid presentations: Implications for biology and disease. *Lab. Invest.* 87(9):851-57, 2007.

271Varki, N. M. and A. Varki. Diversity in cell surface sialic acid presentations: Implications for biology and disease. *Lab Invest* 87(9):851-7, 2007.

272Verdier, C., C. Couzon, A. Duperray and P. Singh. Modeling cell interactions under flow. *Journal of Mathematical Biology* 58(1-2):235-59, 2009.

273Vestweber, D. and J. E. Blanks. Mechanisms that regulate the function of the selectins and their ligands. *Physiol. Rev.* 79(1):181-213, 1999.

274Vogel, J., G. Bendas, U. Bakowsky, G. Hummel, R. Schmidt, U. Kettmann and U. Rothe. The role of glycolipids in mediating cell adhesion: A flow chamber study. *Biochim Biophys Acta* 1372(2):205-15, 1998.

275Walcheck, B., K. L. Moore, R. P. McEver and T. K. Kishimoto. Neutrophil-neutrophil interactions under hydrodynamic shear stress involve l-selectin and psgl-1 - a mechanism that amplifies initial leukocyte accumulation on p-selectin in vitro. *Journal of Clinical Investigation* 98(5):1081-87, 1996.

276Wang, X., A. A. Shah, R. B. Campbell and K. T. Wan. Glycoprotein mucin molecular brush on cancer cell surface acting as mechanical barrier against drug delivery. *Applied Physics Letters* 97(26):2010.

277Weigelt, B., J. L. Peterse and L. J. van't Veer. Breast cancer metastasis: Markers and models. *Nat Rev Cancer* 5(8):591-602, 2005.

278Wilkins, P. P., K. L. Moore, R. P. McEver and R. D. Cummings. Tyrosine sulfation of p-selectin glycoprotein ligand-1 is required for high-affinity binding to p-selectin. *Journal of Biological Chemistry* 270(39):22677-80, 1995.

279Wirtz, D., K. Konstantopoulos and P. C. Searson. The physics of cancer: The role of physical interactions and mechanical forces in metastasis. *Nature Reviews Cancer* 11(7):512-22, 2011.

280Witz, I. P. The selectin-selectin ligand axis in tumor progression. *Cancer Metastasis Rev* 27(1):19-30, 2008.

281Wojciechowski, J. C., S. D. Narasipura, N. Charles, D. Mickelsen, K. Rana, M. L. Blair and M. R. King. Capture and enrichment of cd34-positive haematopoietic stem and progenitor cells from blood circulation using p-selectin in an implantable device. *Br. J. Haematol.* 140(6):673-81, 2008.

282Yago, T., J. H. Wu, C. D. Wey, A. G. Klopocki, C. Zhu and R. P. McEver. Catch bonds govern adhesion through l-selectin at threshold shear. *Journal of Cell Biology* 166(6):913-23, 2004.

283Yamanaka, T., S. Matsumoto, S. Teramukai, R. Ishiwata, Y. Nagai and M. Fukushima. The baseline ratio of neutrophils to lymphocytes is associated with patient prognosis in advanced gastric cancer. *Oncology* 73(3-4):215-20, 2007.

284Yin, L., Y. Li, J. Ren, H. Kuwahara and D. Kufe. Human muc1 carcinoma antigen regulates intracellular oxidant levels and the apoptotic response to oxidative stress. *J Biol Chem* 278(37):35458-64, 2003.

285Yin, L., Y. Q. Li, J. Ren, H. Kuwahara and D. Kufe. Human muc1 carcinoma antigen regulates intracellular oxidant levels and the apoptotic response to oxidative stress. *Journal of Biological Chemistry* 278(37):35458-64, 2003.

286Yin, X. Y., K. Rana, V. Ponmudi and M. R. King. Knockdown of fucosyltransferase iii disrupts the adhesion of circulating cancer cells to e-selectin without affecting hematopoietic cell adhesion. *Carbohydrate Research* 345(16):2334-42, 2010.

287Zen, K., D.-Q. Liu, Y.-L. Guo, C. Wang, J. Shan, M. Fang, C.-Y. Zhang and Y. Liu. Cd44v4 is a major e-selectin ligand that mediates breast cancer cell transendothelial migration. *PLoS ONE* 3(3):e1826, 2008.

288Zhang, K., D. Baeckstrom, H. Brevinge and G. C. Hansson. Comparison of sialyl-lewis a carrying cd43 and muc1 mucins secreted from a colon carcinoma cell line for e-selectin binding and inhibition of leukocyte adhesion. *Tumor Biology* 18(3):175-87, 1997.

289Zhang, K., D. Baeckstrom, H. Brevinge and G. C. Hansson. Secreted muc1 mucins lacking their cytoplasmic part and carrying sialyl-lewis a and x epitopes from a tumor cell line and sera of colon carcinoma patients can inhibit hl-60 leukocyte adhesion to e-selectin-expressing endothelial cells. *Journal of Cellular Biochemistry* 60(4):538-49, 1996.

290Zhang, P., T. Ozdemir, C. Y. Chung, G. P. Robertson and C. Dong. Sequential binding of αvβ3 and icam-1 determines fibrin-mediated melanoma capture and stable adhesion to cd11b/cd18 on neutrophils. *J Immunol* 186(1):242-54, 2011.

291Zollner, O., M. C. Lenter, J. E. Blanks, E. Borges, M. Steegmaier, H. G. Zerwes

and D. Vestweber. L-selectin from human, but not from mouse neutrophils binds directly to e-selectin. *J Cell Biol* 136(3):707-16, 1997.

292Zotter, S., A. Lossnitzer, P. C. Hageman, J. F. M. Delemarre, J. Hilkens and J. Hilgers. Immunohistochemical localization of the epithelial marker mam-6 in invasive malignancies and highly dysplastic adenomas of the large-intestine. *Lab. Invest.* 57(2):193-99, 1987.